Study on Tribological Characteristics of Ceramics in High Temperature and High Pressure Water

1994

Satoshi KITAOKA

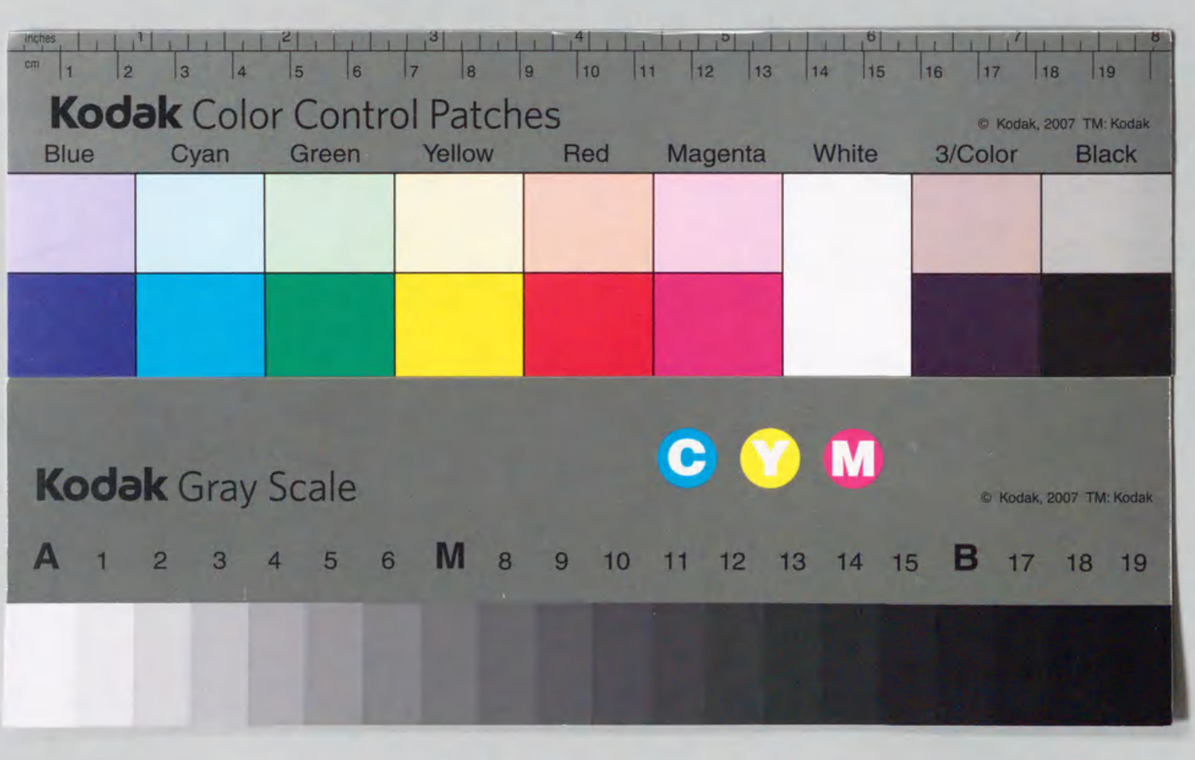

Study on Tribological Characteristics of Ceramics in High Temperature and High Pressure Water

1994

Satoshi KITAOKA

CONTENTS

Chapter 1

Introduction

1 Introduction

1.1 Significance of development of advanced ceramics for nuclear power plants

A supply of electric energy due to nuclear power plants has significantly been needed to solve recent environment problems on evolution of CO_2 and acidic rain. However, we should improve more safety and reliability of the equipments in plants, since the accidents such as Chernovil and Three-mile islands were caused by both trouble of some equipments and human errors. If the reliability of the parts and prolongation of the span of those life is achieved, it will lead to more public acceptance and economy due to rationalization of the periodical inspection.

Radiation exposure of the workers in nuclear atomic plants has been decreased, but still one of the significant problems in the world. Main radiation sources are ^{60}Co and ^{58}Co contained in corrosion products and wear debris, which are released from the structural materials such as stellite and stainless steel etc. in coolant and are transformed to radioactive substances in a reactor core.[1] These radioactive elements are adhered on the pipe and lead to increasing radiation dose rate. Therefore, the dose rate has been decreased by depressing the corrosion of materials due to the control of the coolant, but it has been few years since the dose rate was saturated in Japan.[2] This means that decreasing of the radiation exposure is difficult only due to control of the coolant and countermeasure for the materials is indispensable.

The development of high-performance ceramics is stimulating major advances in a large spectrum of technologies that include machine design, manufacturing techniques and process engineering. Representative examples are alumina (α-Al_2O_3), silicon nitride (α, β-Si_3N_4), silicon carbide (α-SiC), chromium carbide (Cr_3C_2) and titanium carbide (TiC). They have been attracting great deal of attention for applications to equipments in nuclear power plants because of excellent high temperature stability and high hardness in addition to less radioactivity.[3] The development of the advanced ceramics and accumulation of data for the mechanical and chemical properties in the high temperature and high pressure water simulated nuclear power plants is very important since the ceramics is quite a new for the application to tribomaterials compared to the metals.

1.2. Principles of Tribology[4]

During the relative motion of two solid pressed against each other by a normal force F_n, one observes a force F_d that tends to oppose the movement. Associated with this force of friction the breakdown or wear of the two solids is observed.

The measurement of friction and wear is quite simple. The tribometer consists of a moving and a stationary surface pressed against each other. One measures the friction force, and after a chosen time or distance of sliding , one measures the amount of material removed, either by weight change or by volume loss. The wear rate is usually expressed in cubic millimeters removed per newton load and millimeter sliding (mm^2/N). The linear relationship between these quantities implied by this definition is not generally obeyed by ceramics for which this wear rate is not a constant and should be used only for purposes of comparison. Information about the operating wear mechanisms is obtained most often by observation of the wear scars in the scanning electron microscope. Scanning transmission microscopy and optical or electrical spectroscopes can be used to observe defects, dislocations, crystal structures or reaction products.

With few exceptions, the friction force F_d does not depend on apparent contact area A_a nor on the sliding velocity, but is proportional to the normal force F_n usually called "the load". For this reason, one defines a friction coefficient:

$$\mu = \frac{F_d}{F_n} \qquad (1-1)$$

In the absence of lubrication, the friction coefficient varies between 0.2 and 1 in most practical cases. It is lower in the case of diamond and usually higher than one for metals sliding in vacuum. The origin of the friction coefficient is complex and still quite poorly understood. For rough surfaces, plowing of one surface by the hard asperities of the other and other wear processes can make a contribution, but closer examination shows that the wear processes account for less than 10% of the friction energy spent; the latter is almost completely transformed into heat. Systems that approach ideally flat and parallel surfaces do not exhibit lower friction. The real origin of friction lies in the second law of thermodynamics.

Consider an atom A subjected to the moving periodic potential describing its interaction with the other, sliding body (see figure 1-1).[5] As the closest atom B of the counterface moves away, atom A is pulled along and causes a stretch of its bonding to its own

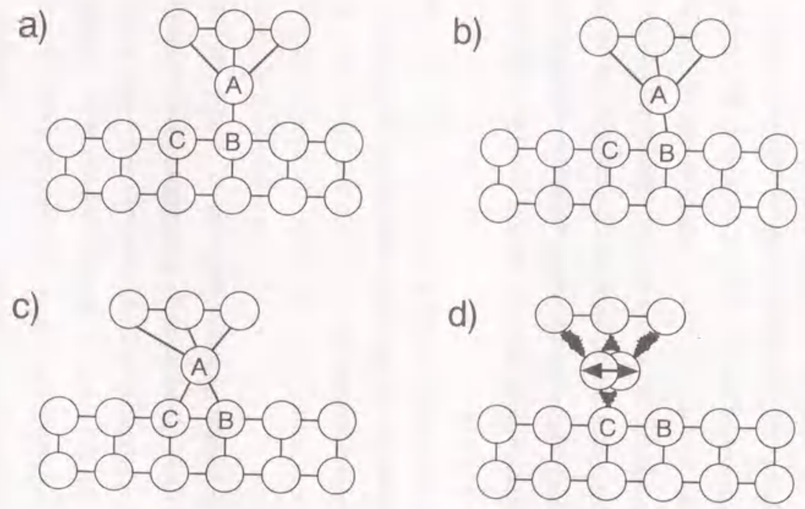

Fig. 1-1 Principle of friction. Atom A of the stationary body is attached to its neighbors by chemical bonds. Atoms B and C belong to the moving body. (a) This is assumed to be the position of minimun energy with closest approach of atoms A and B. (b) After a short distance of sliding, bond A-B is stretched, atom A is pulled away from its equilibrium position by elastic deformation, and the energy increases. (c) Atom A, in its displaced position, is midway between atoms B and C; bond A-B is about to be ruptured. (d) Atom A vibrates about in equilibrium position in regard to atom C by virtue of A-C attraction and release of elastic stretch energy. This vibration is dissipated into body by phonon emission.

substrate. With further sliding, the bonding to atom B breaks and atom A is pulled in the reverse direction by its attraction to atom C. The accumulated elastic energy and the attraction to atom C combine to accelerate an atom backward. With its considerable energy, the atom vibrates in the potential minimum and emits phonons which propagate in the body and add to the thermal vibration energy. Obviously, a lowering of the adhesive energy decreases the friction force. Such a decrease, caused by adsorption of molecules from the ambient, explains why friction is higher in vacuum than in air. A reduction of the friction coefficient to values as low as 0.05 can be achieved by the adsorption of selected surfactans called "*boundary lubricants*".

Wear is defined as the progressive removal of material from the sliding surfaces. It consists of the deformations, cutting and fracture caused by the contact stresses that are due to the normal and frictional forces. In order to understand how wear depends on the properties of materials, let us review briefly the mechanical degradation processes of solids. At moderate stresses (tensile, compressive or shear), all the atoms are displaced from their equilibrium positions. This is elastic deformation. When the shear stress exceeds a threshold value, planes of atoms in the crystals glide on each other by means of dislocation motion; this is plastic deformation. (Note that a pure (i.e., hydrostatic) compressive and tensile stresses do not cause plastic deformation.) Hardness is measured by pressing a diamond pyramid into the surface of the solid and observing the size of the indent and is a measure of the resistance to plastic deformation. Pure metals are soft where the metallic bond is nondirectional because atoms slide on each other easily as long as their distance does not increase. Covalent bonds are strongly directional where in the sp^3 bond of diamond, for instance, the four neighbors attached to an atom must be located at precise positions with respect to each other, and the bending of a bond required to move a dislocation requires large amounts of energy. In ionic crystals, the alternation of positive and negative charges prevents the gliding of atomic planes in all but very few crystal planes. Ionic ceramics are hard and covalently bonded solids are the hardest known.

Fracture always occurs at sharp edge, crack tips or nonspherical voids where the tensile or shear stress is much higher than the average or design stress. At these sites, the local stress can exceed the maximum cohesive force between atoms. Soft solids do not fracture easily: plastic deformation causes a rounding of the edge and a decrease in the maximum stress. Hard materials are brittle because crack tip cannot be blunted by plastic

deformation. The resistance to fracture is called toughness which is related to the strength of the interatomic bond and energy dissipated by bridge between crack surfaces or crack deflection.[6] The interatomic bonds at a crack tip can be weakened strongly by adsorbed molecules. This causes a decrease of the stresses required for crack propagation and this effect is called "*stress corrosion cracking*".

Let's now discuss the wear. There are several types of wear that can be classified and understood in terms of the responses of materials to local stresses. Abrasive wear is caused by the penetration of hard particles into the surface and the cutting of grooves. A.G.Evans and D.B.Marshall have presented the predicted equation for ceramics removal during wear on the base of the lateral fracture mechanism, where cracks initiate and develop horizontally to the worn surface by the residual stress created when the penetrating abrasive particle is removed.[7] This equation is given by:

$$\Delta V = \Omega \frac{F_n^{9/8}}{K_{IC}^{1/2} \cdot H_v^{5/8}} \left(\frac{E}{H_v}\right)^{4/5} L \qquad (1-2)$$

where ΔV is wear volume, Ω is a material-independent constant, E and H_v are elastic modulus and hardness of the material, respectively. K_{IC} is fracture toughness of the wearing material and L is sliding distance. This equation substantiates the strong importance of both the fracture toughness and hardness upon the wear resistance. Adhesive wear is caused by the friction forces described above. In metals, it occurs mostly by plastic deformation and ultimately by crack propagation. According to Archard[8], the resistance to adhesive wear is proportional to the hardness in metals, but contributions from fatigue resistance and toughness have been claimed by others.[9-12] In the case of ceramics, plastic deformation, although observed in the softer and tougher materials, is less important than fracture, but the relative contributions from the material properties to wear resistance are not yet established.

Tribochemical wear is a process governed by a chemical reaction (tribochemical reaction) between surroundings and solid surfaces due to simultaneous friction. The chemical reaction rate of solids is often governed by reaction products that accumulate on the surface and through which the reagent molecules must diffuse. One can see several mechanisms by which such reactions are accelerated by friction: (1) wear removes protective product layer and exposes fresh surface; (2) frictional stresses cause deformation

or microfracture in the layer or the solid and produce diffusion paths or high-energy sites of increased reactivity; (3) frictional heat increases the local temperature; (4) the making and breaking of bonds that accompany friction create highly reactive chemical intermediate states. The wear behavior of ceramics in high temperature and high pressure water may correspond to the tribochemical wear because almost of ceramics are more or less corroded in the environment.

1.3 Chemical effects on tribology of ceramics

1.3.1 Wear reduction by the tribochemical oxidation of Si_3N_4

It is well known that tribology of ceramics is significantly affected by the presence of water.[13,14] For Si_3N_4 ceramics, the wear rate decreases by as much as 2 orders of magnitude in humid air compared with that in dry argon. Minimum wear rate is reached at 90% relative humidity in argon and 50% relative humidity in air. Under these conditions, the wear scar is much smoother than that after sliding in dry gases, and is covered with an amorphous silicon oxide which is probably strongly hydrated. Thus, under the action of friction, enough Si_3N_4 is oxidized to form a several micrometer thick layer ahead of the wear scar of the sliding pin and a thinner but easily detectable layer on the larger wear track of the plate. The friction coefficient of Si_3N_4 is nearly the same in dry and in humid environment.[13] This means that the total mechanical forces acting on the contacting surfaces are the same. In a humid environment, removal of matter by tribochemical oxidation occurs at the asperities; consequently, the contacting surfaces are smoother and the load and friction forces are distributed over wider areas than in the absence of tribochemistry. In other words, the local stresses responsible for microcracking and the mechanical wear of the material are reduced by the tribochemical oxidation. For SiC ceramics, the similar reduction of the local stresses has been reported by Sasaki.[15] Although various tribochemical reactions between Si_3N_4 or SiC and H_2O have been proposed, the progress of the reactions have been hardly confirmed experimentally and have not yet discussed theoretically. It is only confirmed that NH_3 was produced during friction of Si_3N_4 against itself in water at room temperature and the following tribochemical reaction was given by Sasaki.[15]

$$Si_3N_4 + 6H_2O \rightarrow 3SiO_2 + 4NH_3 \qquad (1\text{-}3)$$

Quinn has proposed the mechanism of oxidation wear of steel from the standpoint of

frictional heat.[16] It has been assumed that progress of adhesive wear (plastic deformation) and the oxide layer produced by the tribochemical reaction are removed by friction when its thickness exceeds the critical value ξ . Thus the volumetric wear loss is given by:

$$\Delta V = \frac{2a \cdot A_c \cdot \exp\{-\Delta E/(R \cdot T_c)\}}{3\xi^2 \cdot \rho^2 \cdot v \cdot H_v} F_n \cdot L \qquad (1-4)$$

where A_C and ΔV are frequency factor and activation energy of the static oxidation reaction, respectively, R gas constant, T_C flush temperature at the contact, ρ density of material, v sliding velocity, $2a$ diameter of a junction with two solid surfaces. However, it is hard to predict the wear rate accurately because of the unclear parameters such as T_C , a and ξ . In the case of ceramics, the experimental evidence is not easy to interpret because wear seems to be governed by microfracture rather than plastic deformation. One can speculate that the reaction is accelerated because the hydroxide formed on the surface is continuously removed and fresh surface is exposed by friction, but clear experimental evidence for any mechanism is still lacking.

1.3.2 Tribochemical dissolution of Si_3N_4 and SiC in water

The dissolution of silicon oxide in water is a well-known phenomenon.[17,18] It is also known that silicon nitride dissolves in water slowly but measurably above 200℃ as will be discussed later.[19] When silicon nitride is sliding in water at room temperature, even at velocities and loads for which the temperature at contacting asperities increases little, wear produces very smooth surfaces caused by molecular dissolution of the material.[13] Although measurable quantities of material have been removed, no wear particles are found. It is thought that the dissolution occurs by the oxidation of the material to form water-soluble silicic acid:[17]

$$3SiO_2 + 6H_2O \rightarrow 3Si(OH)_4 \qquad (1\text{-}5)$$

The tribochemical nature of this reaction is responsible for the very smooth surfaces on the rubbing surfaces where the reaction occurs only at contacting asperities. The smoothness of the surfaces leads to hydrodynamic lubrication with attendant near-zero friction when the silicon nitride surfaces slide in water at a velocity of only 6cm/s despite an average bearing load of 4.91N.[20] By assuming that the viscosity of the water is not

changed by the small amount of silicic acid dissolved, the minimum thickness of the hydrodynamic water film is estimated about 70nm which is larger than the surface roughness of the surfaces.[20] Similar experiments with silicon carbide also produce dissolution of the material, but hydrodynamic lubrication is not obtained because the material is mechanically weaker than silicon nitride and suffers local fracture as well as dissolution.[20]

1.3.3 Formation of a lubricious surface

Influence of tribochemical reaction products on friction and wear of silicon nitride has been recently reported at elevated temperature in humid air by using a ball-on flat linear-sliding geometry.[21] The friction coefficient and wear rates are lowered when the wear debris spontaneously forms into rolls, mainly composed of amorphous silicon oxide, probably hydrated with high viscosity, and oriented perpendicular to the sliding direction at high humidity level in the temperature range of 600 to 800℃. Such a cylindrical wear debris were also produced at room temperature in humid argon gas.[13,14] This wear debris on the worn surface may protect the material from further wear. The dramatic effect of these rolls suggests the possibility that conditions in operating devices can be manipulated to produce their formation and extends the operating lifetimes of ceramic/ceramic bearings in service.

Oxide ceramics such as alumina are obviously incapable of undergoing the oxidation reactions that are responsible for the decrease of wear in silicon nitride. This different chemical behavior manifests itself a different reaction between oxide and the environment during friction. Gates, Hsu and Klaus[22] have shown a mechanism for the tribochemical lubrication of the system between α -alumina and water at room temperature. It has been proposed that the sliding in water causes the formation of stable aluminum hydroxides which are modified to a layered structure such as bayerite under high temperature and high pressure at the contact, through a phase transformation from α to γ phase due to anisotropic shear stresses. Easy shear in the layered structure results in lower friction coefficients and wear rate for the surface.

1.3.4 Chemically induced fracture in oxide ceramics

The mechanical strength of many glasses and oxide ceramics decreases with time when

exposed to static loading and ambient environments. This decrease of strength is generally associated with stress corrosion cracking of pre-existing surface flaws in the presence of water. According to Michalske and Freiman[23], the interaction between a strained bridging bond at the crack tip in silica and a water molecule from the environment can be represented by a three-step process as shown in figure 1-2, and each process is explained as follows.

Step 1. A water molecule from the environment attaches to a bridging Si-O-Si bond at the crack tip. The water molecule is aligned by: (1) formation of the hydrogen bond with the $O_{(bridging)}$ atom and (2) interaction of the lone-pair orbital from $O_{(water)}$ with the Si atom. The lone-pair orbital interaction may involve either Van der Walls attraction or some covalent bonding with unoccupied orbital of Si.

Step 2. A concerted reaction occurs in which proton transfer to the $O_{(bridging)}$ is accomplished simultaneously with electron transfer from the $O_{(water)}$ to the Si atom. As a result of this reaction, two new bonds are formed, one between $O_{(water)}$ and Si, and one between hydrogen and $O_{(bridging)}$; the original bridging bond between $O_{(bridging)}$ and Si is destroyed.

Step 3. Rupture of the hydrogen bond between $O_{(water)}$ and transferred hydrogen occurs to yield surface Si-O-H groups on each fracture surface. Since the hydrogen bond is week, this step is expected to occur immediately after proton transfer.

Stress corrosion cracking for Al_2O_3 is also controlled by dissociative chemisorption of electron donor/proton donor species at Al-O-Al crack tip bonds.[24] This has a stress corrosion limit due to crack tip blunting corresponding to the load which stress corrosion crack growth no longer weakens the material.[25] Wallbridge et al.[26] have reported an increase in wear for alumina by an order of magnitude when water was added to their tests which were conducted under the conditions of about 5.7MPa and 0.24m/s in contract to those found by Sasaki[16] and Gates et al.[22] This difference may be related to whether the local stresses at the contact are over the stress corrosion limit or not.

1.4 Corrosion of ceramics in high temperature and high pressure water

1.4.1 Static corrosion

Although ceramics were generally considered to have an excellent corrosion resistance, it has been recently found that non-oxide ceramics are essentially attacked under oxidizing

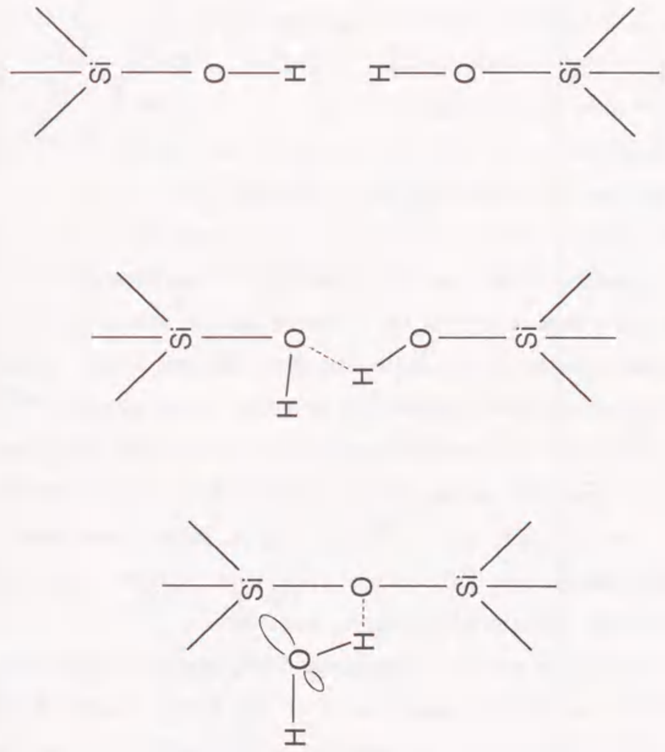

Fig.1-2 Representation of proposed reaction between water and strained Si-O-Si bond at crack tip. Reaction steps involve (1) adsorption of water to Si-O bond, (2) concerted reaction involving simultaneous proton and electron transfer and (3) formation of surface hydroxyl groups.

atmosphere such as dry air[27-33], water vapor[33-37] and water[38-40] at high temperature, and in some cases significant decreases in strength are observed.[33,39,41]

α - or β -silicon nitride (Si_3N_4) and α -silicon carbide (SiC) are significantly oxidized above 700～1000℃ by oxygen or air, and the following chemical reactions have been proposed:

$$Si_3N_4 + 3O_2 \rightarrow 3SiO_2 + 2N_2 \quad (1\text{-}6)$$

$$SiC + 2O_2 \rightarrow SiO_2 + CO_2 \quad (1\text{-}7)$$

Although the oxidation of Si_3N_4 and SiC by water vapor occurs at the similar temperature to that by oxygen, the oxidation by water vapor is completely different from that by oxygen. At higher temperature, it is given by following equations:[35,40]

$$Si_3N_4 + 6H_2O \rightarrow 3SiO_2 + 2N_2 + 6H_2 \quad (1\text{-}8)$$

$$SiC + 4H_2O \rightarrow SiO_2 + CO_2 + 4H_2 \quad (1\text{-}9)$$

At lower temperature, equations (1-3) and (1-10) shown as follows[38,40] are thermodynamically more stable than equations (1-8) and (1-9), respectively.

$$SiC + 2H_2O \rightarrow SiO_2 + CH_4 \quad (1\text{-}10)$$

Since the amorphous silica scale is formed on the surface of the ceramics during the oxidation and plays the role of a protective film, the oxidation kinetics are controlled by the diffusion of gaseous species following parabolic rate law. Moreover, some authors reported that the existence of water vapor enhanced the oxidation of the ceramics.[36,37] These oxidation has been studied by many investigators,[27-32,34-40] but their results are widely scattered. For example, figure 1-3 summarizes the oxidation data of Si_3N_4 and SiC indicates various parabolic rate constants and activation energies. Direct comparison of these kinetics data is impossible because different materials with different impurities, manufacturing techniques and thus different microstructure were used.

Yoshimura et al.[38] have reported the reaction between pure Si_3N_4 powder (average grain size 0.5 μ m, α phase＞90%) and H_2O at temperatures of 200-800℃ under 10 and 100MPa to study the intrinsic oxidation of the material with free of additives and microstructures. Obtained results indicate that the oxidation becomes significant above 200 ℃ and the oxidation kinetics could be sufficiently represented by a Jander-type equation over wide range of reaction. This indicates that the oxidation should be controlled by diffusion processes. The oxidation of the silicon nitride powder gives the apparent activation energies of 73 kJ/mol in water below 400℃ under 100MPa (N1 in fig.1-3) and

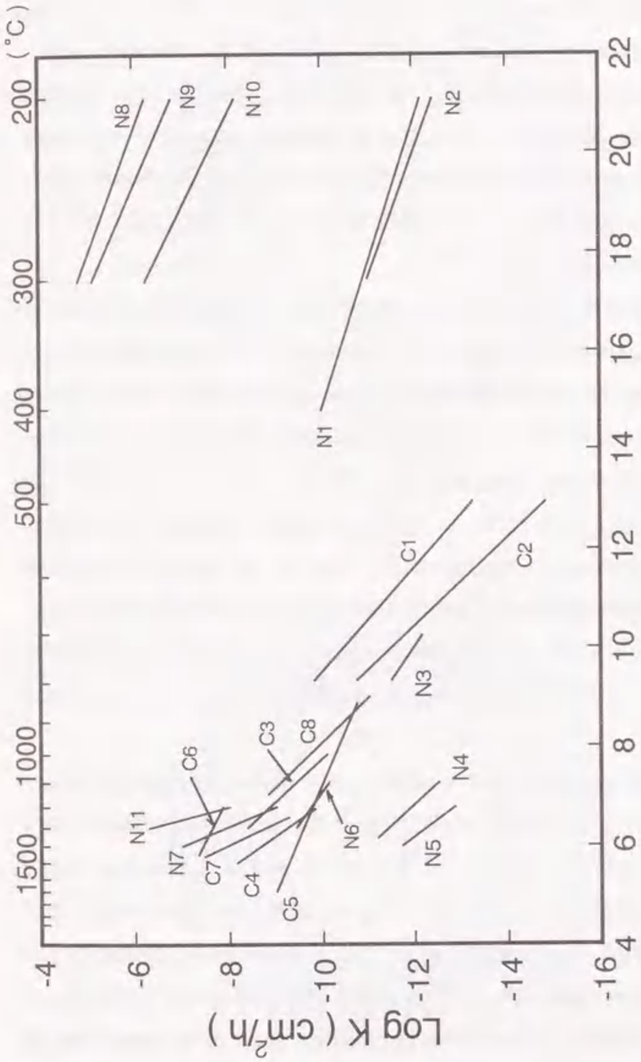

Fig. 1-3 Oxidation of Si_3N_4 and SiC samples in various atmospheres.

N1, N2, N8-N10: Oxidation of Si_3N_4 in water: N1,N2(powder),Yoshimura et al.(38); N8-N10(sintered ceramic),Sato et al.(39) .

N3,N7, N11: Oxidation of Si_3N_4 in water vapour: N3(powder),Yoshimura et al.(38); N7(sintered ceramic),Singhal(34); N11(sintered ceramic),Sato et al.(35).

N4-N6: Oxidation of Si_3N_4 in dry oxygen: N4(powder),Horton (27); N5(powder),Mitomo et al.(29); N6(powder),Tetard et al.(28).

C1: Oxidation of SiC in water: C1(powder),Yoshimura et al.(40); C6(powder),Jorgensen et al.(36);

C2, C6-C8 Oxidation of SiC in water vapour: C2(powder),Yoshimura et al.(38); C8(powder),Suzuki et al.(37) .

C7(sintered ceramic),Singhal(34); C8(powder),Suzuki et al.(37) .

C3-C5 Oxidation of SiC in dry oxygen: C3(powder),Nakatogawa(30); C4(powder),Ervin(31); C5(powder),Jorgensen et al.(32).

84kJ/mol in water below 300℃ under 10MPa (N2 in fig.1-3), which are similar to those of 60-105kJ/mol for H_2O diffusion in amorphous silica.[42,43] T.Sato et al.[39] have also reported the similar apparent activation energies of 83.5-108 kJ/mol (N8-N10 in fig.1-3) for the corrosion of Si_3N_4 ceramics containing Y_2O_3, Al_2O_3 and AlN as sintering aids under hydrothermal conditions at temperatures of 200-300℃ and saturated vapor pressures of water. Yoshimura et al.[38] have proposed a model for the oxidation of Si_3N_4 by H_2O as shown in figure 1-4(a), where the inward diffusion of H_2O in amorphous silica scale is rate-determinant. The outward diffusion of NH_3 might be rather fast. The coupled ionic diffusion, H_3O^+-OH^- and/or NH_4^+-OH^-, may also be possible instead of molecular diffusion of H_2O and NH_3. This model is completely different from that for the oxidation of Si_3N_4 in oxygen where the oxygen diffusion in oxide scale is rate-determinant but the outward diffusion of N_2 might be rather fast.[27-29]

More studies are apparently needed to clarify the true mechanism for H_2O oxidation of Si_3N_4 because we have few data about the chemical state of water in the amorphous silica scale. Tomozawa[44] demonstrated the accommodation of water in amorphous silica phases as hydrated glasses, where it exists as OH^- in early stage of hydration, then as molecular H_2O in more hydrated samples. However, the states of H_2O may be more complicated in the case of the oxidation of Si_3N_4 than those in hydrated glasses because the activity (fugacity) gradient should be considered in the former.[45] That is, the activity of oxidant species has a positive gradient from outside surface to the interface of Si_3N_4/oxide scale, and there is a reverse gradient in nitrogen species. More precisely, the many anionic species such as OH^- and NH_4^+ etc. may exist with their own activities in the oxide scale, and may give different kinetics.

Yoshimura et al.[38] have found quite different kinetics in the oxidation of Si_3N_4 above 500℃ from those below 400℃ in 10MPa H_2O. Especially, under the 10MPa H_2O condition, the oxidation proceeded quite slowly at 500-600℃. The activation energy observed at 700-800℃ was 134kJ/mol as shown in fig.1-3 (N3) and was larger than 84kJ/mol below 300℃ (N2 in fig.1-3). These behavior is considered to be caused by the change of oxidation reaction from equations (1-3) to (1-8) with increasing temperature, which is supported thermodynamically.[38] Therefore, the kinetics seem to be controlled by the diffusion of N_2 in the oxide scale above 500℃, because the smaller H_2 molecule can diffuse more easily than N_2. The higher activation energy at 700-800℃ compared to that

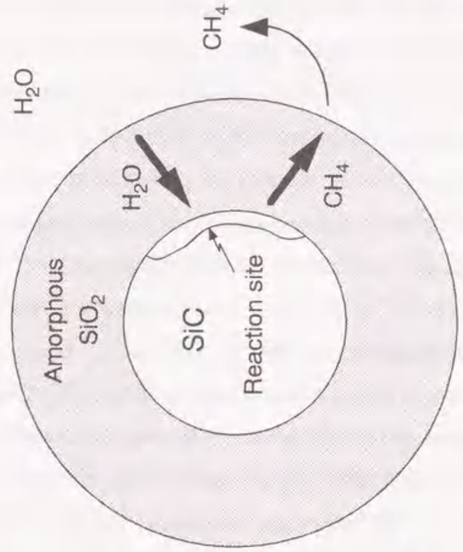

$$SiC + 2H_2O \rightarrow SiO_2 + CH_4$$

(b)

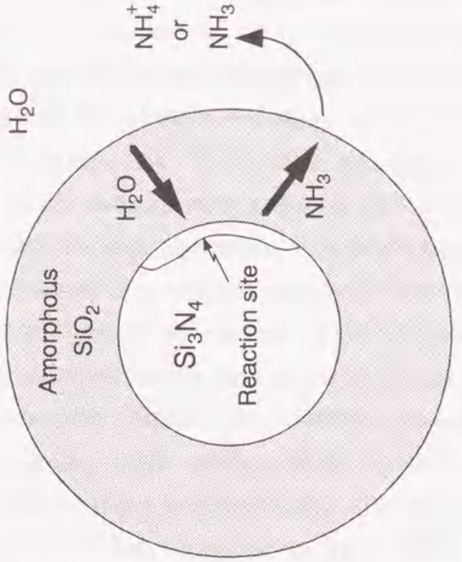

$$Si_3N_4 + 6H_2O \rightarrow 3SiO_2 + 4NH_3$$

(a)

Fig. 1-4 Reaction model of the oxidation of Si_3N_4 and SiC particles by high temperature and high pressure water.

below 400℃ may be related to the lower diffusivity of N_2 rather than H_2O.

Yoshio et al.[46] have also reported the effects of grain morphology in sintered Si_3N_4 ceramics containing Y_2O_3 and Al_2O_3 on the corrosion behavior in water at 300℃ and 8.6MPa. It was found that the specimen with finer grain morphology was corroded rather than that with large grain morphology. For both specimens the traces of machining grooves formed during the surface preparation were observed on the oxide scale even after exposure for 10 days, and this remaining traces during the surface preparation may result in the formation of a layer with high dissolution resistance in high temperature water. Unfortunately, its detail mechanism has not been unknown. Yoshio et al.[47] have shown that Si_3N_4 ceramics containing MgO are attacked more easily than that containing Y_2O_3 and Al_2O_3 under the hydrothermal condition at 300℃. Ono et al.[48] also reported the similar effect of sintering aids on the corrosion behavior in water at 88℃. Ono et al.[19,48] have also found that grain boundaries of the Si_3N_4 ceramics were preferentially dissolved below about 200℃ rather than oxidation of Si_3N_4 surface and the corrosion behavior of the Si_3N_4 ceramics from 120 to 275℃ was not accelerated by the concentration of dissolved oxygen in water. Sato et al.[39] have shown that the corrosion rate of β-Si_3N_4 ceramics containing Y_2O_3, Al_2O_3 and AlN decreased with decreasing crystallinity of the grain boundary phase which was not identified.

Yoshimura et al.[40] have reported the reaction between pure SiC powder (average grain size 0.65 μ m, α phase > 94%) and H_2O at temperatures of 400-800℃ under 10 and 100MPa The oxidation became significantly above 500℃ and amorphous silica scale covered the SiC powder in similar to that of Si_3N_4. The oxidation kinetics of the SiC powder was also approximately represented by a Jander-type equation. Yoshimura et al. suggested that reaction (1-10) is preferentially occurs compared to reaction (1-9) because reaction (1-10) was thermodynamically more stable than reaction (1-9) under the hydrothermal conditions and the obtained activation energy was similar to that estimated by using the Van der Waals diameter of CH_4 to be 0.4nm.[45] They also proposed a reaction model for SiC oxidation in H_2O as shown in fig.1-4(b).[40] After the amorphous silica layer is formed on the surface of SiC particles, H_2O and CH_4 diffuse from outside and from inside of silica layer, respectively in similar to that of Si_3N_4. Calculated apparent activation energies of the oxidation of SiC powder are 167kJ/mol under 100MPa H_2O and 194kJ/mol under 10MPa H_2O. These values are higher than 80kJ/mol for water

diffusion and 134kJ/mol for N_2 diffusion in the case of Si_3N_4 described above. The H_2O diffusion in the silica layer should be the same in the oxidation both of SiC and of Si_3N_4. Thus the oxidation rate of SiC in H_2O is considered to be controlled by the diffusion of CH_4 in the amorphous silica layer.[40] The difference between the oxidation of SiC and Si_3N_4 in pressurized H_2O, therefore, would be due to the difference of produced gases. For further discussion, however, we need more detailed study particularly to know the precise composition of oxide scale and the gaseous species in the scale.

Some authors proposed that the acceleration of the oxidation of SiC due to water vapor is related to the crystallization of amorphous silica scale into cristobalite which creates grain boundaries.[34,36] Yoshimura et al.[40] also observed the crystallization of amorphous silica into cristobalite and tridimite, but this crystallization always occurred only at outside surface of the oxide scale, and the crack tip due to crystallization did not propagate the interface between SiC and oxide scale. Thus the acceleration of the oxidation by the crystallization may be miner effect in high temperature and high pressure water.

Kawakubo et al.[49] have examined corrosion behavior of 14 kinds of sintered ceramics in oxygen-free water (dissolved oxygen less than 0.02ppm) and oxygenated water (dissolved oxygen about 32ppm) at 290℃ using a refreshed-type autoclave system. Obtained results revealed that SiC ceramics (mainly α or β phase) containing boron and carbon as sintering additives had the most excellent dissolution resistance in dissolved oxygen and showed more acceleration of the dissolution rate in oxygenated water than oxygen-free water similarly to Hirayama et al.[50] They have also found that the dissolution rate increases with increasing pH in the solution and the weight loss of the specimen in an oxygenated alkaline solution basically follows a linear rate law, but that in the acidic solution approximately follows a parabolic rate law. Based on the above results, Hirayama et al. [50] considered that the dissolution kinetics depends on the stability of poorly adherent layer such as silica sol because no silica scale on the surface could be detected through scanning electron micrograph, X-ray diffraction analysis and Auger electron spectroscopy examinations; in the alkaline solution, silica sol dissolves rapidly and has no protective effect on the SiC substrate, but the dissolution of silica sol is hard in the acidic solution resulting in the formation of a diffusion layer. This is quite different from the model shown in fig.1-4(b) where the oxidation rate is controlled by diffusion of gaseous species through the protective silica layer. This difference may be caused by the different

experimental methods. That is to say, Hirayama et al.[50] used loop-type autoclave system and controlled composition of the solution, but Yoshimura et al.[40] used batch-type one where composition of the solution changes during the corrosion of the sample and dissolution of silica may be reached in equilibrium in early stage of the oxidation of SiC.

Few reports have been published with respect to corrosion of carbide of titanium or chromium in high temperature and high pressure water.[51,52,53] The reaction between TiC powder (average grain size 1 μ m, C/Ti=0.96) and H_2O has been reported at 200-650℃ under 100MPa.[51] The reaction of TiC with H_2O above 400℃ for 3h yielded anatase, CH_4, CO_2 and H_2, and above 500℃ rutile was formed additionally. The gas analysis revealed that reaction should be the parallel reactions as follows.

$$TiC + 2H_2O \rightarrow TiO_2 + CH_4 \qquad (1\text{-}11)$$

$$TiC + 4H_2O \rightarrow TiO_2 + CO_2 + 4H_2 \qquad (1\text{-}12)$$

The oxidation rate obtained from the weight gain was compared with that calculated from kinetics equations based on various models. In TiC the rate was best described by the Avrami-Erofeyev equation (n=1.3), while the core-shrinking model with an induction period fitted as well. This suggests that the rate-determining step is the nucleation and nuclear growth of TiO_2 at the interface between TiC and TiO_2. The value of n more than unity means that the nuclear growth rate is larger than the nucleation rate. The existence of the induction period may be related to the slow oxidation governed by the diffusion of gaseous species through the amorphous TiO_2. Thus the oxidation model has been proposed as shown in fig. 1-5.[51] First, an amorphous TiO_2 film covered the TiC grains. The gaseous products, CH_4, CO_2 and H_2 might be accumulated beneath this film because these gases appear to be difficult to dissolve in the TiO_2 film at the temperatures of 200-600℃. After a certain period of time, accumulated gases might break the film. This is the end of the induction period. At that time the crystallization occurs from the amorphous TiO_2 into anatase, which also helps to break the film. After that, the reaction occurs at the surface of grains and oxidation is reaction-controlled. Kanno et al.[52] have also suggested that crystallization of the amorphous TiO_2 formed on the TiC film which is coated on a super alloy (*P-20*) by chemical vapor deposition method accelerates the corrosion rate in high temperature and high pressure water.

As regard to corrosion behavior of Cr_3C_2 under hydrothermal conditions, only one study, where Cr_3C_2 matrix composites have similar corrosion resistance to SiC ceramics

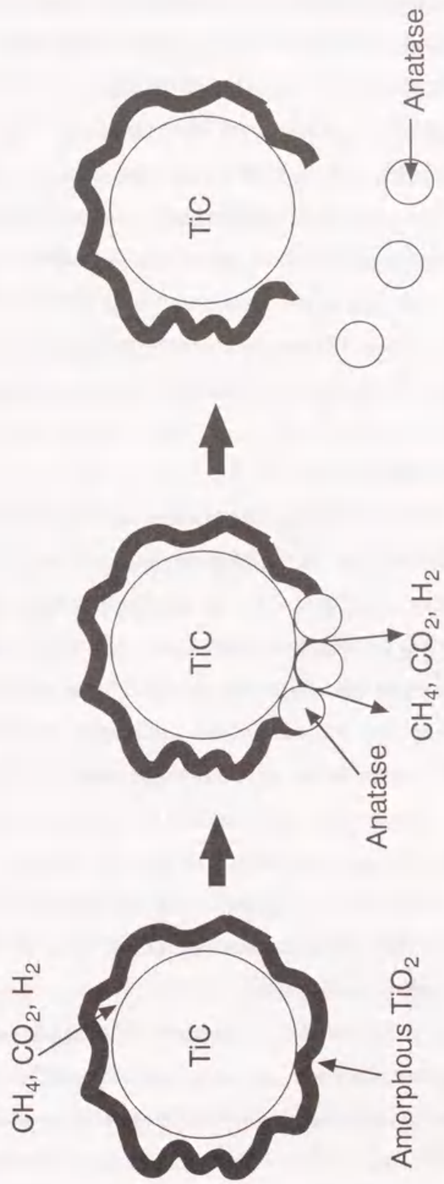

Fig. 1-5 Reaction model of the oxidation of TiC particle by high temperature and high pressure water.

in water at 288℃ simulated Boiling Water Reactors, has been reported.[53] Unfortunately, the effect of sintering aids and corrosion mechanism have not been known.

α -Alumina ceramics have been already applied to a mechanical seal of a primary coolant pump in Pressurized Water Reactors, where is used in water at temperature of 88 ℃. Thus the ceramics are expected for the application as mechanical parts to a severer environment in Light Water Reactors (LWR). Ono et al.[54] have been found that the corrosion resistance of α -Al_2O_3 ceramics increased with increasing the purity of the alumina in distilled water at 275℃ by using the once-through type experimental loop. They have shown that the impurities existed in the grain boundaries such as Si, Ca, Na and K preferentially dissolved into water, resulting in the intergranular corrosion morphology. In addition, boehmite, which is a stable form in the experimental conditions, was observed on the corroded surface. Kawakubo et al.[49] have also reported similar results to above.

1.4.2 Dynamic corrosion due to friction

The study on the corrosion wear of ceramics in high temperature and high pressure water has been just started in Japan.[53,55,56] Saito et al.[53] have reported the tribological behavior of a cylindrical specimen such as Al_2O_3, Si_3N_4, pressureless and hot pressed SiC, Cr_3C_2 composites and stellite rolling against stainless steel (XM-19) in water at 288 ℃ under 7.84MPa, where the ceramics were held by a pin specimen of stellite, in order to evaluate the applicability of the ceramics as guide rollers in a rod cluster control assembly in Boiling Water Reactors (the roller made of stellite is being used now). The wear amounts of the cylindrical specimens decreased in order of Si_3N_4 > hot pressured SiC > Al_2O_3 > stellite > Cr_3C_2 composites > pressureless SiC, and that of the pin specimens decreased in order of Al_2O_3 > hot pressured SiC > Si_3N_4 > Cr_3C_2 composites > stellite > pressureless SiC. It is note that pressureless SiC is promising as the replacement for the stellite, but the wear mechanisms have not been discussed.

Jungo et al.[55] have been reported the effects of load and temperature on the wear rate of hot isotropic pressured Si_3N_4 against itself in water at the temperature of 20～350℃ and the load of 0.07～0.48N under 20MPa by using a pin-on-flat linear-sliding geometry. The specific wear rates increased from 10^{-10} to $10^{-6}mm^2/N$ with increasing the temperature and load, but depended on the temperature larger than the load. The wear mechanisms of the pin were classified into three regions such as "*plastic flow with slightly oxidation of Si_3N_4* (Ⅰ)", "*formation of cylindrical wear debris with oxidation* (Ⅱ)" and "*initiation and propagation of pits with significantly oxidation and subsequent dissolution of silica* (Ⅲ)".[55,56] Region (Ⅰ) appeared at the temperature of about 20～120℃, Region (Ⅱ) at about 120～220℃ and Region (Ⅲ) above 220℃. The appearance of the cylindrical wear debris is strongly affected by the sliding conditions in addition to the existence of water.[13,14,21] However, effect of sintering aids on the tribological behavior of Si_3N_4 ceramics has not been clear under the hydrothermal condition, although the static corrosion behavior are significantly affected by chemical compositions and crystallinity of grain boundaries.[39,47,54]

1.5 Aim of this work

The advanced application of high-performance ceramics as tribomaterials of equipments used in reactor power plants have been desired in order to increase reliability of the mechanical parts and to prolong the span of those life, in addition to decreasing the radiation exposure as mentioned above.[3] However, few reports have been published on the tribological behavior of high-performance ceramics in high temperature and high pressure water simulated the environment in light water reactors.[53,55,56] Furthermore, the wear mechanisms are still uncertain. It is suggested that the friction and wear characteristics of the ceramics in water at room temperature significantly depend on the tribochemical reactions between the worn surface and water,[13,14,15,20] however, the tribochemical reactions have not been experimentally and theoretically well-discussed.

The first purpose is to evaluate the tribological characteristics of the representative structural ceramics such as α -Al_2O_3, α - and β -Si_3N_4, α -SiC, Cr_3C_2-TiC composite (CRT) and Stellite No.6B (ST) sliding on themselves in high temperature and high pressure water. The second purpose is to understand the wear mechanisms. Third purpose is to obtain the information regarding development of the advanced materials with the excellent wear resistance under the hydrothermal conditions.

The reasons for the selection of the above materials are described as follows. Alumina ceramic has been already used as a mechanical seal in water at 88℃ in Pressurized Water Reactors and an application of the ceramics as tribomaterials is expected in water at higher temperature. Since it is well known that Si_3N_4 ceramics generally have excellent mechanical properties such as flexural strength, fracture toughness and thermal shock

resistance, we presume that they have strong resistance to wear due to fracture. The wear rate of Si_3N_4 in water at room temperature is smaller in two orders than that in dry air or argon,[13,15] although it is significantly corroded by water at the temperature above 200℃.[19,38,39] Thus the material may have a good wear resistance in water at temperature below 200℃. SiC ceramic is expected to have an excellent resistance against wear governed only by the corrosion under the hydrothermal condition because of low wear rate in water at room temperature,[15] the excellent corrosion resistance[40,49] and oppositely the inferior mechanical properties. CRT may also have a good wear resistance because the corrosion resistance of CRT is similar to that of SiC. The tribological behavior of ST, which has been widely used for a tribomaterial in LWR, was investigated in order to compare with that of ceramics in water at high temperature and high pressure water. The mechanical and thermal properties of the materials used in these experiments are listed in tables 1-1 and 1-2, respectively. The crystal structure and composition of the ceramics and stellite are shown in table 1-3 and 1-4, respectively.

Friction and wear of a material sliding on itself were to simplify the system of these experiments and to simulate the pair of the materials used as the mechanical seal in Pressurized Water Reactors.

1.6 Summary of this work

The tribological characteristics of the advanced ceramics (Al_2O_3, Si_3N_4, SiC and CRT) sliding on themselves in water were evaluated at various sliding conditions in the temperature range from room temperature to 300℃, and the friction and wear mechanisms were discussed. Moreover, the applicability of these ceramics as tribomaterials in nuclear power plants were estimated. The contents of each chapter were summarized as follows.

In Chapter 2, the effects of temperature, sliding speed, contact load and impurities on the tribological characteristics of two kinds of α -Al_2O_3 ceramics were investigated at the temperatures up to 300℃. The wear mechanisms were discussed on the basis of the examinations of the worn surface morphology, wear participates and static corrosion behavior.

In Chapter 3, the effects of temperature, sliding speed, contact load, hydrostatic pressure, dissolved oxygen concentration and sintering aids of the friction and wear properties of three kinds of Si_3N_4 ceramics in water were evaluated at room temperature and 120℃.

The wear behavior was discussed from the standpoints of the tribochemical oxidation, frictional heat and microfracture.

In Chapter 4, the effects of the temperature and sliding speed on the tribological characteristics of a SiC ceramic in deoxygenated water were investigated in the temperatures up to 300℃. The wear mechanisms were quantitatively elucidated by the participation of the tribochemical oxidation and hydrodynamic lubrication.

In Chapter 5, the effects of the temperature and sliding speed on the friction and wear properties of CRT were studied at the same sliding conditions as those for the SiC ceramic. The tribology of CRT was understood by the contribution of tribochemical oxidation and microfracture, especially thermal shock fracture for the disk specimen.

In Chapter 6, the equations to predict the wear amount of the plate specimen were proposed on the base of these experimental results, and the validity of these equations was verified by using the wear data in the previous studies. The applicability of the ceramics as the mechanical parts in nuclear power plants was also discussed from the viewpoints of the static corrosion, friction and wear resistance of the ceramics, in addition to comparing with the tribology of the stellite. Moreover, the information to develop new materials with the excellent wear resistance in water was described.

In Chapter 7, the results obtained in these experiments were summarized.

Table 1-1 Mechanical properties of materials.

Materials (symbol)	Density (g/cm^3)	Young's modulus (GPa)	Poisson's ratio	Hardness (GPa)	Fracture toughness ($MPa \cdot m^{1/2}$)
Al_2O_3-1 (ALO-1)	3.90	378	0.24	17.1	4.3
Al_2O_3-2 (ALO-2)	3.98	404	0.25	20.1	3.4
Si_3N_4-1 (SN-1)	3.19	304	0.28	17.5	4.7
Si_3N_4-2 (SN-2)	3.24	306	0.28	15.5	5.2
Si_3N_4-3 (SN-3)	3.25	308	0.27	16.3	5.4
SiC (SC)	3.16	428	0.16	22.6	2.4
Cr_3C_2-TiC (CRT)	6.20	396	0.25	19.2	4.3
Stellite No.6B (ST)	8.34	238	0.29	4.1	-

Table 1-2 Thermal properties of materials.

Materials (symbol)	Thermal conductivity κ (W/(m K))	Thermal expansion coefficient α ($\times 10^{-6} K^{-1}$, 20～800℃)	Thermal shock resistance parameter R(℃)
Al_2O_3-1 (ALO-1)	26.9	7.8	83
Al_2O_3-2 (ALO-2)	35.2	7.9	78
Si_3N_4-1 (SN-1)	25.3	3.0	359
Si_3N_4-2 (SN-2)	18.2	3.1	374
Si_3N_4-3 (SN-3)	21.2	3.2	373
SiC (SC)	174	4.5	128
Cr_3C_2-TiC (CRT)	14.2	10.0	63
Stellite No.6B (ST)	12.6	15.5	-

Table 1-3 Crystal structure and composition of ceramics.

Materials (symbol)	Crystal structure of matrix	Compsition (wt%)									
		Al	Si	Mg	Y	Ca	Na	B	Total-C	Cr	Ti
Al_2O_3-1 (ALO-1)	α-phase, trigonal	>52.4	0.114	0.15	-	0.128	0.008	-	-	-	-
Al_2O_3-2 (ALO-2)	α-phase, trigonal	>52.9	0.003	0.025	-	0.004	0.002	-	-	-	-
Si_3N_4-1 (SN-1)	α- and β-phases, hexagonal	2.58	56.5	0.71	-	0.004	0.004	-	-	-	-
Si_3N_4-2 (SN-2)	β-phase, hexagonal	1.88	55.1	-	3.6	0.002	0.002	-	-	-	-
Si_3N_4-3 (SN-3)	β-phase, hexagonal	1.78	55.2	-	3.7	0.002	0.002	-	-	-	-
SiC (SC)	α-phase, hexagonal	-	69.3	-	-	-	-	0.1	30.6	-	-
Cr_3C_2-TiC (CRT)	Cr_3C_2, orthorhombic TiC, cubic	0.02	-	-	-	-	-	-	14.3	68.5	17.2

Table 1-4 Composition of stellite.

Materials (symbol)	Crystal structure	Compsition (wt%)							
		Si	Total-C	Cr	Co	W	Ni	Fe	Mn
Stellite No.6B (ST)	Co, α-phase, hexagonal Co, β-phase, cubic Cr_7C_3, orthorhombic	0.62	1.03	29.94	58.95	3.93	2.51	1.52	1.5

References

1 M.Arii, H.Nagano and Y.Morikawa, *Toshiba review*, 36,No.11,974(1981) (in Japanese).

2 K.Ishigure, *Genshiryoku kogyo*, 37,No.11,8(1991) (in Japanese).

3 S.Nakahigashi, M.Suzuki, I.Tokuda and Y.Yamaguchi, *Genshiryoku kogyo*, 37,No.11,36 (1991) (in Japanese).

4 See for instance: H.Czichos, *Tribology*, Elsevier, Amsterdam, (1978); D.A.Rigney, Ed. *Fundamentals of Friction and Wear Materials*, American Society for Metals, Metals Park, OH(1981); F. P. Bowden and D. Tabor, *The Friction and Lubrication of Solid*, Clarendon Press, Oxford(1986).

5 T.E.Fischer and W.M.Mullins, *J.Phy.Chem.*, 96,5690(1992).

6 A.G.Evans, *J.Am.Ceram.Soc.*, 73,No.2,187(1990).

7 A.G.Evans and D.B.Marshall, *ASM*, 439(1980).

8 J.F.Archard, *J.Appl.Phys.*, 24,No.8,981(1953).

9 I.V.Kraghelsky, *Trans.Am.Soc.Mech.Eng.*, D87,No.3,785(1965).

10 J. Halling, *Wear*, 34,No.3,239(1975).

11 E.F.Finkin, *Wear*, 47,No.1,107(1978).

12 Karl-Heinz Zum Gahr, *Microstructure and Wear of Materials*, Elsevier, 137(1987).

13 T.E.Fischer and H.Tomozawa, *Wear*, 105,29(1985).

14 S.Jahanmir and T.E.Fischer, *Tribol.Trans.*, 31,No.1,32(1988).

15 S.Sasaki, *J.Soc.Lubrication Eng.*, 33,No.8,620(1988) (in Japanese).

16 T.F.J.Quinn, *ASLE Trans.*, 10,No.2,18(1967).

17 R.K.Iler, *The Chemistry of Silica*, John Wiley and Sons, New York (1979).

18 S.H.Chan, *Geothermics*, 18,No.1/2,49(1989).

19 S.Ono, M.Kumagai and K.Hoashi, *Zairyo-to-Kankyo*, 40,315(1991) (in Japanese).

20 H.Tomizawa and T.E.Fischer, *ASLE Trans.*, 30,No.1,41(1987).

21 D.S.Park, S.Danyluk and M.J.McNallan, *J.Am.Ceram.Soc.*, 75,No.11,3033(1992).

22 R.S.Gates, S.M.Hsu and E.E.Klaus, *Tribol.Trans.*, 32,No.3,357(1989).

23 T.A.Michalske and S.W.Freiman, *J.Am.Ceram.Soc.*, 66,No.4,284(1983).

24 T.A.Michalske, B.C.Bunker and S.W.Freiman, *J.Am.Ceram.Soc.*, 69,No.10,721(1986).

25 T.A.Michalske, *Fract.Mech.Ceram.* Vol.5, 277(1983).

26 N.Wallbridge, D.Dowson and E.W.Roberts, *Wear of Materials*; K.C.Ludema, Ed., ASME,New York, 202(1983).

27 R.M.Horton, *J.Am.Ceram.Soc.*, 52,No.3,121(1969).

28 D.Tetard, P.Lortholary, P.Goursat and M.Billy, *Rev.Int.Htes.Temp.*, et' Refract, 10, No.3,153(1973).

29 M.Mitomo and J.H.Sharp, *Yogyo Kyokai Shi*, 84,No.1,33(1976) (in Japanese).

30 T.Nakatogawa, *Kogyo Kagaku Zasshi*, 57,No.5,348(1954) (in Japanese).

31 G.Ervin,Jr., *J.Am.Ceram.Soc.*, 41,No.9,347(1958).

32 P.J.Jorgensen, M.E.Wadsworth and I.B.Cutler, *J.Am.Ceram.Soc.*, 42,No.12,613(1959).

33 G.A.Gogotsi, Y.G.Gogotsi, V.P.Zavada and V.V.Traskovsky, *Materials at High Temperatures*, 9,No.4,209(1991).

34 S.C.Singhal, *J.Am.Ceram.Soc.*, 59,No.1/2,81(1976).

35 T.Sato, K.Haryo, T.Endo and M.Shimada, *J.Mater.Sci.*, 22,2635(1987).

36 P.J.Jorgensen, M.E.Wadsworth and I.B.Cutler, *J.Am.Ceram.Soc.*,44,No.6,258(1961).

37 H.Suzuki, *Yogyo Kyokai Shi*, 67,No.5,157(1959) (in Japanese).

38 M.Yoshimura, J.Kase and S.Somiya, *Yogyo Kyokai Shi*, 94,No.1,129(1986) (in Japanese).

39 T.Sato, T.Murakami, T.Endo, M.Shimada, K.Komeya, T.Kameda and M.Komatsu, *J.Mater.Sci.*, 26,1749(1991).

40 M.Yoshimura, J.Kase and S.Somiya, *J.Mater.Res.*, 1,No.1,100(1986).

41 H.Kim and A.J.Moorthead, *J.Am.Ceram.Soc.*, 73,No.10,3007(1990).

42 I.Burn and J.P.Roberts, *Phys.Chem.Glass.*, 11,No.4,106(1970).

43 S.White, *Nature,Phys.Sci.*, 230,192(1971).

44 M.Tomozawa, *J.Non-Cryst. Solids*, 73,No.2,197(1985).

45 M.Yoshimura, J.Kase, M.Hayakawa and S.Somiya, *Proceedings of the Symposium on Corrosive Degradation of Ceramics, the First Ceramic Science and Technology Congress of the American Ceramic Society*, Nov. 1-2,337(1989).

46 T.Yoshio and K.Oda, *Yogyo Kyokai Shi*, 95,No.4,435(1987) (in Japanese).

47 T.Yoshio and K,Oda, *Yogyo Kyokai Shi*, 95,No.7,730(1987) (in Japanese).

48 S.Ono, M.Yuki, M.Kumagai and K.Hoashi, *Zairyo-to-Kanky* o, 40,533(1991) (in Japanese).

49 T.Kawakubo, H.Hirayama, A.Goto and T.Kaneko, *J.Soc.Mat.Sci.*, 38,No.426,300 (1989) (in Japanese).

50 H.Hirayama, T.Kawakubo and A.Goto, *J.Am.Ceram.Soc.*, 72,No.11,2049(1989).

51 M.Yoshimura, M.Hayakawa and S.Somiya, *Yogyo Kyokai Shi*, 97,No.11,1139(1989) (in Japanese).

52 Y.Kanno, M.Yashima, M.Kakihana and M.Yoshimura, *J.Soc.Mat.Sci.,* 42,No.478,780 (1993) (in Japanese).

53 N.Saito, Y.Fuse, Y.Yasuda and M.Oishi, *Rroceedings of the Symposium on Boshoku Fushoku*, 355(1993) (in Japanese)

54 S.Ono, K.Suzuki, M.Kumagai and K.Hoashi, *Zairyo-to-Kankyo*, 40,655(1991) (in Japanese).

55 X.Jungo and K.Kato, *Proceedings of the Congress on Tribology, Morioka*,205 (1992-10) (in Japanese).

56 X.Jungo, K.Kato, T.Umehara and T.Akiyama, *Proceedings of the Congress on Tribology, Tokyo*, 205(1993-5) (in Japanese).

Chapter 2

Tribological Characteristics of α-Al_2O_3 Ceramics

2 Tribological Characteristics of α-Al_2O_3 ceramics

2.1 Introduction

α-Alumina ceramics (Al_2O_3) have been widely used for tribomaterials because of their excellent wear resistance and chemical stability. They are also being investigated for advanced applications as components and parts of the light water reactor plants which are used in high temperature and high pressure water. Evaluation of the tribological behavior of α-Al_2O_3 ceramics in a hydrothermal environment is extremely important in assessing its applicability as a tribomaterial in high temperature water and improving its wear resistance.

Several investigators have shown the effect of water on the friction and wear behavior of α-Al_2O_3 ceramics at room temperature.[1-3] They have found that the wear rate is remarkably small in water compared with dry sliding tests. Gates et al.[4] have suggested that a lubricious hydroxide layer formed by tribochemical reaction between alumina and water in the sliding interface has a great role in the reduction of friction and wear. Corrosion and dissolution behavior of α-Al_2O_3 ceramics have been investigated in high temperature water[5,6]. The reported results have shown that the grain boundaries of the materials are preferentially attacked. This suggests that the corrosion resistance of α-Al_2O_3 ceramics can be improved by controlling the characteristics of grain boundaries. Because of the corrosion behavior, the influence of water on the tribological properties in high temperature water is considered to be different from that in room temperature water. However, few reports have been published on the friction and wear behavior of alumina in water over 100℃.

This chapter describes the effects of temperature, sliding speed, contact load and impurities on the tribological characteristics of α-Al_2O_3 ceramics sliding on themselves in water at various temperature up to 300℃, and discusses the tribochemical mechanism between alumina and water at 300℃.

2.2 Experimental procedure

The materials used for the wear tests were two kinds of α-Al_2O_3 ceramics (ALO-1 and ALO-2). The ALO-1 specimen (99.2wt% Al_2O_3) contains larger impurities of Si, Ca, Mg and Na than the ALO-2 specimen (99.9wt% Al_2O_3) as shown in table 1-3. The mechanical and thermal properties of the α-Al_2O_3 ceramics are listed in tables 1-1 and 1-2,

respectively.

Wear tests were carried out by sliding the circumferential surface of a rotating disk with plates in water as shown schematically in fig.2-1. The plate specimens were cut to 15mm ×20mm×3mm. Their contact surfaces were ground by an 800 grit diamond wheel to a roughness of about 0.15 μm Ra. The disk specimens were 40mm in diameter and 4mm in thickness. Their contact surface roughness was about 0.20 μm Ra. The plate and disk specimens were ultrasonically cleaned in acetone for 10min, and dried in an oven at 120℃ for 2h. They were cooled in a desiccator to room temperature. After the specimens were fitted to the apparatus, 6.3 liters of distilled water was poured into the autoclave. For ALO-1, the experiments were conducted in water at room temperature, 120℃ and 300℃ under the corresponding saturated vapor pressures of atmospheric pressure, 0.2 and 8.53MPa, respectively. The constant contact load was 19.6N, and the sliding speed ranged from 0.11 to 0.84m/s. The sliding distance was 38,000m. Other experiments were carried out in water at 300℃ at a sliding speed of 0.21m/s and sliding distance of 4,500m under contact loads between 9.8 and 78.4N. For ALO-2, the wear tests were conducted in the same contact load range as that for ALO-1 but at the sliding speeds of 0.42 and 0.84m/s and at sliding distance of 5,000m in water at 300℃. The torque of the driving shaft was monitored during the tests by a torque transducer. The friction coefficient was calculated from the difference of the torque between the load and no-load conditions. Surface profiles of wear scars of the plates parallel to the sliding direction coincided with circular arcs of the disks. Therefore, the wear volume of the plate, ΔV, can be written as

$$\Delta V = \frac{b}{4}\left\{D^2 \sin^{-1}(d/D) - d\left(D^2 - d^2\right)^{1/2}\right\} \qquad (2-1)$$

where b and d are the width (about 4mm) and length of the wear scar, respectively, and D is the diameter of the disk after the test. The wear volume of the disk was obtained from dividing the weight loss of the specimen caused due to the wear by its density. The specific wear rate of the plate, W_s, is defined as

$$W_s = \frac{\Delta V}{F_n \cdot L} \qquad (2-2)$$

where F_n is the contact load and L is the sliding distance. For the calculation of W of the disk, $2F_n$ is used, because the disk was contact with two plates. The worn surfaces were examined by scanning electron microscopy (SEM) and transmission electron microscopy

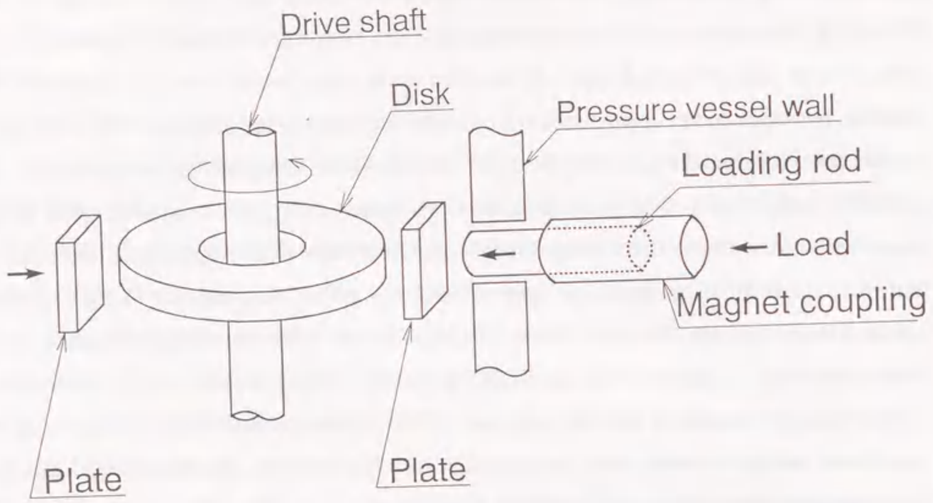

Fig.2-1 Schematic diagram of the wear testing system.

(TEM). The wear debris, which was dispersed into the eluent, was collected by a centrifugal separator and investigated by X-ray diffractometry (XRD).

The tribological characteristics of the α -alumina ceramics in high temperature water seems to depend on the corrosion behavior. In order to examine the corrosion process, the α -alumina specimens were soaked in water at 300℃ for 200h. The surface of the treated specimen was observed by SEM. The components of the eluent after the treatment were analyzed by inductively coupled plasma spectroscopy (ICP).

2.3 Results

2.3.1 Effects of temperature and sliding speed on friction and wear of ALO-1

Figure 2-2 shows the effects of temperature and sliding speed on the steady state friction coefficient of ALO-1. At each temperature, the friction coefficient decreases with increasing sliding speed. As the temperatures are raised, the friction coefficient increases at sliding speeds lower than 0.4m/s, but is weakly dependent on the temperature at 0.4m/s and over. Figure 2-3 shows the effects of temperature and sliding speed on the specific wear rate for the plate and disk of ALO-1. The specific wear rates of the plate and disk at room temperature are extremely small on the order of $10^{-11} \sim 10^{-10} mm^2/N$ and independent of the sliding speed. The specific wear rate increases by several orders of magnitude at elevated temperatures. At 120℃ and 300℃, the specific wear rates of both the plate and disk decrease with increasing sliding speed. The specific wear rates of the disk at all temperature are larger than those of the plate. Figure 2-4 shows the SEM micrographs of the worn surfaces of the plates before and after the tests in water under a contact load of 19.6N. The micrographs of the worn surfaces were taken at the center of the wear scar corresponding to the maximum wear depth. Figure 2-4(b) shows a typical micrograph of the worn surface tested at room temperature. The worn surface is smooth compared to the untested surface shown in fig.2-4(a), but there are some pits. For the untested plate, the depth of surface damage caused by the surface preparation was determined by polishing the plate with 3 μ m -diamond paste to the angle of 1.5×10^{-5} rad. The SEM examination of this surface has revealed that many pits were observed at the surface removal to 10 μ m, but scarcely over 20 μ m. The maximum depth of the wear scar at room temperature test determined from the surface profile was about 5 μ m. Then the pits as shown fig.2-4(b) are

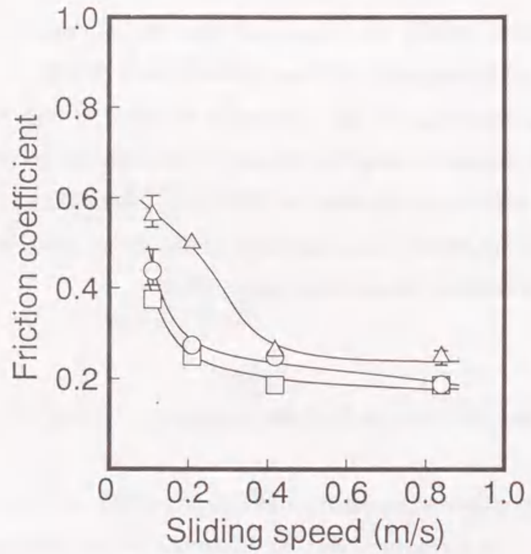

Fig.2-2 Effect of sliding speed on the friction coefficient of ALO-1 specimens in water at room temperature (□), 120℃ (○) and 300℃ (△).

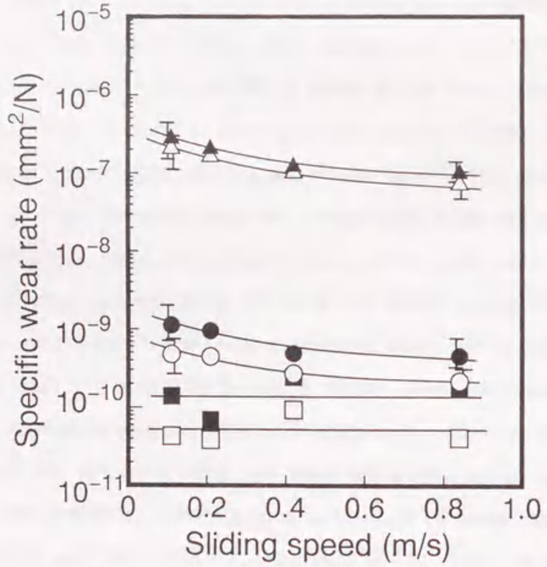

Fig.2-3 Effect of sliding speed on the specific wear rate of the disk and plate of ALO-1 in water at room temperature (□,■), 120℃ (○,●) and 300℃ (△,▲). (Open:plate, filled:disk)

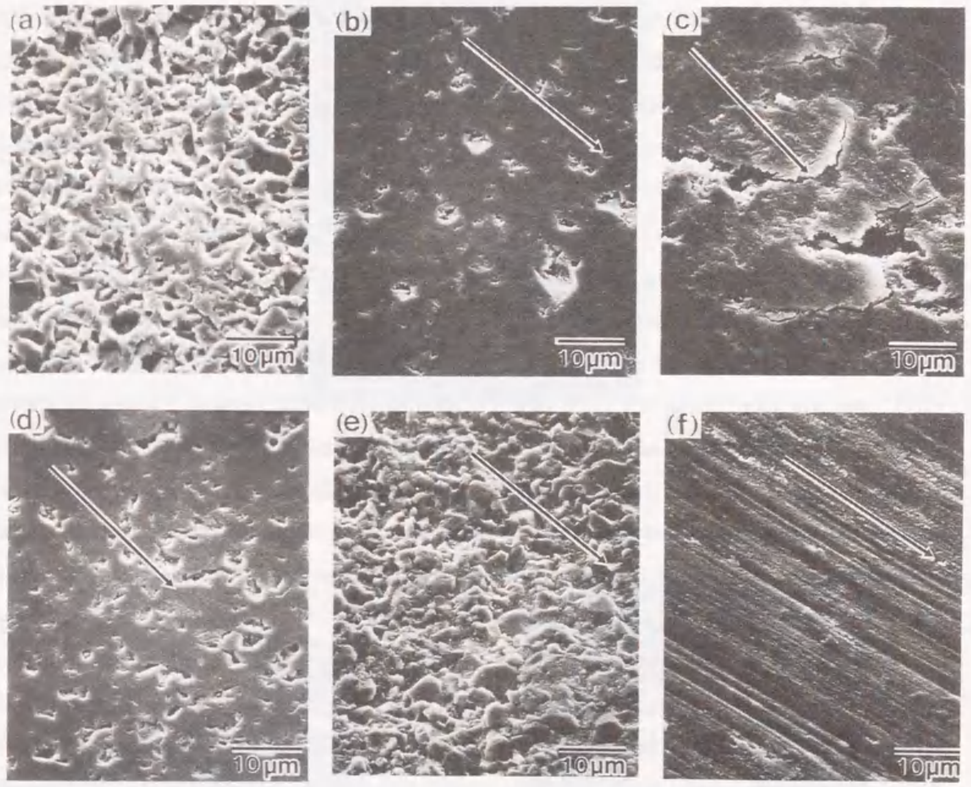

Fig.2-4 Scanning electron micrographs of the worn surfaces of the plate of ALO-1 tested in water under a contact load of 19.6N: (a) the surface of the plate before the test, (b) at room temperature and sliding speed of 0.11m/s, (c) at 120℃ and 0.11m/s, (d) at 120℃ and 0.84m/s, (e) at 300℃ and 0.11m/s, and (f) at 300℃ and 0.84m/s. The arrows shown in the figure indicate the sliding direction of the disk.

thought to be caused by grains pulled out from the surface during surface preparation. No wear debris was found on the worn surfaces of the plates and the disks at any sliding speed. We do not, at this time, have any experimental evidence that would explain this observation, but it is possible to imagine that a thin aluminum hydroxide layer, which is produced by the tribochemical reaction between water and the alumina surface, slightly solves to water as reported by Sasaki.[3] This hydroxide layer possesses some solid lubricating ability[4], resulting in a low specific wear rate. At 120℃, fig.2-4(c) shows many cracks appear on the worn surface at 0.11m/s. Figure 2-4(d) shows few surface cracks and more pits are found at 0.84m/s than that in fig.2-4(b). The maximum depth of the wear scars at 120℃ was about 25～40 μm and was much larger than that at room temperature. The cracks and/or pits on the worn surface were produced during the tests. At 300℃, the worn surface at 0.11m/s shows predominantly intergranular fracture as shown in fig.2-4(e). At the higher sliding speed, a streaked film appears on the worn surface as shown in fig.2-4(f). Figure 2-5 shows that the thickness of this film is approximately 1 μm and that it is loosely attached to the substrate. The nature of the film on the worn surface at a sliding speed of 0.84m/s in water at 300℃ has been investigated in the TEM. The bright field image shown in fig.2-6(a) reveals that this film has the particulates ranging in size from 10 to 30nm. The diffraction pattern includes spotting rings as shown in fig.2-6(b). The spotty ring essentially indicates a crystalline material and the spot pattern of the crystallized phase was identified as γ-alumina. The worn surfaces of the disks have features similar to those of the plates. Wear debris was found for every sliding speed at 300℃. Figure 2-7 shows the XRD patterns of the wear debris produced at 300℃ and the surface of the plate before the test. The debris consists of α-alumina and boehmite, although the diffraction pattern of the plate before the test corresponds to only α-alumina phase. The proportion of boehmite in the wear debris at 0.11m/s is larger than that at 0.84m/s. Boehmite is thermodynamically more stable than α-alumina in water at 300℃ and 8.53MPa. Therefore, the compositions of the debris as a function of sliding speed at 300℃ shows that the hydration of α-alumina wear particles is influenced by the sliding speed, because the exposure time is longer at lower sliding speed in the case of constant sliding distance. The film on the worn surface at 0.84m/s in 300℃ water has γ-alumina particulate as shown in fig.2-6(b), but not observed in the wear debris dispersed into the eluent as shown in fig.2-7. Gates et al.[4] have reported that γ-alumina powder

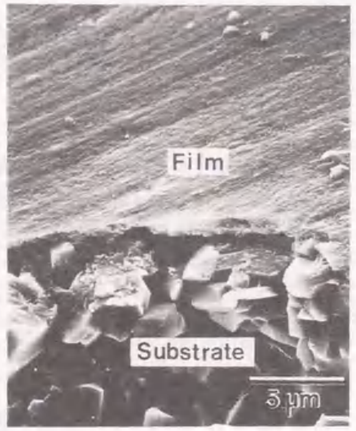

Fig.2-5 Scanning electron micrograph of the fracture surface of the plate of ALO-1 tested in water at 300℃ and sliding speed of 0.84m/s under a contact load of 19.6N.

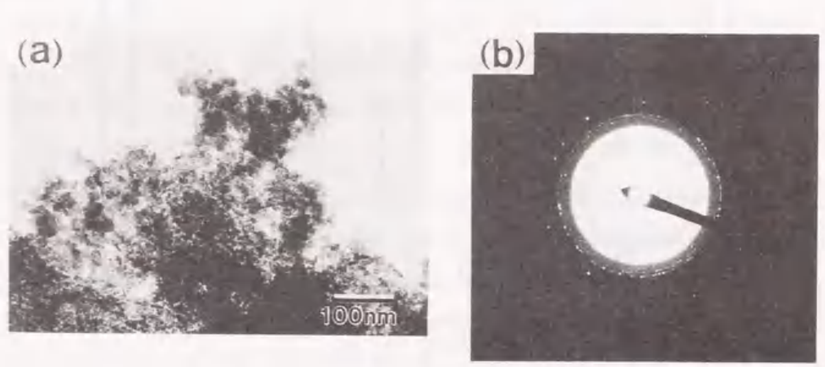

Fig.2-6 Transmission electron micrographs of the film on the worn surface of the plate of ALO-1 tested in 300℃ water at sliding speed of 0.84m/s under a contact load of 19.6N: (a) bright field image and (b) diffraction pattern.

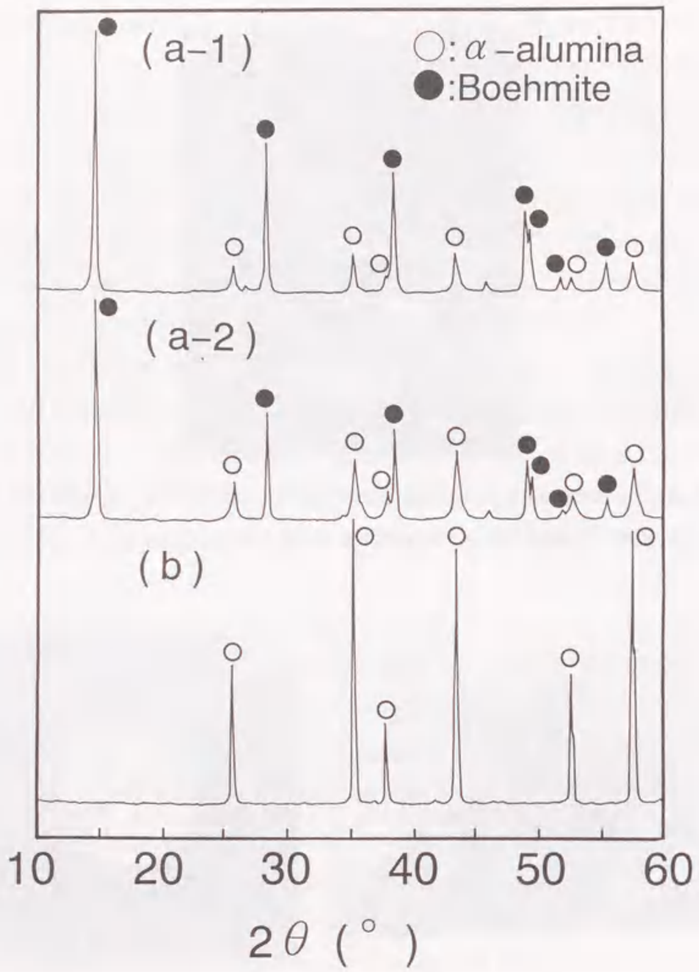

Fig.2-7 X-ray diffraction patterns of (a) wear debris produced from ALO-1 specimens in water at 300℃ under a contact load of 19.6N at sliding speed of (a-1) 0.11 and (a-2) 0.84m/s, and (b) the ground surface of the plate before the test.

easily reacts with water even at temperature of 200℃. Therefore, the γ -alumina debris which falls off from the film are considered to be also immediately hydrated and transformed to boehmite. In fig.2-6, the hydroxide is not found, but, boehmite probably presents in the film according to fig.2-7.

2.3.2 Contact load dependence of friction and wear for ALO-1 and ALO-2

Figure 2-8 shows the effect of contact load on the steady state friction coefficient of ALO-1 and ALO-2 in water at 300℃. The friction coefficient of ALO-1 is similar to that of ALO-2. The friction coefficient of both ALO-1 and ALO-2 gradually decreases with increasing contact load up to 40N and remains constant above 40N. Figure 2-9 shows the effect of contact load on the specific wear rate of the plate and disk in water at 300℃. The specific wear rates of both the plate and disk for ALO-1 are larger than those for ALO-2 at lower contact load of 9.8N, while the specific wear rates for ALO-1 are similar to those for ALO-2 at higher loads of 80N. The specific wear rate of the disk is slightly large compared to that of the plate for both ALO-1 and ALO-2.

For ALO-1 and ALO-2 specimens, the profiles of the worn surface with a contact load of 9.8N were similar to fig.2-4(e), which shows predominantly intergranular fracture. When the contact loads were increased, the substrate surfaces were covered with the film as shown in fig.2-4(f). The wear debris produced in water at 300℃ for both ALO-1 and ALO-2 were found to consist of α -alumina and boehmite by XRD. The proportion of boehmite in the debris produced at 19.6N and at the sliding distance of 4,500～5,000m, but was smaller than that at the different sliding distance of 3,8000m for ALO-1 as shown in fig.2-7. The hydration of α -alumina wear debris probably proceeds with increasing the duration of exposure in water at 300℃. So the proportion of boehmite might increase with increasing the sliding distance related to the exposure time.

2.3.3 Corrosion behavior of ALO-1 and ALO-2 in high temperature water

The weight loss of ALO-1 specimen soaked in water at 300℃ for 200h was 5.6×10^{-4}g/cm^2, while that of ALO-2 specimen was only about 10 percent of the weight loss of ALO-1. Figure 2-10 shows the SEM photomicrograph of the surface of the ALO-1 specimen after the hydrothermal treatment. The intergranular region of the material is attacked preferentially, and many α -alumina grains are removed from the surface. But the

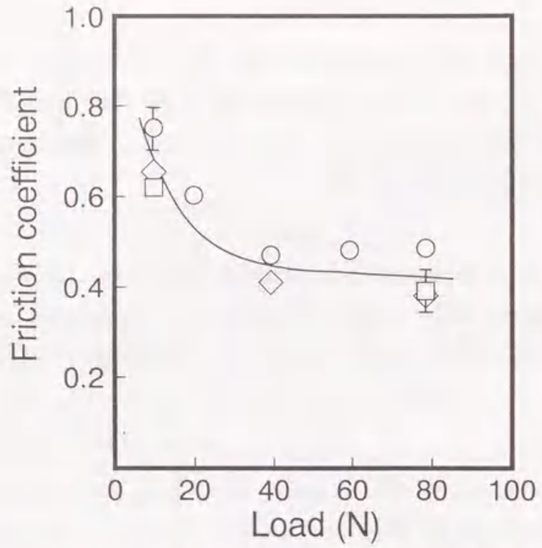

Fig.2-8 Effect of contact load on the steady state friction coefficients of ALO-1 (○) at the sliding speed of 0.21m/s and at the sliding distance of 4,500m, ALO-2 (□) at 0.42m/s and 5,000m, and ALO-2 (◇) at 0.84m/s and 5,000m in water at 300℃.

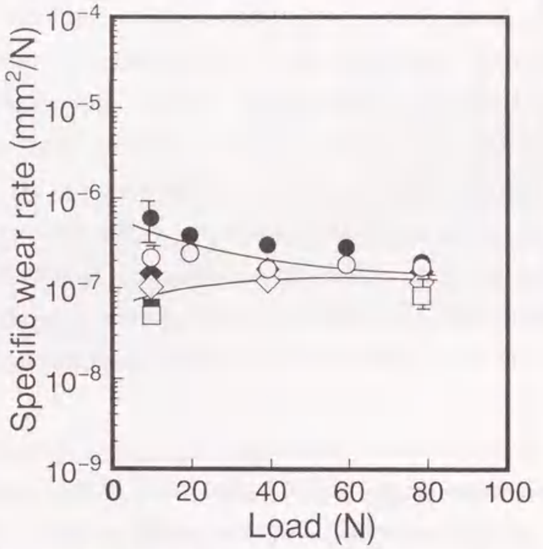

Fig.2-9 Effect of contact load on the specific wear rates of the plate and disk of ALO-1 (○, ●) at the sliding speed of 0.21m/s and at the sliding distance of 4,500m, ALO-2 (□,■) at 0.42m/s and 5,000m, and ALO-2 (◇,◆) at 0.84m/s and 5,000m in water at 300℃. (Open: plate, filled: disk)

morphology of the intergranular corrosion was hardly found on the surface of ALO-2 soaked. So the microstructure of the materials before the treatment was examined by TEM with energy dispersive spectroscopy (EDS). Figure 2-11 shows that a large amount of amorphous material segregates at triple points of the grain boundaries of ALO-1, where these amorphous deposit consists of an Si-Al-Ca-O system, compared to that of ALO-2.

Table 2-1 shows the solubility of each constituent element of ALO-1 in water at 300℃. $M(x)$ and $M(Al)$ are the amounts of the element x and aluminum in the eluent, respectively. They are subtracted blank values. $A(x)$ and $A(Al)$ are those in ALO-1 before the corrosion. If the ratio of $M(x)/M(Al)$ to $A(x)/A(Al)$ is larger than unity, the element x is more soluble than Al. Table.2-1 reveals that the solubility of Si, Ca and Na is extremely higher than that of Al. But the ratio of Mg is similar to that of Al. This suggests that Mg has little effect on the corrosion of ALO-1 ceramic. In spite of the intergranular corrosion and the large amount of Na in the eluent, Na was not detected at the grain boundaries of the material by the EDS analysis. Na probably segregates at the grain boundaries below the detection limit of EDS for sodium. Accordingly, the corrosion of ALO-1 ceramic is considered to have been caused by solution of the intergranular components such as Si, Ca, and Na.

2.4 Discussion

These studies have shown that the specific wear rate of ALO-1 significantly increases at elevated temperatures. This behavior could be explained as follows. The attacked layer, which is formed by the intergranular corrosion, is easily removed at the sliding interface, and then the worn surfaces become rough. The microfracture occurs with the increase in the local contact stress at these asperity surfaces. It is accelerated with progress of the corrosion at elevated temperatures. In addition, α -alumina ceramics have slow crack growth (*S.C.G.*) behavior due to stress corrosion cracking in the presence of water[7,8]. The subcritical crack propagation velocity is increased with increasing temperature.[9] Therefore, the stress corrosion reaction induced by the friction force, especially tension, is considered to be accelerated with increasing temperature and to contribute to the increase in the wear rate. The preferential dissolution of the grain boundary layer also proceeds in higher temperature water. Thus, the microfracture, which occurs with the stress corrosion cracking and the dissolution of the grain boundary layer, affects greatly the wear

Fig.2-10 Scanning electron micrographs of the surface of ALO-1 soaked in water at 300 ℃ for 200h.

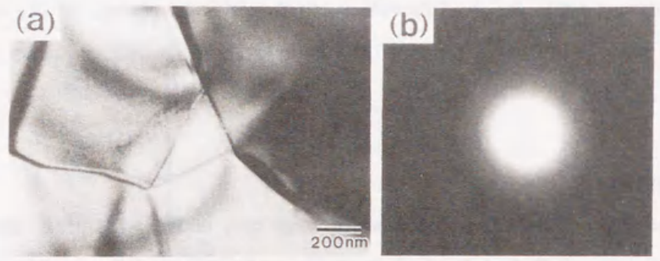

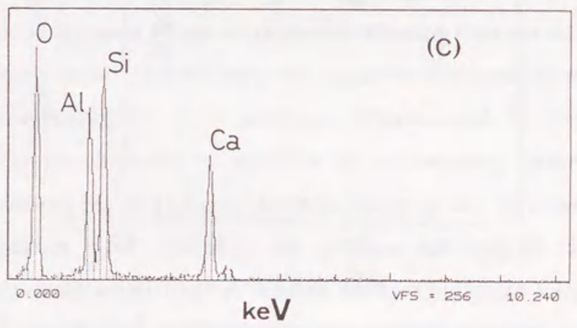

Fig.2-11 Transmission electron micrographs of the ALO-1 ceramic before the test: (a) bright field image, (b) electron diffraction pattern at the triple point of grain boundary, and (c) EDS spectrum at that.

Table 2-1 Solubility of constituent elements of ALO-1 in water at 300℃.

Element x	$[M(x)/M(Al)]/[A(x)/A(Al)]$*
Al	1
Si	720
Mg	1.7
Ca	637
Na	1662

* $M(x)$ and $M(Al)$ are the amounts of element x and aluminium in the eluent, respectively. $A(x)$ and $A(Al)$ are those in ALO-1 before the corrosion test.

characteristics in higher temperature water rather than lubricious effect due to the formation of the hydrated alumina layer. In water at 300℃, the specific wear rate of ALO-1 specimens is similar to that of ALO-2 specimens at 80N as seen in fig.2-9, although the corrosion resistance of ALO-1 was significantly inferior to that of ALO-2 in water at 300℃. This behavior can be explained as follows. The stress corrosion limit greatly depends on crack tip geometry[10,11]. For ALO-1, the crack tip blunting due to the corrosion may depress the stress corrosion cracking compared to ALO-2, but the wear of ALO-1 will be controlled by the removal of α -alumina grains caused by the dissolution of the grain boundary layer, which may strongly affect to the tribological behavior of ALO-1 with decreasing the contact load.

As the sliding speed increased in water at 120℃ and 300℃, the friction coefficient and the wear rate of ALO-1 decreased. The reduction of the wear rate can be associated with the decrease in the intergranular corrosion depth because of short testing duration resulting from the increase in sliding speed under constant sliding distance. In water at 120℃, the pits shown in fig.2-4(d) were thought to be produced by the removal of the α -alumina grains from the surface due to intergranular corrosion, according to the comparison of the surface damage depth during surface preparation and wear scar depth. The cracks shown in fig.2-4(c) seem to appear by the microfracture on the surface, because the local contact stress at the asperity surfaces increases with the progress of the grains pull-out compared to the higher sliding speed.

In water at 300℃, the streaked film with particulates appeared on the worn surface of ALO-1 and ALO-2 at increasing sliding speeds and contact loads. These particulates are much smaller than the gain size of the original material. This seems to be caused by the repeated crushing of the grains and other large fragments that were broken off the substrate at the sliding interface. The film is thought to be formed by the subsequent accumulation of the particulates on the substrate. This suggests that the crushing and accumulation preferentially occurred rather than grain pull-out from the substrate due to the intergranular corrosion. The worn surface roughness decreases from 0.5 to 0.1 Ra by the film formation. This film prevents the direct contact of the substrates and reduces the local stress with increasing the real contact area on the worn surface. However, it does not seem probably to act as lowering the wear because of loosely attached film on the substrate and easily pull-out.

Finally, the formation mechanisms of γ -alumina in the film are discussed. At the sliding interface, anisotropic shear forces are applied. If the real area of contact, A_r, is given by

$$A_r = \frac{F_n}{p} \qquad (2-3)$$

where p is the yield pressure of the materials (= H_v),[12] the shear stress of ALO-1 and ALO-2 specimens at the sliding interface in water at 300℃ was about 4～13GPa. Gates et al.[4] reported that shear stresses in the sliding interface, which is similar value to our experiments, could cause stress induced phase transformation from α - to γ -alumina, subsequently reacting with water to form hydroxides. Therefore, γ -alumina particulates in the film may be formed by pure transformation. Boehmite is stable in water at 300℃, however, γ -alumina particulates exist in the film, which suggests the occurrence of incomplete reaction between γ -alumina and water. In addition, it is well known that boehmite decomposes through the transition of γ -, δ -, and θ -alumina as at elevated temperatures, forming finally α -alumina.[4,13] Therefore, the γ -alumina in the film is considered to be produced by dehydration of boehmite formed on the worn surface because of elevated temperature due to friction heat at the sliding interfaces. The film may be formed by accumulation of the particulates produced during the repeated process of the hydration and dehydration. Torkar et al.[14] have found that γ -alumina was formed under unsaturated vapor pressure in the range from 400 to 500℃ and from 10 to 15MPa. At high sliding speed and high contact load in 300℃ water, the sliding interfaces seem to be locally in the environment mentioned above or over because of frictional heat and local stress. In water at 120℃, the film with γ -alumina particulates did not appear on the worn surface at any sliding speed. Then the stress induced phase transformation and/or decomposition of boehmite formed on the surface seem not to occur at the sliding interface.

2.5 Conclusions

(1) The friction coefficient of ALO-1 decreased with the increase in the sliding speed at each temperature. The friction coefficient of ALO-1 increased with increasing temperature at sliding speeds lower than 0.4m/s, but was weakly dependent on the temperature at 0.4m/s and over. The friction coefficient of ALO-1 in water at 300℃, which was similar to that of ALO-2, gradually decreased with increasing contact load up to 40N and remains constant above 40N.

(2) The specific wear rates of both the plate and disk for ALO-1 increased remarkably with increasing temperature. The specific wear rate of ALO-1 decreased with increasing sliding speed in water at 120 and 300℃. In water at 300℃, the specific wear rates of ALO-1 at lower contact load of 9.8N were larger than those of ALO-2, whereas those of both ALO-1 and ALO-2 were similar values at higher loads. This behavior of ALO-1 at 300℃ seems to be mainly caused by falling off the Al_2O_3 grains due to the vigorous dissolution of the impurities segregated at the intergranular layers rather than microfracture due to stress corrosion cracking, which may be influenced by the crack tip blunting due to the dissolution. On the other hand, the tribological behavior of ALO-2 at 300℃ may be related only to the stress corrosion cracking because of a small amount of the impurities.

(3) The streaked film containing γ-alumina particulates appeared on the worn surface at increasing sliding speeds and contact loads in water at 300℃. γ-alumina particulates may be formed by the stress induced phase transformation and/or decomposition of boehmite produced on the worn surface.

References

1 J.E.Hines, Jr.,R.C,Bradt and J.V.Biggers, *ASME Wear of Materials*, 462(1977).

2 J.E.Hines, Jr.,R.C,Bradt and J.V.Biggers, *ASME Wear of Materials*, 540(1979).

3 S.Sasaki, *J.Soc.Lubrication Eng.*, 33,No.8,620(1988) (in Japanese).

4 R.S.Gates, S.M.Hsu and E.E.Klaus, *Tribol.Trans.*, 32,No.3,357(1989).

5 T.Kawakubo, H.Hirayama, A.Goto and T.Kaneko, *J.Soc.Mater.Sci*., 38,No.426,300 (1989) (in Japanese).

6 S.Ono, K.Suzuki, M.Kumagai and K.Hoashi, *Zairyo-to-Kankyo*, 40,655(1991) (in Japanese).

7 A.G.Evans, *J.Mater.Sci.*, 7,1137(1972).

8 T.A.Michalske B.C.Bunker and S.W.Freiman, *J.Am.Ceram.Soc.*, 69,No.10,721(1986).

9 S.M.Wiederhorn and L.H.Bolz, *J.Am.Ceram.Soc.*, 53,No.10,543(1970).

10 K.Hirao and M.Tomozawa, *J.Am.Ceram.Soc.*, 70,No.6,377(1987).

11 T.A.Michalske, *Fracture Mechanics of Ceramics,Vol.5.*, Edited by R.C.Bradt, A.G. Evans, D.P.H.Hasselman, and F.F.Lange. Plenum,New York, (1983).

12 See for instance: H.Czichos,*Tribology*, Elsevier, Amsterdam, (1978); D.A.Rigney, Ed. *Fundamentals of Friction and Wear Materials*, American Society for Metals, Metals Park, OH(1981); F. P. Bowden and D. Tabor, *The Friction and Lubrication of Solid*, Clarendon Press, Oxford(1986).

13 T.Sato, *Thermochimica Acta*, 88,69(1985).

14 K.Torkar and H.Krischner, *Ber.Dtsch.Keram.Ges.*, 39,No.11.2,131(1962).

Chapter 3

Tribological Characteristics of Si_3N_4 Ceramics

3 Tribological Characteristics of Si_3N_4 Ceramics

3.1 Introduction

Silicon nitrid ceramicse (Si_3N_4) have been attracting great deal of attention for engineering applications because of their high fracture strength and excellent thermal shock resistance. They are also being investigated for applications as a mechanical seal in a coolant pump in Pressurized Water Reactor, which is used at a maximum temperature of 120℃ in water, and are required to have high wear and corrosion resistance. Evaluation of the tribological and corrosion behavior of the Si_3N_4 ceramics under this environment is crucial for its applicability as the sealing materials.

The effects of water on the friction and wear behavior of Si_3N_4 ceramics sliding on itself at room temperature have been studied by several investigators[1-4]. Fischer et al.[1,3] have reported that the specific wear rate in very humid environments and water is about 100 times lower than that in dry argon at sliding speed of 1×10^{-3}m/s. They have found that a tribochemical reaction between silicon nitride and water plays a role in the reduction of friction and wear. They have also reported that the wear occurs by dissolution of the material, since wear particles are not observed. Tomizawa et al.[2] have shown that the friction coefficient remarkably decreases with increasing sliding speed from 1×10^{-3} to 0.2m/s at a normal load of 5N in water and this behavior may be related to hydrodynamic forces in addition to the tribochemical reaction.

Some studies on corrosion behavior of Si_3N_4 ceramics have been conducted in high temperature water. Yoshio et al.[5,6] have reported that Si_3N_4 ceramics are significantly attacked at 300℃ and 8.6MPa, and the corrosion characteristics of Si_3N_4 ceramics may depend on the Si_3N_4 grain morphology and the dissolution behavior of components added as sintering aids. Sato et al.[7] have found that the corrosion behavior at temperatures of 200～300℃ and at saturated vapor pressures of water is dependent on the crystallinity of the grain boundary phase, which is produced by the reaction of sintering additives with SiO_2 formed on the surface of Si_3N_4 powder. Yoshimura et al.[8] have studied about the reaction between Si_3N_4 powder and H_2O at temperatures of 200～800℃ under 10 and 100MPa, and proposed the following reaction[8]:

$$Si_3N_4 + 6H_2O \rightarrow 3SiO_2 + 4NH_3 \ . \qquad (3\text{-}1)$$

The oxidation of Si_3N_4 powder by H_2O seems to be controlled by the H_2O diffusion in amorphous SiO_2 layer.[8] Ono et al.[9] reported the influence of dissolved oxygen on corrosion behavior of Si_3N_4 ceramics containing MgO from 120 to 275℃ in water. They found that dissolved oxygen does not promote the corrosion behavior at the temperatures of 120～275℃ and grain boundaries of the Si_3N_4 ceramics are preferentially dissolved, rather than oxidation of Si_3N_4 surface below 200℃. Because of these corrosion behavior, the influence of water on the tribological properties at 120℃ in water, where a sliding interface is probably at higher temperature and higher pressure, is considered to be different from that at room temperature in water. However, few reports have been published on the friction and wear behavior of Si_3N_4 ceramics in water over 100℃.

In this chapter as a part of investigations on tribology of advanced ceramics, the effects of temperature, sliding speed, contact load, hydrostatic pressure, dissolved oxygen and sintering aids on the tribological characteristics of Si_3N_4 ceramics by sliding on themselves are presented in water. The friction and wear characteristics of Si_3N_4 are also discussed.

3.2 Experimental procedure

Wear tests were carried out by sliding the circumferential surface of a rotating disk with plates in a high pressure vessel (inner volume 10.5 liters) as shown schematically in fig.2-1. The materials of disk and plate used for the wear test were three kinds of hot-pressed Si_3N_4 ceramics (SN-1, SN-2 and SN-3 samples). For SN-1 ceramic, MgO and Al_2O_3 were added as sintering aids. Both SN-2 and SN-3 ceramics contained Y_2O_3 and Al_2O_3. It has been found by TEM and XRD that the grain boundary phases of SN-1 and SN-2 were amorphous, while that of SN-3 consisted of a crystalline phase identified as $Y_{10}(SiO_4)_6N_2$ and an amorphous phase. The matrix phase of SN-1 was α - and β -Si_3N_4, but those of SN-2 and SN-3 were only β -Si_3N_4 as seen in table 1-3. The mechanical and thermal properties of the Si_3N_4 ceramics are listed in table 1-1 and 1-2, respectively. The chemical compositions of the materials are shown in table 1-3. The plate specimens were cut to a size of $15\times20\times4$mm and their contact surfaces were ground by an 800 grit diamond wheel to a roughness of about 0.05 μm R_a. The surface roughness of the disk specimen (40mm in diameter and 4mm in thickness) was about 0.3 μm R_a. Before the wear tests, the two plates and disk were ultrasonically cleaned in acetone for 10min, dried in an

oven at 120 ℃ for 2h, and then cooled in a desiccator to room temperature. After the two plates and disk were fitted to the apparatus shown in fig.2-1, the atmosphere in the vessel was replaced with the argon or mixed gases of argon and oxygen for the bubbling, and 7 liters of the testing solution were poured into the vessel. The testing solutions were distilled water, which was controlled to achieve a dissolved oxygen concentration of below 0.02 by bubbling with argon or that of 8.5mg/l by using the mixed gas of argon and oxygen.

The torque of the driving shaft during the test was monitored by a torque transducer. The friction coefficient was calculated from the difference of the torque between loaded and unloaded conditions. The wear volume of the specimens was obtained from dividing the weight loss of the specimens due to the wear by their density. The wear volume calculated from weight loss of the plates was in good agreement with that determined from the geometry of the wear scar at all sliding conditions. This means that weight change of the plate due to corrosion is negligible. The specific wear rate of plate was determined by using equation (2-2).

The worn surfaces of the specimens after the test were examined by SEM. The wear debris particles, which were dispersed into the solution, were collected by a centrifugal separator and observed by TEM with EDS and an X-ray photoelectron spectroscopy (XPS). The ammonia concentration in the solution after the wear test was determined by the indophenol blue spectrophotometric method which was described in JIS K0101[10]. The elements except NH_3 in the solution were analyzed by ICP. Gaseous species from the reactions were analyzed by gas chromatography.

The temperature and pressure at the sliding interface of the specimens are higher due to the flush temperatures. In order to determine the relationship between the tribological characteristics of the materials in water and the corrosion behavior at the sliding interface, the specimens were statically soaked in water at temperatures from 120 to 300℃ for 100h under the corresponding saturated vapor pressures. The dissolved oxygen in water for corrosion tests was controlled to the same concentration as that for the wear tests. After the experiment, the specimens were dried and the weight change was measured. The attacked surface of the sample, the testing solution and gaseous product after the static corrosion test were analyzed by the same methods as the wear tests.

The sliding conditions are listed in table 3-1. In mode Ⅰ, effects of sliding speed and

Table 3-1 Sliding conditions of the wear tests of Si_3N_4 ceramics.

Experimental mode	Materials	Temperature /Hydrostatic pressure	Dissolved oxygen concentration	Sliding speed	Contact load	Sliding distance
Ⅰ	SN-1	R.T./0.1MPa	<0.02mg/l	0.11～0.84m/s	19.6N	38,000m
		120℃/0.2MPa	8.5mg/l			
Ⅱ	SN-1	120℃/0.2MPa	<0.02mg/l	0.84m/s	9.8～78.4N	10,000m
		120℃/100MPa				
Ⅲ	SN-2	120℃/0.2MPa	<0.02mg/l	0.11～0.84m/s	19.6N	38,000m
	SN-3					

dissolved oxygen (D.O.) on the tribological characteristics of SN-1 sliding on itself in water at room temperature and 120℃ were investigated. In mode Ⅱ, dependence of hydrostatic pressure and contact load on the friction and wear behavior of SN-1 in water at 120℃ was evaluated. In mode Ⅲ, effect of sintering aids on the tribology of SN-1 and SN-2 in water at 120℃ was discussed with the results of SN-1 obtained in mode Ⅰ. In the following section, results and discussion in mode Ⅰ, Ⅱ and Ⅲ will be discussed in this order.

3.3 Results and discussion

3.3.1 Effects of temperature, sliding speed and dissolved oxygen concentration on tribological behavior of SN-1 (experimental mode Ⅰ)

(a) Friction coefficient and specific wear rate of SN-1

Figure 3-1 shows the effect of sliding speed on the friction coefficient of SN-1 in the steady state at the dissolved oxygen concentration less than 0.02mg/l at room temperature and 120℃. At room temperature, the friction coefficients are very low on the order of 0.01, and decrease slightly with increasing sliding speeds. The friction coefficients at 120 ℃ are much larger than those at room temperature and rapidly decrease with increasing sliding speed, passing through a minimum value of 0.3 at a sliding speed of 0.4m/s, and then abruptly increase. For all sliding speeds, the friction coefficients at a dissolved oxygen concentration of 8.5mg/l at room temperature and 120℃ exhibited the same values as those at dissolved oxygen concentration below 0.02mg/l shown in fig.3-1.

Figure 3-2 shows the specific wear rate of plate and disk of SN-1 at dissolved oxygen concentration below 0.02mg/l at room temperature and 120℃ as a function of sliding speed. The specific wear rates of both plate and disk at room temperature are small on the order of $10^{-10}mm^2/N$ and decrease with increasing sliding speed, similarly to the friction coefficient shown in fig.3-2. At 120℃, the specific wear rates are large, and the wear behavior of the plate on the sliding speeds is different from that of the disk. The specific wear rate of the plate shows a minimum value at the sliding speed of 0.4m/s, similarly to the friction behavior as seen in fig.3-1, but that of the disk increases with increasing sliding speed.

Figure 3-3 shows the effect of dissolved oxygen on the specific wear rate of SN-1 specimens at room temperature and 120℃. As seen in the fig.3-3, the specific wear rates

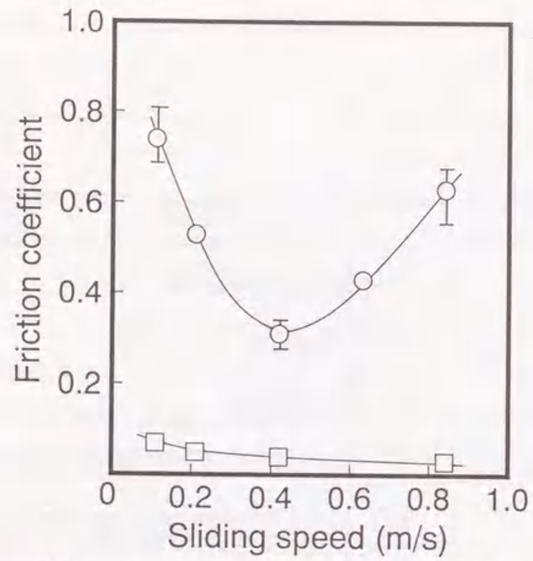

Fig.3-1 Effects of sliding speed on the friction coefficient of SN-1 specimens in water of dissolved oxygen concentration below 0.02mg/l at room temperature (□) and 120℃ (○).

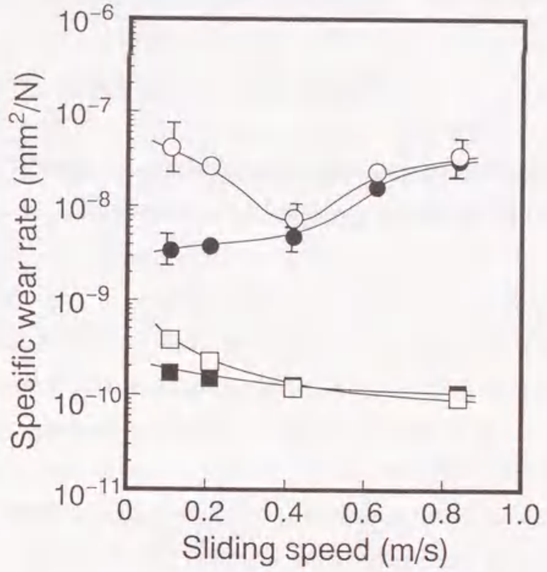

Fig.3-2 Effects of sliding speed on the specific wear rate of the disk and plate of SN-1 in water of dissolved oxygen concentration below 0.02mg/l at room temperature and 120℃ : disk (■) and plate (□) at room temperature, disk (●) and plate (○) at 120℃.

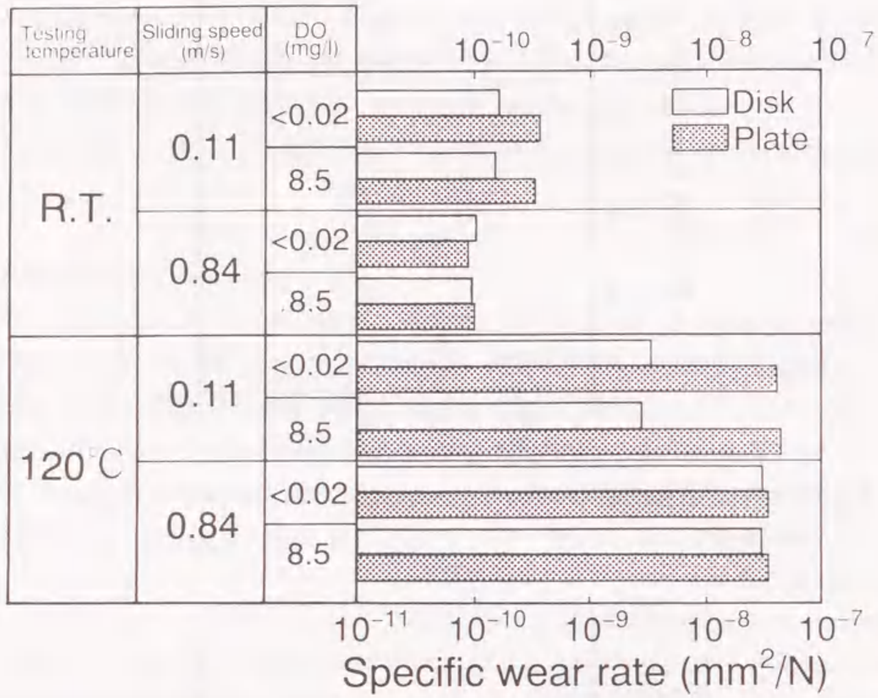

Fig.3-3 Effects of dissolved oxygen concentration on the the specific wear rate of the disk and plate of SN-1 at the sliding speed of 0.11 and 0.84m/s.

of both disk and plate are independent of dissolved oxygen concentrations at all testing conditions and the specific wear rates of the plate at lower sliding speeds in water at 120 ℃ are larger than those of disk.

(b) Analysis of the worn surfaces and wear debris of SN-1

Figure 3-4 shows the SEM micrographs of the worn surfaces of the SN-1 plates before and after the tests in water of dissolved oxygen concentration below 0.02mg/l at room temperature and 120℃. The micrographs of the worn surfaces were taken at the center of the wear scar corresponding to the maximum wear depth. The surface of the specimen before the test, which is shown in fig.3-4(a), shows evidence of plastic flow of the substrate caused by the surface grinding. As seen in fig.3-4(b), the worn surface of a specimen after the test at room temperature and sliding speed of 0.11m/s is very smooth. It is interesting to note that cylindrical debris, which is orientated vertically to the sliding direction, can be observed on the worn surface. This debris is similar shape to that formed by tribological reactions during sliding of Si_3N_4 ceramic in humid environments[1,3]. Fischer et al.[1] have reported from TEM and Secondary Ion Mass Spectroscopy (SIMS) that the cylindrical debris is an amorphous silicon oxide. We have not examined the wear debris here, but the wear debris in this experiment seems to be the same compound as that reported by Fischer et al.[1] and probably exists as silica which is rolled to a cylindrical form at the contact surface during the sliding action. At room temperature, the features of the worn surfaces were very smooth, independent of sliding speed. However, at 120℃ and sliding speed of 0.11m/s, many streaked scars on the worn surface are observed as shown in fig.3-4(c). These scars are caused by the direct contact between plate and disk surfaces, although wear debris is not found on the worn surface. The grain boundaries of the material are preferentially attacked as seen in fig.3-4(c). The morphology of the worn surfaces at sliding speed up to 0.4m/s was similar to that at 0.11m/s. At a higher sliding speed of 0.84m/s, two different micrographs of the worn surface show the different morphology; one worn surface becomes more rough and indicates a transgranular cracking as seen in fig.3-4(d), and in the another worn surface, the formation of a thin film is observed partly as seen in fig.3-4(e). It was found from the examinations of the cross section of this film by SEM and EDS that the film (1 μ m thickness) consisted of a flat silicon oxide layer which contained Al, Mg and N. This thin film may be formed by the

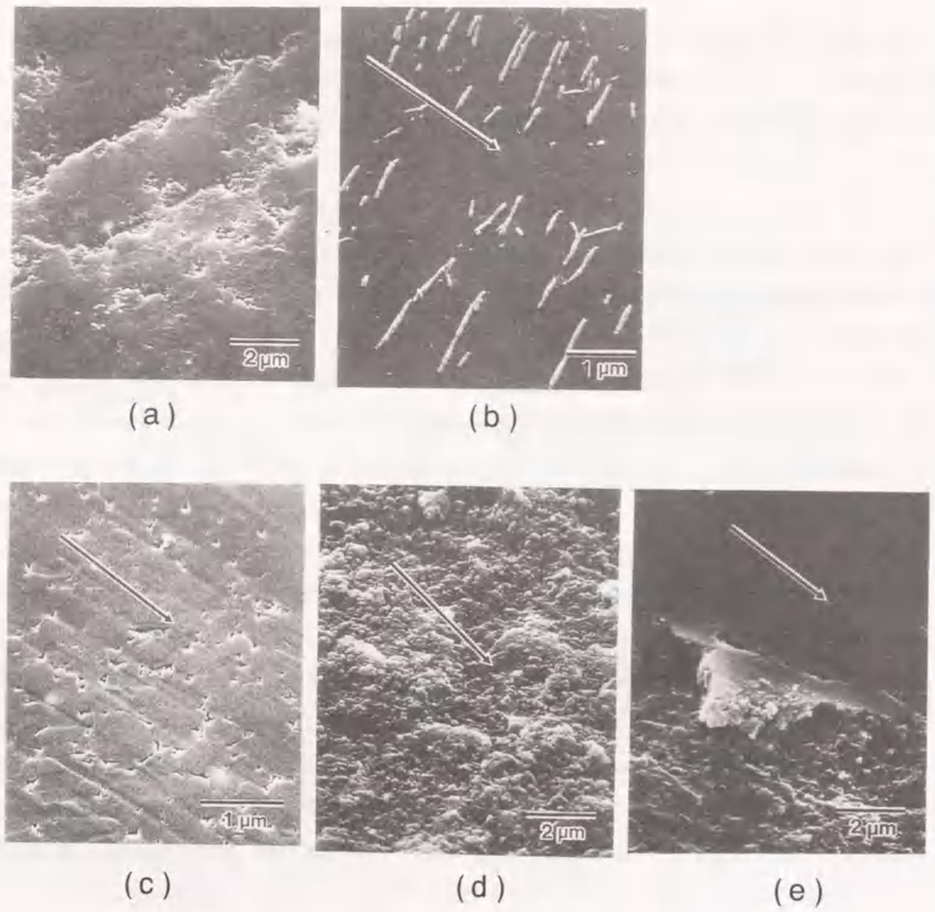

Fig.3-4 Scanning electron micrographs of the worn surfaces of the plate tested for SN-1 in water of dissolved oxygen concentration below 0.02mg/l under a contact load of 19.6N: (a) before and (b) after the test at sliding speed at room temperature of 0.11m/s, (c) the sliding speed of 0.11m/s, and (d) and (e) those of 0.84m/s after the test at 120℃. The arrows shown in the figure indicate sliding direction of the disk.

hydrothermal corrosion of SN-1 at the interface between the plate and disk.

The wear particles appear at sliding speeds above 0.6m/s in water at 120℃ and the amount of the debris tends to increase with increasing sliding speed as will be shown in fig.3-10. Figure 3-5 shows the results of TEM observations of the wear particles produced from the SN-1 specimens at the sliding speed of 0.84m/s in water of dissolved oxygen concentration below 0.02mg/l at 120℃. The bright field image shown in fig.3-5(a) reveals that the wear particles have a granular form ranging from 10 to 400nm in size, which is different from cylindrical form at room temperature. Figs. 3-5(b) and (c) show the electron diffraction patterns for the large particle A and the aggregated fine particle B in fig.3-5(a), respectively. The electron diffraction pattern for the large particle A reveals a crystalline material identified as β -Si_3N_4, whereas the diffraction pattern for the aggregated fine particles B indicates the presence of an amorphous material in addition to β -Si_3N_4 particles. The EDS spectrum for the fine particles (B) in fig.3-5(d) shows the existence of oxygen, which was scarcely detected for the large particle(A).

Figure 3-6 shows XPS spectrum of the Si 2p level for the fine wear particles produced from the SN-1 specimens. The spectrum is resolved into two peaks corresponding to the binding energies of 101.3 and 103.4eV, which can be assigned to Si_3N_4 and SiO_2 gel by literature data[11], respectively. Thus we conclude that the fine wear particles consist of β -Si_3N_4 and amorphous silicon dioxide. This means that mechanical wear such as microfracture occurs concurrently with the oxidation of Si_3N_4 grains at higher sliding speeds in water at 120℃.

(c) Analysis of the solution and gaseous products after the test for SN-1

The presence of NH_3 in the solution after all wear tests was confirmed by indophenol blue spectrophotometric method, indicating the tribochemical reaction of Si_3N_4 with H_2O which is given by eq.(3-1). Figure 3-7 shows the NH_3 concentration in the solution as a function of sliding speed for dissolved oxygen concentration below 0.02mg/l at room temperature and 120℃. This figure also involves the data measured after soaking the SN-1 specimens statically in the same deoxygenated solution at 120℃ for 100h corresponding to the wear test at 0.11m/s. As shown in fig.3-7, the NH_3 concentrations at room temperature are about 0.1mg/l and decrease slightly with increasing sliding speed, similarly to the behavior of the friction coefficient and specific wear rate as seen in figs.

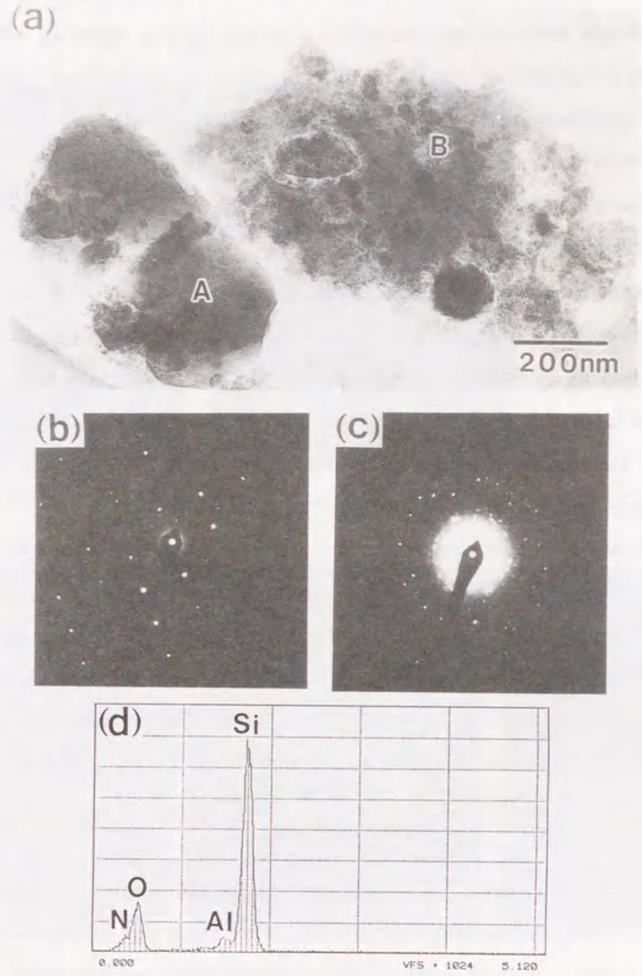

Fig.3-5 Transmission electron micrographs of the wear particles produced from SN-1 in water at 120℃ of dissolved oxygen concentration below 0.02mg/l at the sliding speed of 0.84m/s under a contact load of 19.6N: (a) bright field image, (b) diffraction patterns for the large particle A and (c) that for the aggregated fine particles B, and (d) EDS spectrum for the particles B.

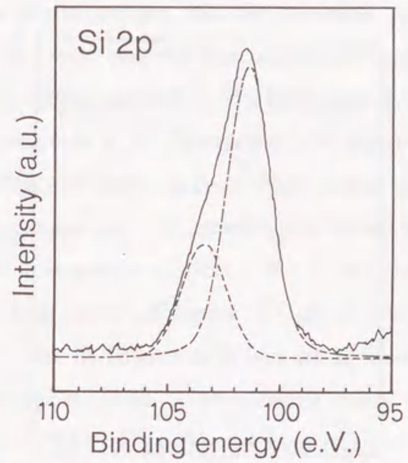

Fig.3-6 XPS spectrum of the Si 2p level for the fine wear particles produced form SN-1 in water at 120℃ of dissolved oxygen concentration below 0.02mg/l at the sliding speed of 0.84m/s under a contact load of 19.6N; ——— observed spectrum, ------- Si_3N_4 spectrum and ---------- SiO_2 gel spectrum.

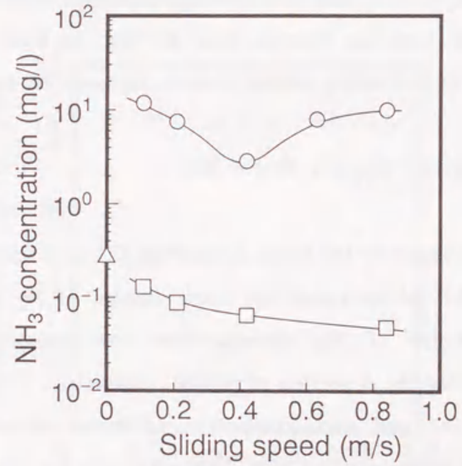

Fig.3-7 The NH_3 concentration after the test of SN-1 in water of dissolved oxygen concentration below 0.02mg/l as a function of sliding speed at room temperature (□) and 120℃ (○,△). Triangle's symbol is the data measured after soaking SN-1 specimens statically in the same deoxygenated solution at 120℃ for 100h.

3-1 and 3-2, respectively. However, the NH_3 concentrations at 120℃ are significantly larger than those at room temperature and decrease with increasing sliding speed up to about 0.4m/s, but then increase, similarly to friction coefficient and specific wear rate of plate as shown in figs.3-1 and 3-2, respectively. It is also seen from fig.3-7 that the NH_3 concentration for the wear test at 120℃ is larger than that at a static corrosion.

The amount of wear of the SN-1 specimens, W_c, corresponding to the NH_3 concentration is estimated from eq.(3-1). The W_c/W_w ratio is shown as a function of sliding speed at room temperature and 120℃ in fig.3-8, where W_w is the total amount of wear determined from the weight loss of both plates and disk before and after the test. As seen in fig.3-8, the ratio of W_c/W_w at room temperature is unity, independent of the sliding speeds, indicating that the wear proceeds only by eq.(3-1). At 120℃, the ratio of W_c/W_w is unity at the sliding speed up to about 0.2m/s, but decreases with increasing sliding speed. This suggests the participation of the microfracture due to the production of the wear debris containing the Si_3N_4 particles at higher sliding speeds shown in fig.3-5.

In the wear experiments for SN-1, H_2 gas was detected only at the sliding speeds above 0.4m/s in water at 120℃. Figure 3-9 shows the relationship between the sliding speed and the amount of H_2 existing in both gas- and liquid-phases, where the gases dissolved in water are calculated by applying Henry's law. As seen in fig.3-9, the amount of H_2 production increases with increasing sliding speeds. H_2 may be formed by the following reaction:

$$Si_3N_4 + 6H_2O \rightarrow 3SiO_2 + 2N_2 + 6H_2 \qquad (3\text{-}2)$$

Nitrogen gas was also detected in the range from about 0.1 to a few volume percent for all wear tests, but we could not determine the exact amount of N_2 gas produced by wear, because the reproducibility of N_2 concentration was poor, probably due to the contamination of air during the collection of gaseous products.

The total wear volume and each component of wear volume of SN-1 specimens contributing to the wear mechanisms at 120℃ are shown in fig.10 as a function of sliding speed. The total wear volume is determined from the total weight loss of both plates and disk, and each wear component is estimated from eqs.(3-1) and (3-2) to produce NH_3 and H_2, respectively. The remaining wear component appeared at sliding speeds above 0.6m/s is assumed to be due to microfracture, which abruptly increases with increasing sliding

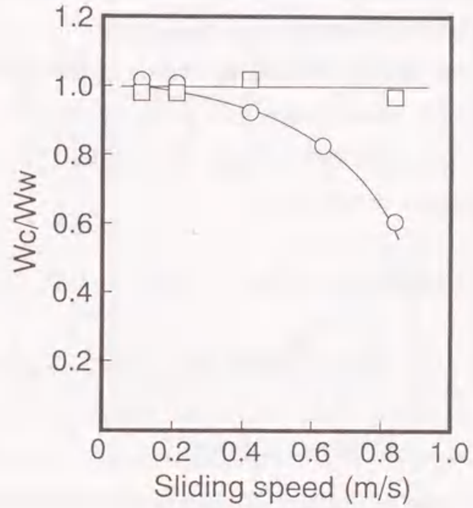

Fig.3-8 W_c/W_w ratio as a function of the sliding speed: W_c and W_w are the wear amounts estimated from the reaction to produce NH_3 and that determined from the weight loss of both plates and disk, respectively, at room temperature (□) and 120℃ (○) in water of dissolved oxygen concentration below 0.02mg/l.

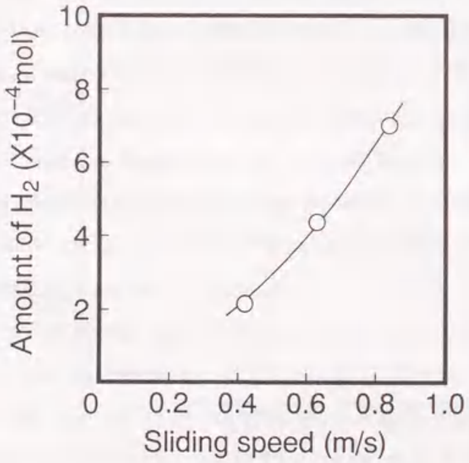

Fig.3-9 The amount of H_2 gases existed in the gas- and liquid-phases as a function of sliding speed in water at 120℃ (○). The gases dissolved in water are calculated by applying the Henry's law.

speed. It is seen from fig.10 that the corrosion reaction (3-1) due to the hydrothermal oxidation makes a major contribution to the wear mechanism.

If the ideal gaseous species of NH_3, N_2 and H_2 remain at the interface between Si_3N_4 and SiO_2 scale of the reaction product until their partial pressures become equal to the outside pressure (p_i MPa), the Gibbs free energies of reactions (3-1) and (3-2) under the pressure of p_i MPa are calculated as follows:

$$\Delta G_{(3\text{-}1)} = 3G^0_{SiO_2} + 4G^0_{NH_3} + 4RT\ln(p_i/0.1) - \left(G^0_{Si_3N_4} + 6G^0_{H_2O} + 6\int_{G^0}^{G} dG_{H_2O}\right) \qquad (3-3)$$

$$\Delta G_{(3\text{-}2)} = 3G^0_{SiO_2} + 2G^0_{N_2} + 6G^0_{H_2} + 8RT\ln(p_i/0.1) - \left(G^0_{Si_3N_4} + 6G^0_{H_2O} + 6\int_{G^0}^{G} dG_{H_2O}\right) \qquad (3-4)$$

where T is the temperature in K, R is the gas constant, G^0_i is the Gibbs free energy of formation for substance i under 0.1MPa at T. Recent thermodynamic data of β-Si_3N_4 suggested by Hendry[12] and JANAF data[13] of other substances are used for the calculation of the Gibbs free energies of the reactions. $\int_{G^0}^{G} dG_{H_2O}$ is the difference of the Gibbs free energy for H_2O between 0.1 and p_i MPa at temperature T (calculated from ref.14). Gibbs free energy changes for Si_3N_4 and SiO_2 due to pressure difference are negligibly small compared to those for gas species. Figure 3-11 shows the temperature dependence of ΔG for the reactions (3-1) and (3-2) at 0.2 and 10MPa. At 0.2MPa, the reaction (3-1) for the production of NH_3 is thermodynamically more stable than the reaction (3-2) for production of H_2 up to 200℃, but above this temperature the stabilities of these reactions reverse. At 10MPa, this change from the reaction (3-1) to (3-2) occurs at about 400℃. In the static corrosion, NH_3 was produced in water up to 300℃ saturated vapor pressure, but H_2 gas was not evolved as will be discussed later. This behavior agreed with the thermodynamic predictions. Although thermodynamics equilibriums are not established for wear tests, it is possible to imagine that the interfaces at higher sliding speeds, where H_2 gas is slightly produced, are locally at very high temperatures as suggested from the thermodynamic calculations. The other mechanism for the production of H_2 may be considered to be the decomposition of NH_3, which is produced with the further progress of the reaction (3-1), at the sliding interface.

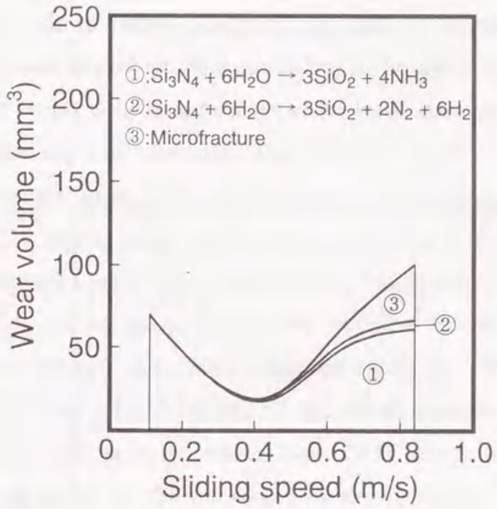

Fig.3-10 The total wear volume and wear component at 120℃ in water of dissolved oxygen concentration below 0.02mg/l as a function of sliding speeds, where the total wear volume is determined from the weight loss of both plates and disk and wear component are estimated from the reactions ① and ② to produce NH_3 and H_2, respectively. The remaining wear component ③ is due to the microfracture.

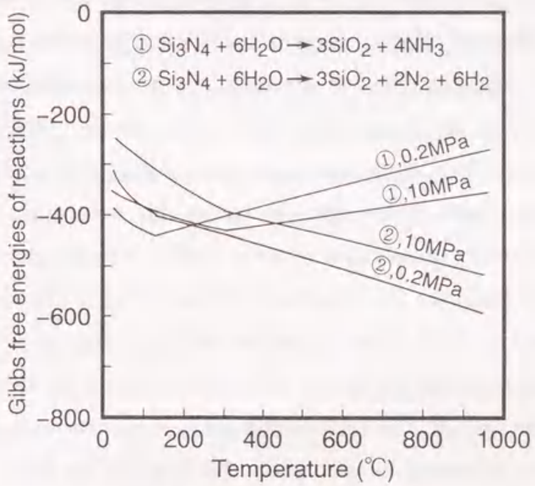

Fig.3-11 The temperature dependence of the Gibbs free energies for the reactions to produce NH_3 and H_2 in water under the pressure of 0.2 and 10MPa as a function of temperature.

(d) Corrosion behavior in high temperature water of the Si_3N_4 ceramics

Figure 3-12 shows the effect of the temperature on the weight loss of the SN-1, SN-2 and SN-3 specimens in water with dissolved oxygen concentration below 0.02mg/l. As seen in fig.3-12, the weight loss is observed for all specimens and significantly increases with increasing temperature, especially above 170℃. The corrosion resistance of SN-2 is inferior to that of SN-3 in water at temperatures up to about 200℃, but above this temperature SN-3 is attacked slightly greater than SN-2. This behavior probably relates to the preferential hydrothermal oxidation of $Y_{10}(SiO_4)_6N_2$ existing as the secondary phase in SN-3, since $Y_{10}(SiO_4)_6N_2$ of the secondary phase was found to be readily oxidized at about 800℃ in air compared to Si_3N_4 of matrix[15]. The surface of all samples after corrosion tests up to about 150℃ was found to have an intergranular corrosion morphology in similar to that shown in Fig.3-4(c). On the other hand, for the corrosion tests above about 170℃ the surfaces of the samples were confirmed to be coated with porous silicon oxide layer containing Al and Mg for SN-1 (or Y for other materials) by SEM and EDS. The concentrations of Al, Mg and Si in the solution after the corrosion test for SN-1 in water at 120℃ for 100h were measured by ICP. The molar ratios of Al (0.25) and Mg (0.11) to Si in the solution were similar to those of Al (0.23) and Mg (0.14) to Si at the triple point of the grain boundary of SN-1 ceramic before the corrosion test. Further, the concentration of NH_3 was slightly detected in the solution below 120℃ for SN-1, but not detected for other materials. For all ceramics, the concentration of NH_3 remarkably increased with increasing the temperature in similar to the dependence of soaking temperature on the weight loss of the specimens seen in Fig.3-12, while H_2 gas was not detected at all corrosion tests. These behavior means that only grain boundaries of the Si_3N_4 ceramics preferentially dissolve below about 150℃, whereas above about 170℃ all surfaces of the Si_3N_4 ceramics are remarkably dissolved after the oxidation of Si_3N_4 following to the reaction (3-1). These corrosion behavior did not also depend on the dissolved oxygen concentrations of below 0.02 and 8.5mg/l in similar to the wear experiments as seen in fig.3-3. The relationship between the corrosion and tribology of SN-1 in water will be discussed in the section 3.3.1(e), but for other materials in the section 3.3.3.

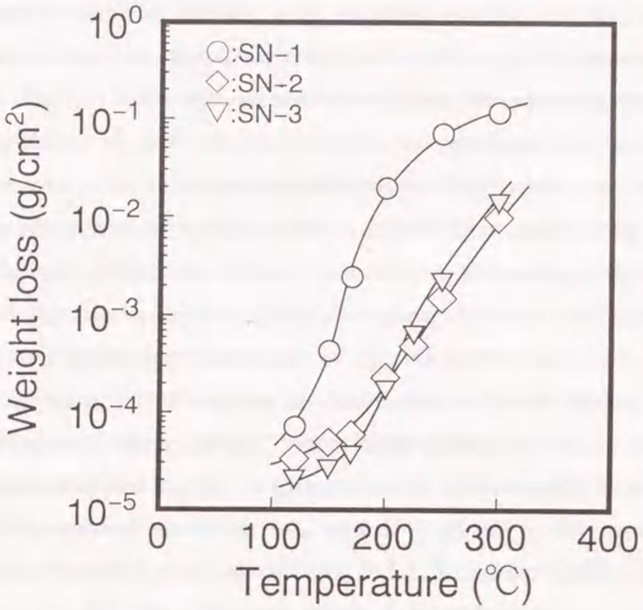

Fig.3-12 Weight loss of the specimens soaked in water at various temperature for 100h: SN-1 (○), SN-2 (◇) and SN-3 (▽). *V/A* was 2.6m, where *V* (m^3) was the amount of water and *A* (m^2) was the sum of the initial surface areas of the specimens.

(e) Friction and wear mechanisms of SN-1 in water

The tribological behavior of SN-1 in water depends on the temperatures and sliding speeds, but does not on dissolved oxygen concentrations. The experimental results presented here provide clear evidence of tribochemical reactions between Si_3N_4 and H_2O. Although the tribochemical reaction at room temperature as well as at the lower sliding speeds in water at 120℃ consists of only eq.(3-1), the friction coefficients and specific wear rates in water at room temperature are sufficiently lower than those at 120℃.

At room temperature, cylindrical wear debris was found. This is considered to be the same amorphous silica produced by the tribochemical reaction at room temperature in wet argon by Fischer and Tomizawa[1]. There are two possible reaction mechanisms of the silica surface in the presence of water; one reaction mechanism may be partially hydroxylation of silica as a silanol group, which is capable of adsorbing more water by hydrogen bonding. The other mechanism may be slow dissolution of silica to form silicic acid $Si(OH)_4$[16]. The existence of the cylindrical debris suggests that the former dominantly occurs more than the latter in water at room temperature. Since this hydrated silica layer, which is softer than Si_3N_4, probably prevents the direct contact between plate and disk, it can reduce the magnitude of the local stresses due to contact between plate and disk, resulting in a low friction and wear rate[1,4]. Because the worn surfaces become flat after the sliding tests at room temperature, the hydrodynamic lubrication due to a wedge film of water may participate in the tribological behavior[3]. However, the thickness of the water film is about 10nm (calculated from ref.17), which is estimated from contact geometry of the specimens at the sliding speed of 0.11m/s and the viscosity of water at 20℃ (1×10^{-3}Pas). This value of thickness is considerably smaller than the diameter (approx. 100nm) of the cylindrical wear debris on the worn surface. Therefore, the wear particles should prevent the achievement of hydrodynamic lubrication. Since the hydrated silica layer with lubricating ability may not be sufficiently formed in the early stage of sliding, higher frictional heat is produced at the higher sliding speeds, and subsequently accelerates the reaction (3-1). However at higher sliding speeds, this layer which is able to protect the substrate, is formed in a shorter testing duration, resulting in the decrease of the specific wear rate with increasing sliding speed.

At 120℃, the friction coefficient and specific wear rate of SN-1 are significantly larger than those at room temperature as seen in figs.3-1 and 3-2, respectively. These behavior

can be explained as follows. The solubility of amorphous silica in water increases with increasing temperature, pH and pressure[16,18]. Since oxidation of Si_3N_4 in water is controlled by the diffusion of H_2O into an amorphous silica layer[5,8], the decrease of this layer due to dissolution would result in a rapid increase of the oxidation rate. Moreover, by the production of NH_3 with the progress of the reaction (3-1), the dissolution of the silica layer, which acts as a protective film on the substrate, is promoted. These behavior leads to the direct contact between plate and disk, and many streaked scars appear on the worn surface. The wear caused by the corrosion is considered to be rapidly accelerated by a rise of temperature on the worn surface due to the direct contact between plate and disk, since the Si_3N_4 ceramic is significantly corroded in water above about 170℃ as seen in fig.3-12. The worn surface becomes rough due to the more vigorous corrosion at higher sliding speed, and then the microfracture occurs with the increase of the local contact stress at these asperity surfaces, producing the wear debris with the amorphous silica particles. The layer containing this silica debris on the worn surface at 120℃ can not be expected to have the same lubricious as that produced at room temperature, because the temperature of sliding interface may be locally very high and the hydrogen-bonded water molecules on the hydrated silica surface come off at 150℃ in air[16].

After the wear test of SN-1 at the sliding speed of 0.11m/s at 120℃, the molar ratios of Al (0.052) and Mg (0.011) to Si in the solution were similar to those of Al (0.048) and Mg (0.015) to Si in the SN-1 specimen, but were lower than those in the grain boundary. The molar ratios in the solutions after the wear tests at 120℃ were independent on sliding speed. The worn surfaces at the sliding speeds below 0.42m/s showed the morphology of the grain boundary corrosion in similar to the attacked surfaces in the static corrosion tests below 150℃. These behavior seems to be explained by the fact that the amounts of intergranular attacked layer at lower sliding speeds are too small compared with the total amounts of the wear of SN-1 dissolved in the testing solution.

As shown in figs.3-1 and 3-10, the friction coefficient and the total wear volume caused by the reaction (3-1) have a minimum value at the sliding speed of about 0.4m/s in water at 120℃. This behavior can be explained as follows. When SN-1 is statically immersed in water, the intergranular phase is at first attacked at temperatures up to 150℃. For the wear tests the grain boundary corrosion at lower sliding speeds is supposed to affect to the tribological characteristics. Therefore, the higher friction coefficient and wear volume

observed at the lower sliding speeds may be caused by the increase of the contact stress on the asperities formed by the dissolution of the grain boundaries. This effect probably becomes stronger at the lower sliding speed, because the testing duration increases with decreasing sliding speed under the constant sliding distance.

On the other hand, the increasing sliding speed leads to the acceleration of the direct oxidation of SN-1 substrate due to the temperature rise on the worn surface. This corrosion also leads to the rougher surface and simultaneously increases the friction coefficient, resulting in the appearance of microfracture. Thus the tribological behavior of the material at 120℃ at lower sliding speed may be controlled by the dissolution of the grain boundaries, while that at higher sliding speed by the direct oxidation of SN-1 substrate. This suggests that at lower sliding speed the wear resistance of Si_3N_4 ceramics in water at 120℃ can be improved by controlling the characteristics of grain boundaries, but at the higher sliding speed the improvement will be difficult by using this method.

As shown in fig.3-2, the specific wear rate of the disk of SN-1 at the lower sliding speeds in water at 120℃ is significantly different from that of the plate. Since the disk contacts with the plates periodically, the corrosion wear of the disk is considered to be prevented by the surrounding cooling water compared to the plates, where the temperature on the worn surface could rise readily. At higher sliding speeds, the disk can not be cooled down by the surrounding cooling water, and the temperature on the worn surface of the disk becomes so high that the corrosion wear rate can increase with increasing sliding speeds. For the plates the microfracture involving the removal of the oxide scale in addition to the tribochemical reaction can occur because of a slight excess of water at the sliding interface.

3.3.2 Effects of hydrostatic pressure and contact load on tribological behavior of SN-1 (experimental mode Ⅱ)

Figure 3-13 shows the effect of load on the friction coefficient of SN-1 ceramic in the steady state at the sliding distance of 10,000m under the hydrostatic pressures of 0.2 and 10MPa. The friction coefficient increases with increasing the load and saturates at about 60N under both hydrostatic pressures of 0.2 and 10MPa. The friction coefficients at 0.2MPa are larger than those at 10MPa.

Figure 3-14 shows the effect of load on the specific wear rate for the plate and disk

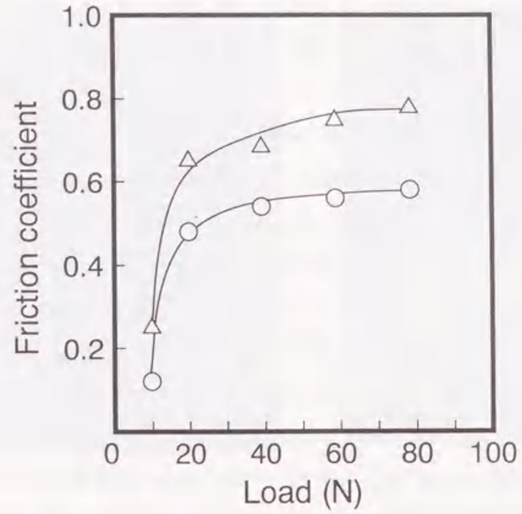

Fig.3-13 Effect of the load on the friction coefficient of SN-1 specimen under 0.2 (△) and 10MPa (○).

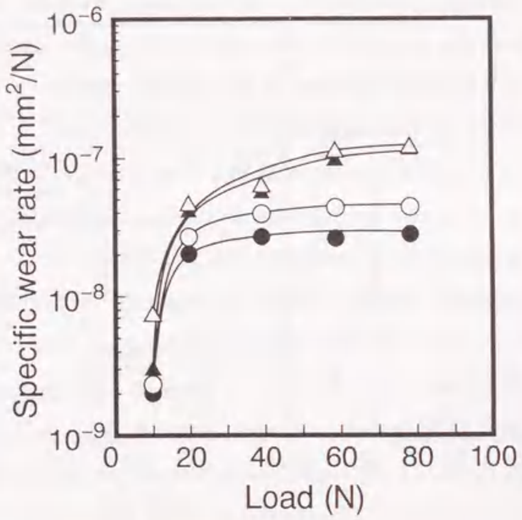

Fig.3-14 Effect of the load on the specific wear rate of the disk and plate of SN-1 in water at 120℃ under 0.2 and 10MPa: disk (▲) and plate (△) at 0.2MPa, disk (●) and plate (○) at 10MPa.

under the hydrostatic pressures of 0.2 and 10MPa. The dependence of load and hydrostatic pressure on the specific wear rate is similar to those of the friction coefficient. This behavior is considered to be caused by the hydrothermal oxidation and microfracture of Si_3N_4 as will be discussed later.

Figures 3-15(a) and (b) show the SEM micrographs of the worn surfaces of the plates after the tests in the water at 120℃ under the hydrostatic pressure of 10MPa. As seen in fig.3-15(a), many streaked scars are observed on the worn surface at load of 9.8N. This suggests the direct contact between disk and plates, although wear debris was not found on the worn surface. The grain boundaries of the material are preferentially attacked as seen in fig.3-15(a). The morphology of the worn surface at lower load under the hydrostatic pressure of 0.2MPa was similar to that under 10MPa. At higher load of 78.4N under 10MPa shown in fig.3-15(b), the worn surface becomes more rough and thin film, which was similar to that observed at the load of 19.6N under 0.2MPa as seen in fig.3-4(e), is observed partly on the worn surface, but the intergranular corrosion is absent. This flat film may contribute to depression of the friction and wear because of the decrease of the local stress at the interface. However, at the load of 78.4N under 0.2MPa, the film was not observed on the worn surface, and more wear particles were produced, compared with that at 10MPa. The wear particles were found to consist of Si_3N_4 and oxide products by XRD and EDS. This means that the microfracture of SN-1 occurs remarkably at higher load and at lower hydrostatic pressure. This microfracture probably relates to the absence of the film on the worn surface at 78.4N under 0.2MPa. The presence of NH_3 in the solution after all wear tests was confirmed by indophenol blue spectrophotometric method. H_2 gas was detected at the load above 19.6N under both 0.2 and 10MPa.

The total and each component of wear volume relating to the wear mechanisms under 0.2 and 10MPa are shown in fig. 3-16 as a function of the load. The total and each wear component were determined by using the same method as that mentioned in the section 3.3.1(e). As seen in figs.3-16(a) and (b), the wear at lower loads is mainly caused by the reaction (3-1), whereas the wear at higher loads occurs by the microfracture and the hydrothermal oxidation following the reactions (3-1) and (3-2). The microfracture remarkably increases with decreasing the hydrostatic pressure from 10 to 0.2MPa at higher load. It seems to be caused by the direct contact between disk and plates because vaporization of water with increasing frictional surface temperature occurs more easily at

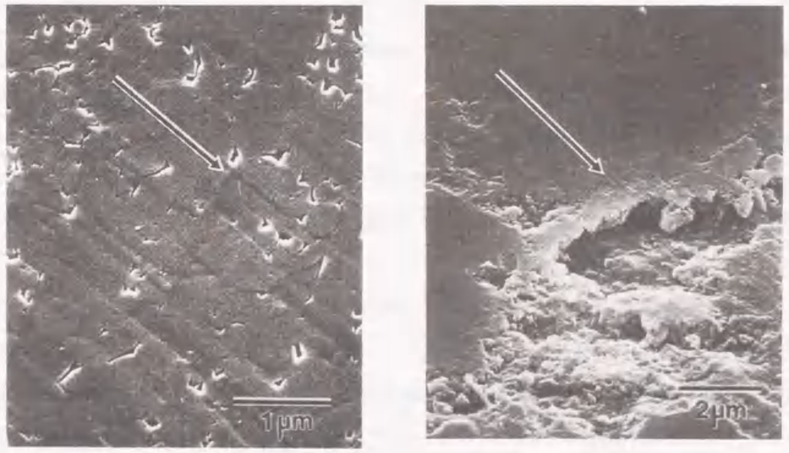

(a) (b)

Fig.3-15 Scanning electron micrographs of the worn surfaces of the plates after the tests in water at 120℃ under 10MPa (a) at 9.8 and (b) at 78.4N. Allows show sliding direction.

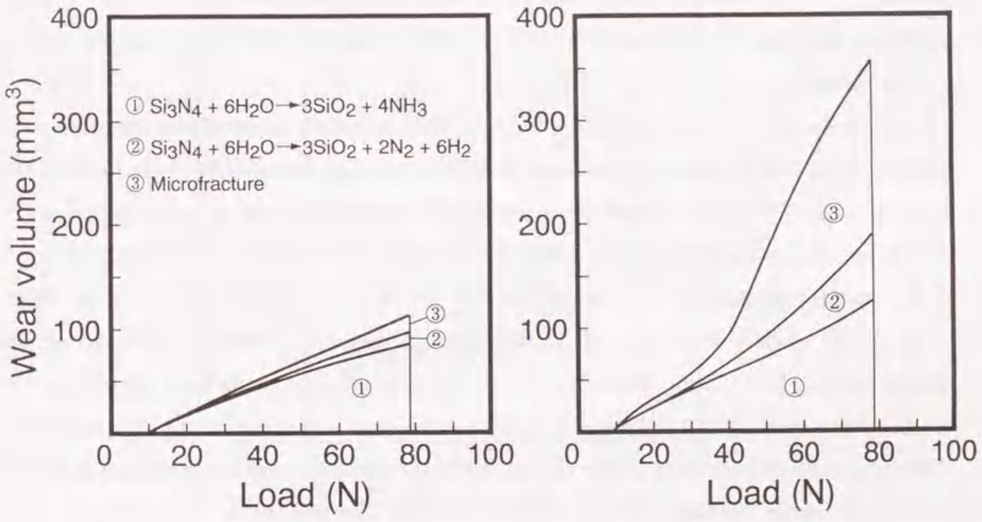

(a) (b)

Fig.3-16 The total wear volume and each wear component (a) at 0.2MPa and (b) at 10MPa as a function of the load.

0.2MPa than that at 10MPa. The microfracture probably leads to the absence of the thin film on the worn surface, resulting in the increases of the friction coefficient and specific wear rate. The microfracture may be also caused by cavitation erosion, which is induced by impact stress due to collapse of water vapor at the sliding interface. The tribological behavior of SN-1 would not be affected by "*cushion effect*", where cavities on the worn surface depress the direct contact of plate with disk, because the friction and specific wear rate at 0.2MPa are larger than those at 10MPa as seen in figs. 3-13 and 3-14.

3.3.3 Effect of sintering aids on tribological behavior (experimental mode Ⅲ)

Figure 3-17 shows the effect of sliding speed on the friction coefficient of the samples in the steady state sliding condition in water at 120℃. The friction coefficient of SN-1 at lower sliding speeds is significantly larger than those of SN-2 and SN-3. The friction coefficient of SN-1 rapidly decreases with increasing sliding speed, passing through a minimum value of 0.3 at a sliding speed of 0.4m/s, and then abruptly increases. The friction coefficient of SN-2 is constant at approximately 0.3, whereas that of SN-3 increases with increasing sliding speed. At sliding speeds above 0.4m/s, the friction coefficient decreases in order of SN-3, SN-1 and SN-2, and the value of SN-3 at the sliding speed of 0.84m/s is close to that of SN-1.

Figure 3-18 shows the specific wear rates of plate and disk of the Si_3N_4 ceramics as a function of sliding speed. The dependence of sliding speed on the specific wear rates of the plates is similar to that on the friction coefficients, suggesting that the wear of the plates mainly proceeds with development of the shear stress at the sliding interface. At lower sliding speed, the specific wear rate of the disk for SN-1 is similar to those of the other samples. The specific wear rates of the disks for all samples increase with increasing the sliding speed, and at sliding speeds above 0.4 m/s they are near to those of the plates. The specific wear rates of the disks are smaller than those of the plates at all sliding speeds. This is considered to be affected by the surroundings water in addition to the shear stress, because the worn surface of the disk periodically contacts with two plates in this experiment.

Figure 3-19 shows the SEM micrographs of the worn surfaces of the plates tested in water at the sliding speed of 0.84m/s for SN-2 and SN-3. As seen in fig.3-19(a), the worn

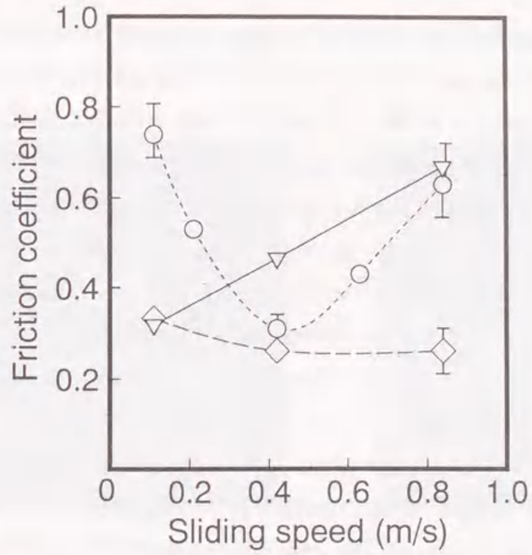

Fig.3-17 Effect of sliding speed on the friction coefficient of the specimens in water at 120℃: SN-1 (○), SN-2 (◇) and SN-3 (▽).

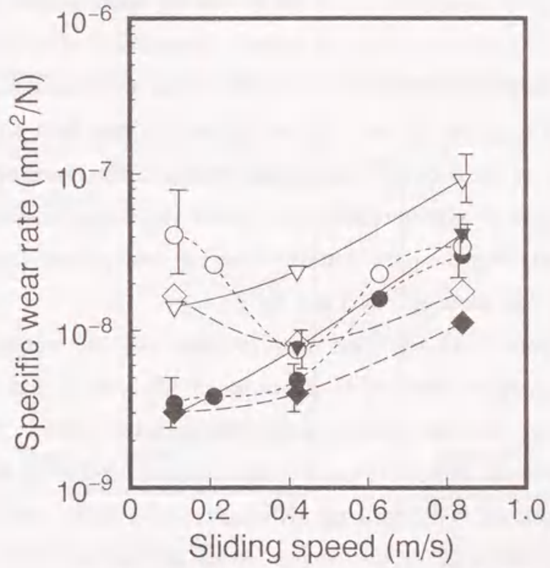

Fig.3-18 Effect of sliding speed on the specific wear rates of the disk and plate in water at 120℃: disk (●) and plate (○) of SN-1, disk (◆) and plate (◇) of SN-2 and disk (▼) and plate (▽) of SN-3.

surface of SN-2 is smoother than the other samples and many streaked scars are observed. Further, this material does not show any wear particles and film formation on the worn surface. The grain boundaries of SN-2 are preferentially attacked. In fig.3-19(b), the worn surface of SN-3 shows both the intergranular and transgranular cracking. A large amount of wear particles were produced, but no film was formed on the worn surface. At lower sliding speed of 0.11m/s, the morphology of the worn surfaces for all samples was similar to that for SN-2 at 0.84 m/s seen in fig.3-19(a). The worn surface of SN-1 mainly indicated a transgranular cracking and the thin film, which was produced by the hydrothermal oxidation of SN-1, was observed partly on the worn surface as seen in fig.3-4(c).

The total and each component of wear volume of SN-2 and SN-3 relating to the wear mechanisms are shown in fig.3-20 as a function of sliding speed. Those of SN-1 are shown in fig.3-10. At lower sliding speed, the wear due to reaction (3-1) is predominant for all samples, while at higher sliding speed, the wear behavior is governed by the progress of reaction (3-1) and the microfracture, especially for SN-1 and SN-3 as seen in figs.3-10 and 3-20. The amount of wear component ② at higher sliding speed is the largest for SN-1. Since the reaction (3-2) easily occurs at higher temperature thermodynamically, the temperature at the sliding interface for SN-1 may be higher than those for other samples. However, we can also image that the total amount of the frictional heat produced is largest for SN-3 from a result of the friction coefficient in fig.3-17. Therefore, the H_2 production for SN-1 probably occurs at higher temperature, where the transgranular fracture of the material proceeds locally, but the total contact region for SN-3, where the frictional work is done, may be larger than those for SN-1 and SN-2.

At lower sliding speed, both the total wear volume and the weight loss at lower temperature in the immersion tests are in the order of SN-1, SN-2 and SN-3 as seen in figs.3-10, 3-12 and 3-20, and the worn surfaces of all samples showed the morphology of the grain boundary corrosion similar to the attacked surfaces exposed in water up to about 150℃ in the corrosion tests. Therefore, the tribological behavior at lower sliding speeds may be caused by the increase of the contact stress on the asperities formed by the dissolution of the grain boundaries. This effect probably becomes stronger at lower sliding speed, because the testing duration increases with decreasing sliding speed at the constant sliding distance of 38km.

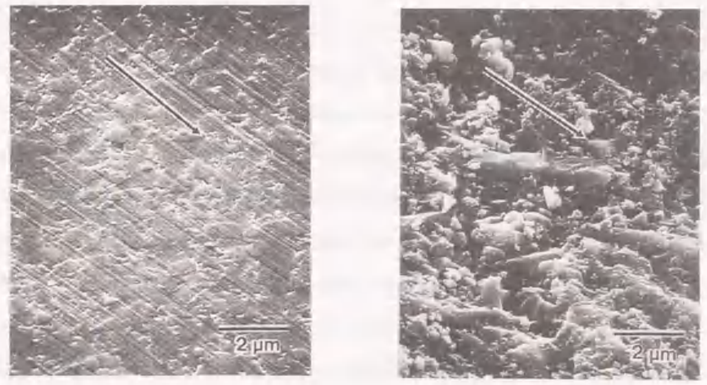

Fig.3-19 Scanning electron micrographs of the worn surfaces of the plates tested in water at sliding speed of 0.84m/s: (a) SN-2 and (b) SN-3. The arrows shown in the figure indicate sliding direction of the disk.

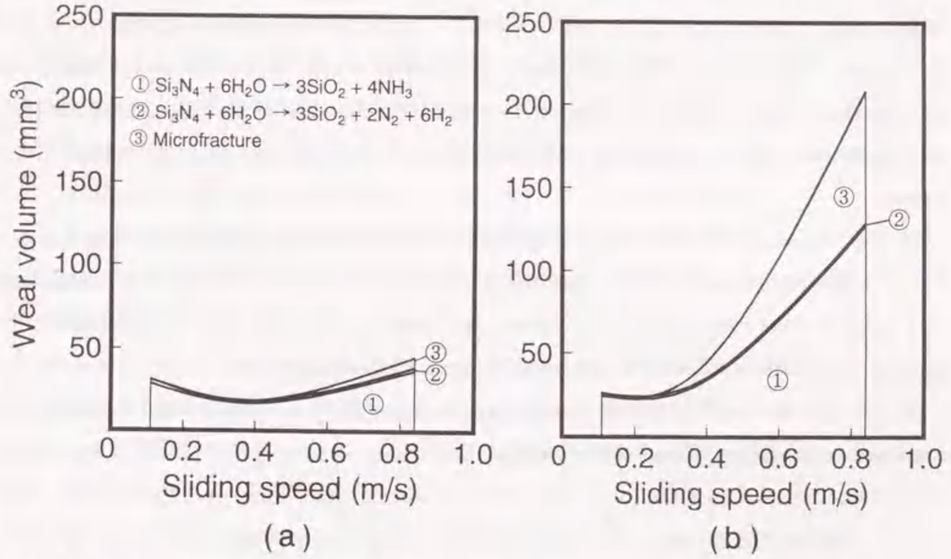

Fig.3-20 Total wear volume and each wear component as a function of the sliding speed: (a) SN-2 and (b) SN-3.

Increasing sliding speed leads to the acceleration of the direct oxidation of the Si_3N_4 substrate due to the temperature rise on the worn surface as seen in figs.3-10 and 3-20. This corrosion also leads to rougher surface and simultaneously increases the friction coefficient, resulting in the appearance of the microfracture. At higher sliding speeds, the total wear volume of the sample is the largest for SN-3, although SN-1 was significantly attacked in water at the temperatures up to 300℃ compared to other samples at all immersion tests as seen in fig.3-12. The thin film formed on the worn surface of SN-1 may contribute to depression of the friction and wear because of the decrease of the local stress at the interface. A large total wear volume of SN-3 may be caused by the inferior oxidation resistance of the crystalline secondary phase and the stress induced by the volume change accompanying this oxidation, leading to the intergranular cracking on the worn surface and the increase of reaction (3-1) due to the temperature rise. The low friction and wear of SN-2 may be correlated to the excellent corrosion resistance of the amorphous grain boundary phase in high temperature water.

3.6 Conclusions

(1) The friction coefficients and specific wear rates of disk and plates of SN-1 at room temperature were on the order of 0.01 and $10^{-10}mm^2/N$, respectively, and decreased with increasing sliding speed. The hydrated silica layer, which possessed some lubrication ability, is probably formed in a shorter testing duration at higher sliding speeds, resulting in a slight decrease of the friction coefficient and specific wear rate with increasing sliding speed.

(2) The friction coefficients and specific wear rates of disk and plates of SN-1 in water at 120℃ were significantly larger than those at room temperature. The friction coefficients and specific wear rates of plates showed a minimum value at about 0.4m/s, whereas the specific wear rate of the disk increased with increasing sliding speed.

(3) The friction coefficient and specific wear rate of SN-1 increased with increasing the load and saturated at about 60N under 0.2 and 10MPa in water at 120℃. The friction coefficient and specific wear rate at 0.2MPa were larger than those at 10MPa. This seems to be caused by the direct contact between disk and plates and cavitation erosion due to vaporization of water with increasing the asperity temperatures, resulting in the absence of the oxide layer on the worn surface.

(4) The friction coefficients and the specific wear rates of disk and plates of SN-1 were independent of dissolved oxygen concentrations for all sliding conditions in water at room temperature and 120℃.

(5) In water at 120℃, the friction coefficients and specific wear rates of plate for SN-1 were larger than those of SN-2 and SN-3 at lower sliding speeds, but decreased in order of SN-3, SN-1 and SN-2 at higher sliding speeds above 0.4m/s.

(6) The wear of the materials at lower sliding speeds and lower loads in water at 120℃ was caused mainly by the hydrothermal oxidation of Si_3N_4 to produce NH_3. This phenomenon seems to be responsible for the contact stress on the unevenness formed by the dissolution of the grain boundaries, and the subsequent dissolution of the silica layer of the reaction product. On the other hand, the wear at higher sliding speeds and higher loads occurred by the microfracture and the hydrothermal oxidation to produce H_2 in addition to NH_3. Especially, the tribological behavior of SN-1 at higher sliding speeds may be affected by the film formed on the worn surface, and that of SN-3 by the preferential oxidation of $Y_{10}(SiO_4)_6N_2$.

References

1 T.E.Fischer and H.Tomizawa, *Wear*, 105,29(1985).

2 H.Tomizawa and T.E.Fischer, *ASLE Trans.*, 30,No.1,]41(1987).

3 S.Jahanmir and T.E.Fischer, *Tribol.Trans.*, 31,No.1,32(1988).

4 S.Sasaki, *J.Soc.Lubrication Eng*, 33,No.8,620(1988) (in Japanese).

5 T.Yoshio, K.Oda, and K.Oda, *Yogyo Kyokai-Shi*, 95,No.4,435(1987).

6 T.Yoshio and K.Oda, *Yogyo Kyokai-Shi*, 95,No.7,730(1987).

7 T.Sato, T.Murakami, T.Endo, M.Shimada, K.Komeya, T.Kameda and M.Komatsu, *J.Mater.Sci.*, 26,1749(1991).

8 M.Yoshimura, J.Kase and S. Somiya, *Yogyo Kyokai-Shi*, 94,No.1,129(1986).

9 S.Ono, M.Kumagai and K.Hoashi, *Zairyo-to-Kankyo*, 40,315(1991).

10 *Testing methods for industrial water, JIS K 0101*, Japanese Standards Association, 139(1991).

11 M.Peuckert and P.Greil, *J.Mater.Sci.*, 22,3717(1987).

12 A.Hendry, *Proceedings of the 11th RISO International Symposium on Metallurgy and Materials Science*, 27(1990).

13 JANAF Thermochemical Tables Third Edition, *J.Phys.Chem.Ref. Data*, Vol.14, Suppl.1,1985.

14 U.Grigull, J.Straub and P.Schiebener, *Steam Tables in SI-Units: Wasserdampftafeln,* Springer-Verlag, Berlin(1984).

15 J.B.Veyret and M.Billy, *EURO-CERAMICS, Vol.3, Engineering Ceramics*, Edited by G.de With, R.A.Terpstra and R.Metselaar, Elsevior Applied Science, Maastricht, The Netherlands, 512(1989).

16 R.K.Iler, *The Chemistry of Silica*, John Wiley and Sons, New York(1979).

17 A.Cameron, *Basic Lubrication Theory*, Ellis Horwood Ltd. and John Wiley and Sons, 48(1976).

18 S.H.Chan, *Geothermics*,18,No.1/2,49(1989).

Chapter 4

Tribological Characteristics of α -SiC Ceramic

4 Tribological Characteristics of α-SiC Ceramic

4.1 Introduction

Advanced ceramics have been attracting great attention for engineering applications in nuclear power plants under conditions of high temperature and high pressure water. Particularly, SiC ceramics are expected to be one of the candidates for tribological materials because of their excellent corrosion resistance under the hydrothermal conditions[1,2]. However, so far studies were mainly focused on static oxidation behavior in high temperature water, where the oxidation reaction of SiC with H_2O shows a parabolic rate law[1,3] and is proposed to be as follows[2,3]

$$SiC + 2H_2O \rightarrow SiO_2 + CH_4 . \qquad (4\text{-}1)$$

Several reports have suggested that the tribological characteristics of SiC in water at room temperature are greatly influenced by specific chemical reaction with water at the sliding interface, namely tribochemical reaction[4,6]. However, experimental evidence to support the reaction process and/or thermodynamic approaches has not been reported in detail. Moreover, the friction and wear properties of SiC ceramics in water at temperature above 100℃, which seem to be accompanied by the hydrothermal oxidation reaction (4-1), have not been studied yet.

In this chapter, as a series of investigations on tribology of advanced ceramics[7,8], effects of temperature and sliding speed on the tribological characteristics of SiC ceramic by sliding on the same material in water at room temperature, 120℃ and 300℃, are reported and the friction and wear mechanisms of SiC ceramics are discussed.

4.2 Experimental procedure

Wear tests were carried out by sliding the circumferential surface of a rotating disk on two plates as shown in fig.2-1. The materials of disk and plate used in this experiment were of a commercial sintered α-SiC ceramic containing 0.1wt%B and 1.0wt%C (free-carbon) as seen in table 1-3, and the basic mechanical and thermal properties are listed in tables 1-1 and 1-2, respectively. The plate specimens were cut to a size of $10 \times 20 \times 4$mm and their contact surfaces were ground by an 800 grit diamond wheel to a roughness of 50nm Ra. The roughness of the sliding surface of disk specimen of 40mm diameter and

4mm thickness was about 360nm Ra. Before the wear tests, the specimens of two plates and a disk were ultrasonically cleaned in acetone for 10min, dried in an oven at 120 ℃ for 2h, and then cooled in a desiccator to room temperature. After the two plates and the disk were fitted to the apparatus, the atmosphere in the vessel was replaced with argon (≥99.9999% purity), and 3.65 liters of distilled water which was controlled to have the dissolved oxygen concentration below 0.02mg/l by bubbling with argon were poured into the vessel. Experiments were conducted at room temperature under the atmospheric pressure(0.1MPa) and at 120 and 300℃ under the corresponding saturated vapor pressures of 0.2 and 8.53MPa, respectively. Wear tests were carried out in the sliding speed range from 0.11 to 0.84m/s at the constant contact load of 19.6N and up to the sliding distance of 38,000m. The torque of the driving shaft during the test was monitored by a torque transducer. The friction coefficient was calculated from the difference of the torque between loaded and unloaded conditions. The wear volume of the specimens was obtained from dividing the weight loss of the specimens due to the wear by their density. The wear volume calculated from weight loss of the plates was in good agreement with that determined from the geometry of the wear scar at all sliding conditions. This means that any weight change of the plate from causes other than the wear is negligible. The specific wear rate was determined by using equation (2-2).

The worn surfaces of the plate specimens after the test were examined by SEM. The depth profiling of the worn surfaces for XPS analysis was carried out by ion-sputter etching, which was performed with an applied beam voltage of 4kV at a beam current density of $1mA/cm^2$ using argon gas. Gaseous species of reaction products, which were collected by replacing the gas-phase in the vessel by distilled water, were analyzed by gas chromatography. The amount of Si in the solution after the wear tests was determined by ICP.

4.3 Results and discussion

4.3.1 Temperature and sliding speed dependence of friction and wear

Figure 4-1 shows the effects of temperature and sliding speed on the friction coefficient of the SiC ceramics in the steady state where the friction coefficient was constant at the sliding distance above about 5,000m. The friction coefficients are very low, of the order of 0.01 at room temperature, but increase with increasing temperature. At higher

temperatures, the friction coefficients remarkably decrease with increasing sliding speeds.

Figure 2 shows the effect of the sliding speed on the specific wear rate for the plate and disk of SiC in water at room temperature, 120 and 300℃. The specific wear rate of SiC at room temperature is extremely small, of the order of 10^{-11} mm^2/N, and little dependent of the sliding speed. This value is of the same order as that for ALO-1 specimens in fig.2-3, but is smaller than that for SN-1 specimens in fig.3-2. The specific wear rate of SiC increases by several orders of magnitude at elevated temperatures as seen in fig.4-2. The SiC ceramic had a greater wear resistance than α-Al_2O_3 and Si_3N_4 in water at 120 and 300℃ as seen in figs 2-3, 3-2 and 4-2. As seen in fig.4-2, at 120℃ and 300℃, the specific wear rate of SiC decreases with increasing sliding speed, and this behavior is similar to that of the friction coefficient. The friction coefficient and specific wear rate in high temperature water are thought to depend on tribochemical reactions and hydrodynamic lubrication as will be discussed later. The worn surface of the disk is considered to be readily affected by the surroundings water compared with that of plate because a given place on the disk contacts with the plate only periodically. However the specific wear rate of the disk shows the same behavior as that of the plate. This suggests that the wear of the plate and disk mainly proceeds with development of the shear stress at the sliding interface.

4.3.2 Analysis of the worn surfaces

Fine mirror-like worn surfaces of the two plates and the disk were observed at all sliding conditions and their roughness was less than 5nm Ra. Figure 4-3 shows a typical micrograph of the plate tested at a sliding speed of 0.11m/s in water at 300℃. As seen in fig.4-3, the worn surface is very smooth. The pits shown in the micrograph seem to be pores formed during the sintering process of the material, because the surface of the plate polished with 3 μm-diamond paste before the wear test had similar shape and distribution of pits to those on the worn surface. No wear debris was observed by SEM on the worn surfaces at all sliding conditions.

Figure 4-4 shows depth profiles of silicon, carbon and oxygen measured by XPS on the worn surface at a sliding speed of 0.11m/s in water at 300℃. In the first 10 min of sputtering, the content of silicon increases rapidly, but that of carbon decreases. Thereafter the contents of both silicon and carbon gradually increase with increasing the sputtering

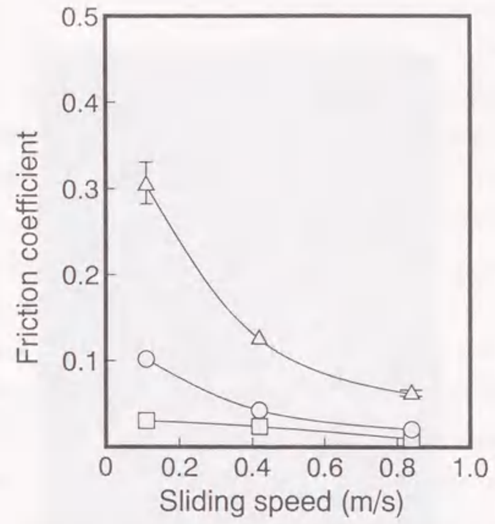

Fig.4-1 Effect of sliding speed on the friction coefficient of SiC specimens in water at room temperature (□), 120℃ (○) and 300℃ (△).

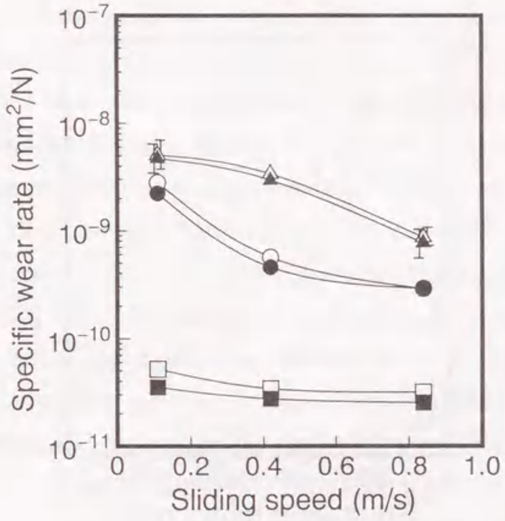

Fig.4-2 Effect of sliding speed on the specific wear rate of the disk and plate in water at room temperature (□,■), 120℃ (○,●) and 300℃ (△,▲). (Open:plate, filled:disk)

Fig.4-3 Scanning electron micrograph of the worn surface of SiC plate tested at sliding speed of 0.11m/s in water at 300℃.

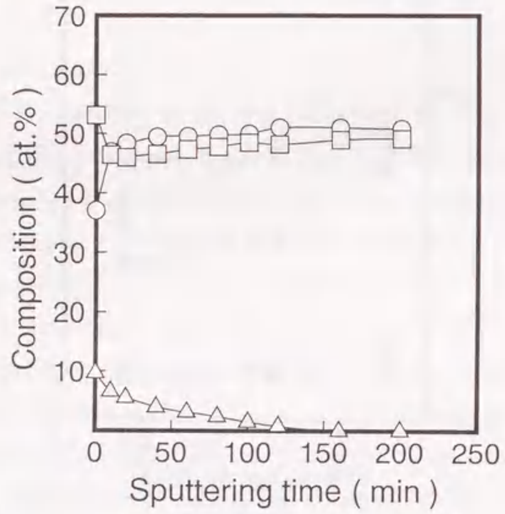

Fig.4-4 Depth profiles of silicon (○), carbon (□) and oxygen (△) on the worn surface of SiC at a sliding speed of 0.11m/s in water at 300℃.

time and saturate at about 120 min. On the other hand, the content of oxygen decreases with increasing the sputtering time and is not detected over more than the etching time of about 120 min. The thickness of silicon oxide is estimated to be of the order of about 10nm. These similar profiles to those shown in fig.4-4 were observed for other sliding conditions and also for the surfaces before the wear test and for statically soaked specimen under the same hydrothermal condition as the wear test. These results reveal that a surface oxidation layer does not develop at the sliding interface in water. On the other hand, the presence of carbon in the most surface layer may be caused by contamination during the procedures before the XPS analysis.

After the test at the sliding speed of 0.11m/s in water at 120℃, a slight amount of black particulates was floated on water and a part of them was adhered on the surface of the container around the waterline. Unfortunately these particulates could not be characterized because of a small amount of the wear particulates. The particulates may consist of carbon, which is formed by the reaction of SiC with H_2O because H_2 produced due to friction was observed as will be discussed later. At other sliding conditions, any particulates were not detected.

4.3.3 Analysis of the gaseous products after the wear tests

In the gases collected from the vessel after the wear tests at room temperature, no gas species were detected other than argon. However, H_2 and CH_4 gases were present after testing at 120 and 300℃. The amount of CO_2 gas was not detected by the gas chromatography except at 300℃. A slight amount of C_2H_6 in addition to the above gases was detected only after testing at 300℃. Figure 4-5 shows the relationship between the sliding speed and each amount of the reaction products (H_2, CO_2, CH_4 and C_2H_6) existing in both gas- and liquid-phases, where the gases dissolved in water are calculated by applying Henry's law. This figure also includes the corrosion data measured after immersing the SiC specimens statically in the same hydrothermal conditions as the wear tests at 300℃. No gases were detected after static corrosion of the specimens below 120℃. As seen in fig.4-5, the evolution of H_2, CO_2 and CH_4 is accelerated by friction in water at 300℃. It is noted that the C_2H_6 gas is produced only by friction in water at 300℃. At higher temperatures, the quantities of the gaseous products decrease with increasing the sliding speeds, as seen in fig.4-5. The formation of H_2, CO_2, CH_4 and C_2H_6 gases may be

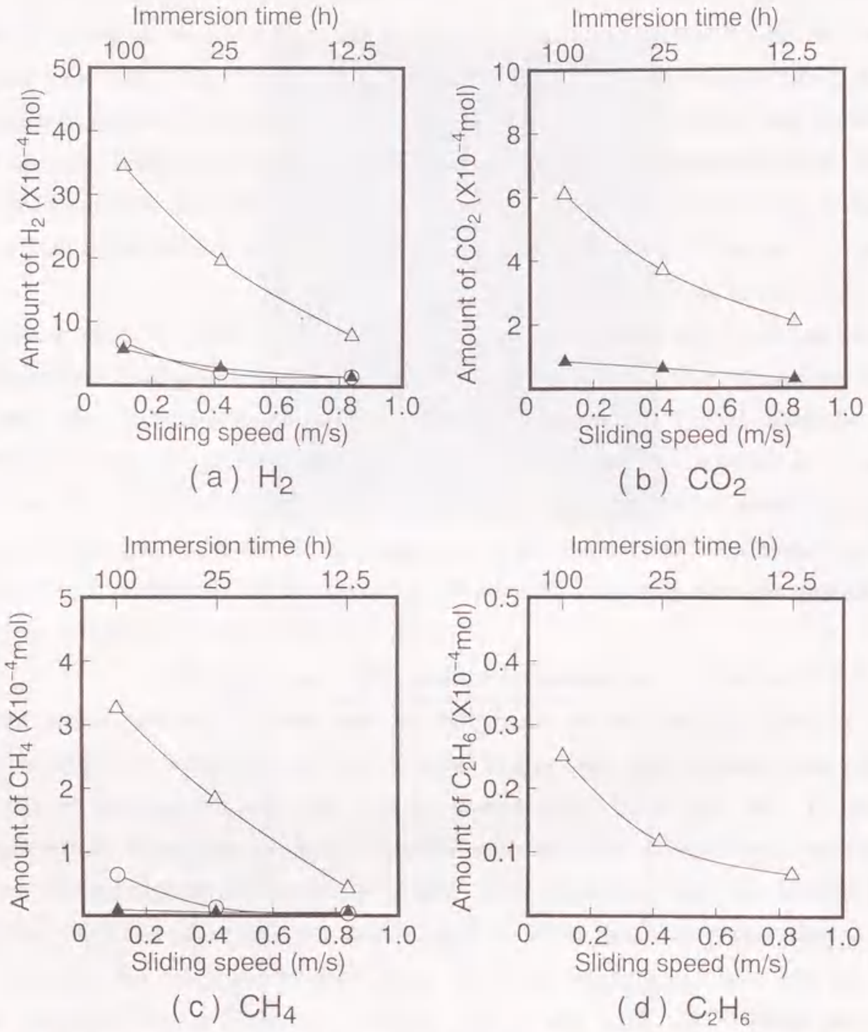

Fig.4-5 The each amount of H_2, CO_2, CH_4 and C_2H_6 gases existed in the gas- and liquid-phases as a function of sliding speed at 120℃ (○) and 300℃ (△). In the figure, static corrosion data of SiC specimen at 300℃ (▲) under the same hydrothermal conditions as the wear tests are also shown as a function of immersion time. The gases dissolved in water are calculated by applying the Henry's law: (a) H_2, (b) CO_2, (c) CH_4 and (d) C_2H_6.

expressed by the following reactions in addition to the equation (4-1):

$$SiC + 4H_2O \rightarrow SiO_2 + CO_2 + 4H_2 \quad (4\text{-}2)$$

$$SiC + 2H_2O \rightarrow SiO_2 + 1/2\ C_2H_6 + 1/2\ H_2 \quad (4\text{-}3)$$

$$SiC + 2H_2O \rightarrow SiO_2 + C + 2H_2 \quad (4\text{-}4)$$

During the wear and static immersion tests at 300℃ as seen in fig.4-5, the molar ratio of CO_2 to H_2 is about 0.2, suggesting reaction (4-1). The silica produced by reactions (4-1), (4-2) and (4-3) during the wear test at 300℃ seems to be dissolved immediately because any silica layer due to friction does not grow as seen in fig.4-4. On the other hand, the amount of H_2 production during the wear tests at 120℃ is equal to that during the static corrosion at 300℃ as seen in fig.4-5(a), but CO_2 which is observed during the static corrosion at 300℃ corresponding to reaction (4-2) is not detected during the wear at 120 ℃. The carbon-like particulates were observed at lower sliding speed in water at 120℃. Therefore, H_2 may be mainly produced by reaction (4-4) during the wear tests at 120℃. The content of carbon in water is estimated from the amount of H_2 production to be about 1 ppm at the sliding speed of 0.11m/s at 120℃. This extremely small amount of the carbon-like particulates may lead to the difficulty of quantitative chemical analysis of carbon. Carbon produced by reaction (4-4) is probably removed during dissolution of silica, since no evident increase in carbon and silicon oxide on the worn surface after the test in water at 120℃ was observed by the XPS analysis. In water at room temperature similarly to that at 120℃, reaction (4-4) may proceed more preferentially rather than reaction (4-2). However, carbon-like particulates could not be observed after the wear test at room temperature. Even if total carbon in the removed disk and two plates transforms to solid debris at room temperature, the content of carbon in water is on the order of 0.01 ppm. The presence of this amount must be very hard to detect.

4.3.4 Analysis of the solution after the wear tests

The silicon in the solution after the wear tests was evidently present at 120 and 300℃, but was not detected at room temperature. The silica produced by tribochemical reactions of SiC is considered to dissolve in water to form a silicic acid. Figure 4-6 shows the W_c/W_w ratio as a function of the sliding speed at 120 and 300℃. In this figure, W_w is

the total amount of wear determined from the weight loss of two plates and disk. W_c is calculated as the wear amount of the SiC corresponding to the Si concentration in the solution, which is corrected by subtracting the value measured after soaking the SiC specimens statically under the same hydrothermal conditions. As seen in fig.6, the ratios of W_c/W_w at both 120 and 300℃ are approximately unity, independent of the sliding speeds, indicating that the wear of SiC ceramic in high temperature water mainly proceeds with the dissolution of silica produced by reactions (4-1)~(4-4). This result reflects that growth of a silica layer was not observed on the worn surface by the XPS analysis shown in fig.4-4.

4.3.5 Wear and corrosion mechanisms

Figure 4-7 shows the temperature dependence of the Gibbs free energies of reactions (4-1) ~(4-4) calculated from refs.9 and 10 under 0.1MPa pressure which corresponds to the atmospheric pressure at room temperature. Reaction (4-1) for the production of CH_4 at 0.1MPa is thermodynamically the most stable reaction up to about 550℃. In the range from 550 to 620℃, the most stable reaction is reaction (4-4) and changes to reaction (4-2) above 620℃. Under the pressure of 8.53MPa, corresponding to the saturated water vapor pressure at 300℃, this change in the stabilities from the reaction (4-1), through (4-4), to (4-2) occurs at about 1,000-1,100℃, as calculated from refs.9, 10 and 11.

Figure 4-8 shows the relative molar ratio of H_2/CH_4 which is calculated by subtracting amount of each product such as H_2 and CH_4 obtained during static corrosion from that during the wear test, indicating the relative molar ratio of the gases produced at the sliding interface by the friction. This figure also involves the static corrosion data of the SiC specimens in water at 300℃. In the statical immersion at 300℃, the production of H_2 is larger than that of CH_4. Moreover, the molar ratio of CO_2 to H_2 corresponds to the ratio expected from reaction (4-2) as seen in fig.4-5. These results suggest that reaction (4-2) is preferred to reaction (4-1) for the static oxidation of SiC in water at 300℃, although reaction (4-1) is thermodynamically most stable in all reactions at this temperature. Since the oxidation of SiC in redistilled water or acidic solution follows to parabolic rate law[1,3], these phenomena seem to be due to the difference of diffusion coefficient of the produced gases in $Si(OH)_4$ which would exist as a sol on the SiC surface as reported by Hirayama et al.[1] The Van der Waals' radius of CO_2 is the same value as

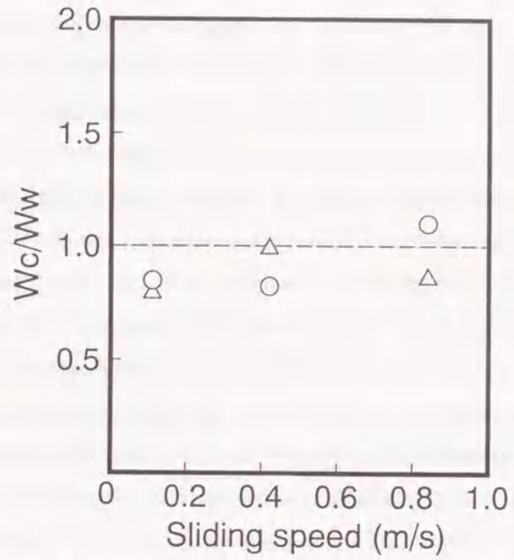

Fig.4-6 W_c/W_w ratio as a function of the sliding speed: W_c and W_w are the wear amounts of the SiC specimens corresponding to the concentration of Si in the solution and that determined from the weight loss of two plates and disk, respectively, at 120℃(○) and 300℃(△) in water.

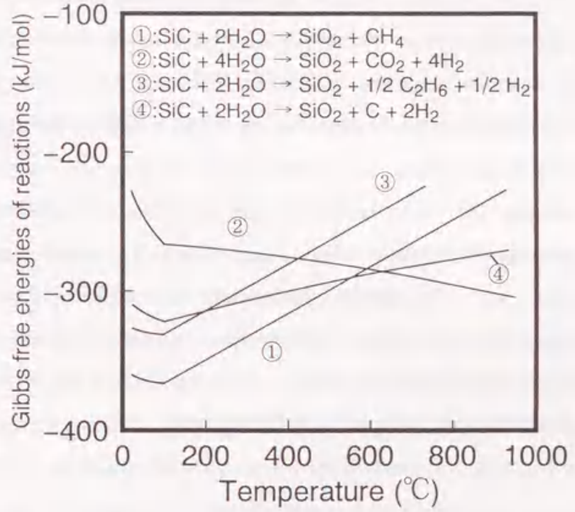

Fig.4-7 Gibbs free energies for the reactions ①, ②, ③ and ④ under the pressure of 0.1MPa as a function of temperature.

of CH_4(0.414nm), but smaller than that of C_2H_6 (0.473nm)[12]. The CO_2 gas has a polarity, while the hydrocarbon gases are nonpolar. In addition, CO_2 gas dissolves easily into water and transforms to carbonic acid. For these reasons, the preferential progress of the reaction (4-2) may be caused by easy diffusion of polar CO_2 and/or carbonic acid in the $Si(OH)_4$ sol. During the static corrosion of the specimens at 300℃, the increase of the relative molar ratio of H_2 to CH_4 with increasing the immersion time probably contributes to an enlargement of the difference of diffusivity of H_2 (or CO_2) and CH_4 due to the development of the $Si(OH)_4$ layer formed on the SiC substrate. As seen in fig.4-8, the relative molar ratio at the wear tests in water at 300℃ is lower than that at the static corrosion test. This behavior may be attributed to the favorable progress for reaction (4-1) because of the decrease of the $Si(OH)_4$ diffusion layer thickness by friction and wear.

The relative molar ratio of H_2 to CH_4 tends to increase with increasing sliding speed at 120 and 300℃, as seen in fig.4-8. This tendency cannot be explained by frictional heating at the sliding interface, because higher friction coefficient at low sliding speed as seen in fig.1 thermodynamically prefers reaction (4-2) or (4-4) to reaction (4-1), accompanying the increase of the temperature at the sliding interface. It is probably explained by the fact that the higher hydrodynamic lubrication of water at higher sliding speeds would contribute to the tribological behavior on the smooth worn surface which is formed by the solution of the silica into water. The dependence of the sliding speed on the relative ratio of H_2 to CH_4 at 120℃ is more apparent than that at 300℃. This may be correlated with easy of the formation of the hydrodynamic lubrication film at 120℃ because the viscosity of water increases with decreasing temperature.

The author now discusses the contribution of each tribochemical reaction to the total wear, which is determined from the total weight loss of both plates and disk. The amounts of CH_4, H_2 and C_2H_6 formed at the sliding interface are defined as the values corrected by subtracting the quantity of gaseous products in both gas- and liquid-phases under the static corrosion of the specimens from those obtained in the wear tests. Each wear component at 300℃ is estimated from the corrected values of H_2, CH_4 and C_2H_6 by assuming the evolution of the gaseous products following the equations (4-1), (4-2) and (4-3). The amount of H_2 due to reaction (4-2) is calculated by subtracting the quantity of H_2 produced with the progress of the reaction (4-3) from the total amount of H_2. On the other hand, the wear components at 120℃ are calculated by using the equations (4-1) and (4-4) because of the

detection of H_2, CH_4 and carbon-like particulates during the wear test. The total and each component contribution to the wear volume relating to the wear mechanisms at 120 and 300℃ are shown against the sliding speeds in fig. 4-9. It is seen from fig.4-9 that the hydrothermal oxidation reactions (4-1) and (4-2) are the main participants in the wear mechanism in water at 300℃, and reaction (4-3) gives only a small contribution. Since the worn surface at 300℃ was very smooth, it is imagined that microfracture scarcely occurred. Therefore, the residual wear component, which is less than 10% of the total wear volume in water at 300℃, is presumed to be caused by the slight contribution of reaction (4-4) and/or the scatter of the experimental data.

As shown in fig.4-9, wear behavior at 120℃ is governed by tribochemical reactions (4-1) and (4-4). Because no development of carbon layer on the worn surface due to friction at 120℃ was observed by the XPS analysis, carbon produced by reaction (4-4) would be worn off during the test. The remaining wear component at lower sliding speed exists, but at higher sliding speed the tribochemical wear is slightly larger than the total wear determined by the weight loss of the disk and two plates. We imagine that microfracture did not occur, because the worn surface morphology at 120℃ similarly to that at 300℃ was very smooth. Therefore, the difference between the total and tribochemical wears at 120℃ may be due to the scatter of the experimental data.

The gaseous products and wear particulates due to wear in water at room temperature could not be detected because of a slight wear volume. However, taking into consideration that the worn surface morphology at room temperature is similar to those at 120 and 300 ℃, the tribological behavior at room temperature also seems to be mainly influenced by tribochemical reactions.

From these experiments, the wear mechanisms of SiC in high temperature water can be explained by the tribochemical reactions of SiC with H_2O at the sliding interface. The increase of the specific wear rate with a rise of the temperature seems to be attributed to the acceleration of the hydrothermal oxidation of SiC, simultaneously with dissolution of the reaction product such as silica. The decreases of the specific wear rate and friction coefficient with increasing sliding speed are probably caused by the hydrodynamic lubrication due to a wedge film of water because of the flat worn surfaces. It is also considered that the total hydrothermal oxidation is reduced by the decrease of testing duration with increase of sliding speed under the condition of the constant sliding distance.

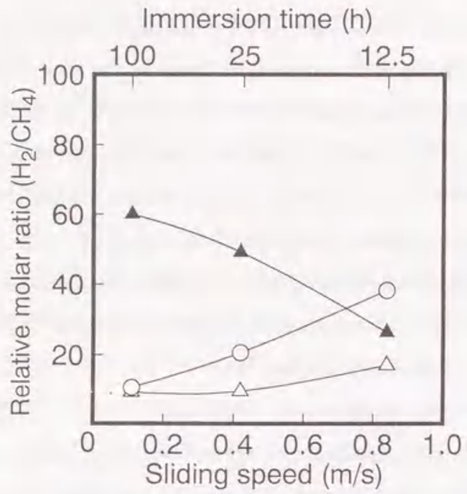

Fig.4-8 The relative molar ratio (H_2/CH_4) of SiC as functions of sliding speed at 120 ℃(○) and 300℃(△), and of static immersion time at 300℃(▲).

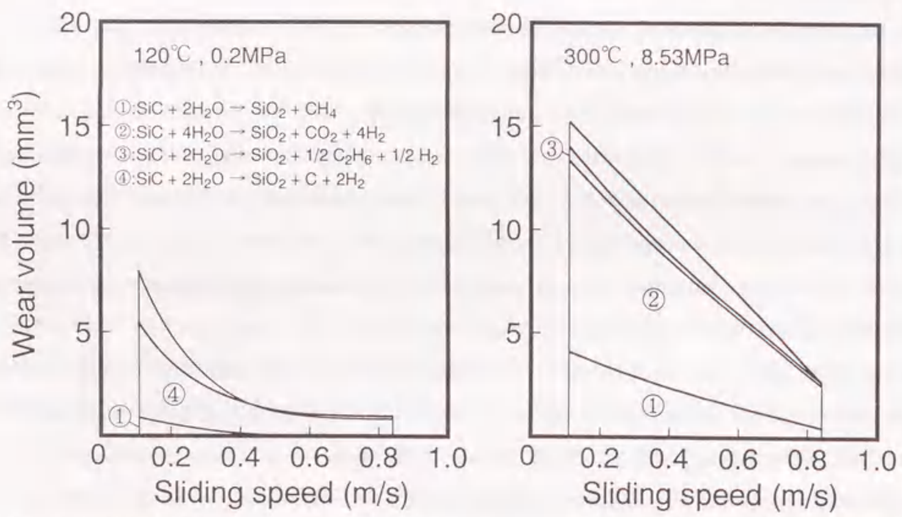

Fig.4-9 The total wear volume and each wear component of SiC at 120 and 300℃ in water as a function of sliding speeds. In the figure, the total wear volume is determined from the weight loss of both the plates and disk, and each wear component is estimated from the reactions ① , ② (or ④) and ③ to produce CH_4, H_2 and C_2H_6 gases, respectively.

4.4 Conclusions

(1) The friction coefficient and specific wear rates of disk and plate increased with a rise of the temperature at all sliding speeds. These behavior was considered to be caused by the acceleration of the hydrothermal oxidation of SiC, simultaneously with dissolution of silica.

(2) The decreases of the friction coefficient and specific wear rate with increase of the sliding speed at 120 and 300℃ were caused by the hydrodynamic lubrication and by depressing the hydrothermal oxidation due to a decrease of the testing duration with increase of the sliding speed.

(3) The relative molar ratio H_2/CH_4 of H_2 and CH_4 produced by the wear test at 300℃ was smaller than that from the static corrosion of the SiC specimens under the same hydrothermal condition. This phenomena may be considered to be caused by a decrease of the $Si(OH)_4$ sol layer thickness at the sliding interface due to friction and by the difference of the diffusivity between H_2 (or CO_2) and CH_4 through the $Si(OH)_4$ layer.

(4) The wear amounts estimated from the evolution of the gaseous products such as H_2, CH_4 and C_2H_6 and/or from the Si concentration in the testing solution were the similar values to that determined from the weight loss of two plates and disk at 120 and 300℃. The worn surfaces at room temperature resembled very closely in morphology that at 300 ℃. The wear mechanisms of the SiC ceramic in the range from room temperature to 300℃ was therefore governed by the tribochemical reactions at the sliding interface.

References

1 H.Hirayama, T.Kawakubo ,A.Goto, and T.Kaneko, *J.Am.Ceram.Soc.*, 72,No.11,2049 (1989).

2 S.Ono, K.Suzuki, M.Kumagai, K.Hoashi, T.Moriguchi and Y.Imamura, *JAIF International Conference on Water Chemistry in Nuclear Power Plants,* 315(1991).

3 M.Yoshimura, J.Kase and S.Somiya, *J.Mater.Res.*, 1,No.1,Jan/Feb,100(1986).

4 H.Tomizawa and T.E.Fischer, *ASLE trans.*, 30,No.1,41(1987).

5 S.Sasaki, *J.Soc.Lubrication Eng.*, 33,No.8,620(1988) (in Japanese).

6 P.Andersson, *Wear*, 154,37(1992).

7 S.Kitaoka, Y.Yamaguchi, and Y.Takahashi, *J.Am.Ceram.Soc.*, 75,No.11,3075(1992).

8 S.Kitaoka, T.Tuji, T.Katoh, Y.Yamaguchi and K.Sato, *J.Am.Ceram.Soc.,* 77,No.2,580 (1994).

9 JANAF Thermochemical Tables Third Edition, *J.Phys.Chem.Ref.Data,* Vol.14, Suppl.1, (1985).

10 Ihsan Barin, Fried Sauert, Ernst Schultze-Rhonhof and Wang Shu Sheng, *VCH* (1989).

11 U.Grigull, J.Straub, and P.Schiebener, *Steam tables in SI-Units: Wasserdampftafeln* , Springer-Verlag, Berlin(1984).

12 A.R.Berens and H.B.Hopfenberg, *J.Menb.Sci.*, 10,283(1982).

Chapter 5

Tribological Characteristics of CRT Ceramic

5 Tribological Characteristics of CRT Ceramic

5.1 Introduction

Advance ceramics are being investigated for a progress of reliability of the mechanical parts in Light Water Reactor Plants (LWRP) and prolongation of the span of their life due to applications as a tribomaterials, because the ceramics generally have high hardness, the excellent wear resistance and high temperature stability.[1] Since ^{60}Co is the main source for radiation exposure of the workers and is mainly produced from stellite (ST) in LWRP, which is being used as the tribomaterials, the application of the ceramics as the replacement of ST is expected from the standpoint of the decrease of the radiation exposure.[1,2]

Chromium carbide (Cr_3C_2)-titanium carbide (TiC) composite (CRT) is considered to be a possibility of the tribomaterials as a guide roller of the rod cluster control assembly, because CRT ceramic has the above mentioned properties and excellent fracture resistance as cutting tools.[3] However, no reports have been published on the tribological characteristics of CRT in high temperature and high pressure water simulated the environments of LWRP. Saito et al.[4] have been found that CRT has the excellent corrosion resistance in water at 288℃ in similar to SiC ceramics. Unfortunately, its corrosion mechanism have not been known. Yoshimura et al.[5] have found that the reaction of TiC powder with H_2O above 400℃ for 3h yielded anatase, CH_4, CO_2 and H_2, and above 500 ℃ rutile was formed additionally. They have also proposed the model of the hydrothermal oxidation of TiC as follows. First, an amorphous TiO_2 film covered the TiC grains. The gaseous products, CH_4, CO_2 and H_2 might be accumulated beneath this film because these gases appear to be difficult to dissolve in the TiO_2 film at the temperatures of 200-600℃. After a certain period of time, accumulated gases might break the film. At that time the crystallization occurs from the amorphous TiO_2 into anatase, which also helps to break the film. After that, the reaction occurs at the surface of grains, where oxidation reaction is controlled. Kanno et al.[6] have also suggested that crystallization of the amorphous TiO_2 formed on the TiC film which was coated on a super alloy (*P-20*) by chemical vapor deposition method accelerates the corrosion rate in high temperature and high pressure water

The tribological characteristics of Al_2O_3, Si_3N_4 and SiC in high temperature water have been found to be strongly affected by the corrosion behavior as described in the

previous chapters. This chapter reports the effects of temperature and sliding speed on the friction and wear behavior of CRT by sliding on itself in water at room temperature, 120 ℃ and 300℃, and discusses the friction and wear mechanisms.

5.2 Experimental procedure

The materials of disk and plate used in this experiment were of hot-pressed CRT. The mechanical and thermal properties are listed in tables 1-1 and 1-2, respectively. The crystal structure and composition of the CRT are shown in table 1-3. It has been reported that Cr_7C_3 and $Cr_{23}C_6$ are produced during the solution of Cr_3C_2 into TiC[7], however, only Cr_3C_2 and TiC in CRT ceramics were detected by XRD. The amount of CrC dissolved in TiC, which was calculated by using Hachisuka's equation, was about 10mol%.[7]

The experimental procedures of the wear tests were fundamentally similar to that for SiC as described in chapter 4. Wear tests were carried out by sliding the circumferential surface of a rotating disk on two plates as shown in fig.2-1. The roughnesses of the sliding surface of the plate and disk of CRT were 0.08 and 0.3 μm, respectively.

The testing solution was the distilled water which was controlled to have the dissolved oxygen concentration below 0.02mg/l by bubbling with argon. Experiments were conducted at room temperature under the atmospheric pressure (0.1MPa) and at 120 and 300℃ under the corresponding saturated vapor pressures of 0.2 and 8.53MPa, respectively. Wear tests were carried out in the sliding speed range from 0.11 to 0.84m/s at the constant contact load of 19.6N and up to the sliding distance of 38,000m. The friction coefficient was calculated from the difference of the torque between loaded and unloaded conditions. The wear volume of the specimens was obtained from dividing the weight loss of the specimens due to the wear by their density. The wear volume calculated from weight loss of the plates was in good agreement with that determined from the geometry of the wear scar at all sliding conditions in similar to Si_3N_4 and SiC ceramics as described in chapters 3 and 4. This means that any weight change of the plate from causes other than the wear is negligible. The specific wear rate was determined by using equation (2-2).

The worn surfaces of the plate specimens after the test were examined by SEM, EDS and XPS. The depth profiling of the worn surfaces for the XPS analysis was carried out by ion-sputter etching, which was performed for 10min with an applied beam voltage of 4kV at a beam current density of 1mA/cm^2 using argon gas. The wear debris particles, which

were dispersed into the solution, were collected by a centrifugal separator and identified by XRD. The wear debris was also examined in O_2 atmosphere at the temperature up to 1,000 ℃ by thermogravimetry (TG) and differential thermal analysis (DTA). Gaseous species of reaction products, which were collected by replacing the gas-phase in the vessel by distilled water, were analyzed by gas chromatography. The amounts of Cr and Ti in the solution after the wear tests were determined by ICP.

5.3 Results and discussion

5.3.1 Temperature and sliding speed dependence of friction and wear

At all sliding conditions, the friction coefficient in the initial stage was about 0.6～0.8, but decreased with increasing the sliding distance and saturated above about 15,000m. Figure 5-1 shows the effects of temperature and sliding speed on the friction coefficient of CRT ceramics in the steady state. As shown in fig.5-1, the friction coefficient increases with increasing temperature and decreases with increasing sliding speed.

Figure 5-2 shows the specific wear rates of the plate and disk as a function of sliding speed. The specific wear rates of the plate at room temperature are in the order of 10^{-10} mm^2/N, whereas those at 120 and 300℃ are about 10 times larger than that at room temperature. The specific wear rate of the plate at the constant temperature slightly decreases with increasing the sliding speed. On the other hand, the specific wear rates of the disk at all sliding conditions are larger than that of the plate. This suggests the wear of the disk proceeds due to the influence of the ambient environment in addition to development of the shear stress at the sliding interface. As seen in fig.5-2, the specific wear rate of the disk at 0.11m/s does not depend on the temperature and is constant ($5\times10^{-9}mm^2/N$). However, the specific wear rate of the disk at room temperature decreases with increasing the sliding speed, that at 120℃ is constant and that at 300℃ oppositely increases.

5.3.2 Analysis of the worn surfaces

Figure 5-3 shows the SEM micrographs and EDS spectra of the worn surfaces after the tests at the sliding speed of 0.11m/s in water at room temperature and 300℃. For the comparison, those after the tests, the morphology and EDS spectrum of the lapped surface before the tests are shown in fig.5-3(a). As seen in fig.5-3(a), the white and black regions

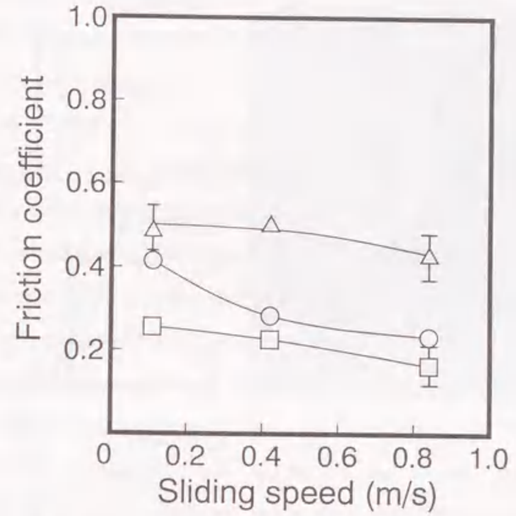

Fig.5-1 Effect of sliding speed on the friction coefficient of CRT specimens in water at room temperature (□), 120℃ (○) and 300℃ (△).

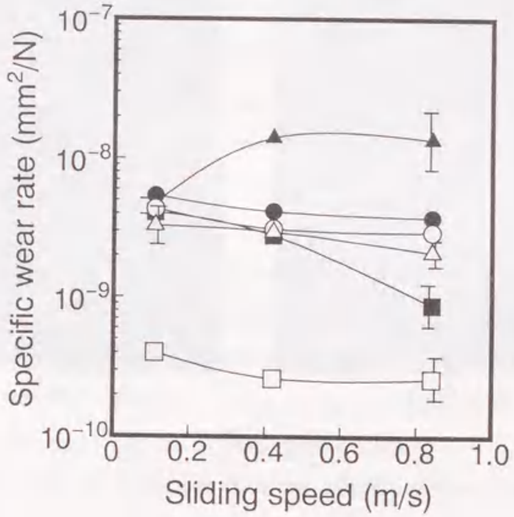

Fig.5-2 Effect of sliding speed on the specific wear rate of the disk and plate in water at room temperature (□,■), 120℃ (○,●) and 300℃ (△,▲). (Open:plate, filled:disk)

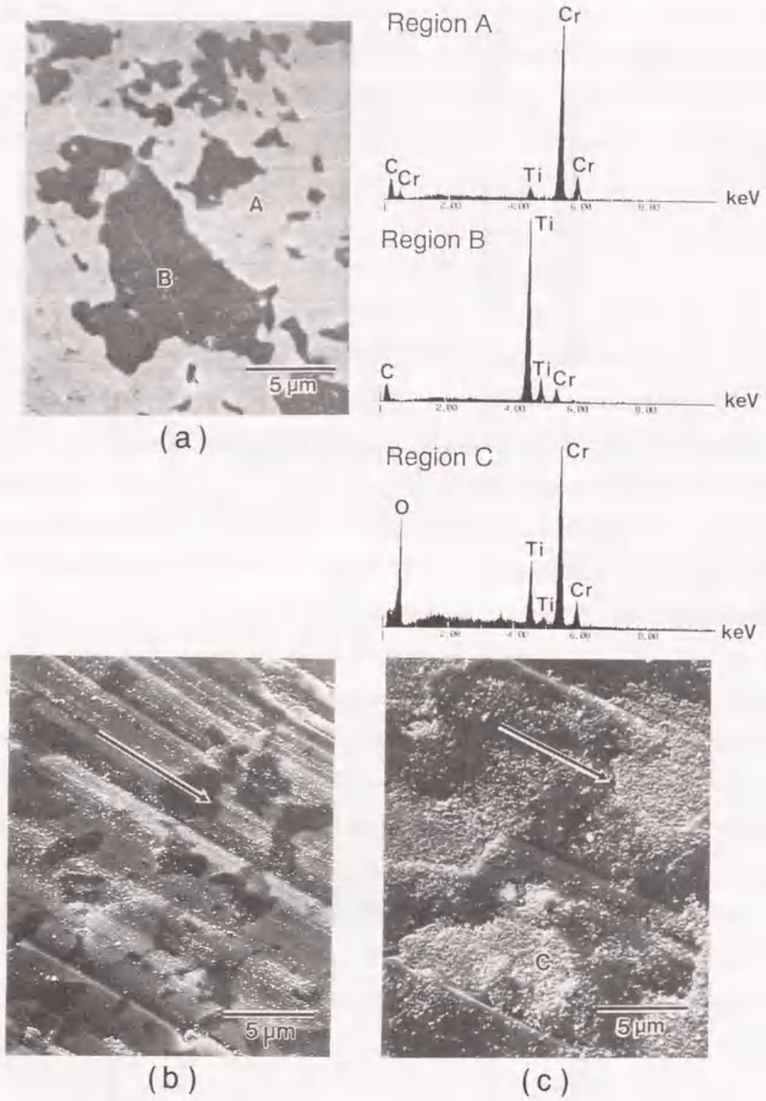

Fig.5-3 Scanning electron micrographs and EDS spectra of the worn surfaces of the plate tested in water at sliding speed of 0.11m/s for CRT: (a) before and (b) after the test at room temperature and (c) those after the test at 300℃. The arrows shown in figs (b) and (c) indicate the sliding direction of the disk.

are found to be corresponded to Cr_3C_2 and TiC, respectively. The sliding interface at room temperature seems to be in the condition of boundary lubrication, because many streaked scars on the worn surface are observed as shown in fig.5-3(b). It is imaged that the region of TiC is removed hardly compared to that of Cr_3C_2, since the hardness of $TiC_{1.0}$ at room temperature (HV2900) is significantly larger than that of Cr_3C_2 (HV1300). However, the morphology of the worn surface does not have the preferential fracture, but the uniform one. The wear debris is found to be slightly adhered on the worn surface as seen in fig.5-3(b). The morphology of the worn surface at higher sliding speed in water at room temperature was similar to that in fig.5-3(b), corresponding to the constant specific wear rate of the plate against the sliding speed as seen in fig.5-2.

On the other hand, the worn surface at lower sliding speed in water at 300℃ is rougher than that at room temperature as seen in fig.5-3(c). The region of TiC on the worn surface is preferentially removed and the particulates, which consists of mixture of Cr- and Ti-oxides, are accumulated on the damaged surface. It was found from the EDS analysis of this region that the molar ratio (Cr/Ti) of Cr and Ti in the particulates was 3.5 in similar to the value (3.7) of the bulk sample determined by ICP. This suggests that the amount of the preferential removal of the TiC region is significantly small compared to the total wear amount of the specimens and the Cr and Ti components removed from the bulk are homogeneously mixed by the friction. At higher sliding speed in water at 300℃, the whole of the worn surface was covered with this oxide film (0.5～1 μm thickness). The worn surface of the plate in water at 120℃ had the intermediate morphology between those at room temperature and 300℃.

The Cr 2p and Ti 2p levels for the worn surface of the plate at 0.84m/s in water at 300℃ was examined by XPS. Two peaks corresponding to the binding energies of Cr_2O_3 (Cr 2p=576.6eV) and TiO_2 (Ti 2p=458.4eV) were detected. The spectra for the surface of the specimen after immersing the CRT specimens statically in the same hydrothermal conditions as the wear tests at 300℃ were similar to those at the wear test, confirming the existence of Cr_2O_3 and TiO_2 on the corrosion surface too.

5.3.3 Analysis of the wear particles

Figure 5-4(b) shows the XRD pattern of the wear debris (dark green) produced by the wear at 0.84m/s in water at 300℃. As seen in fig.5-4(b), the pattern is identified as

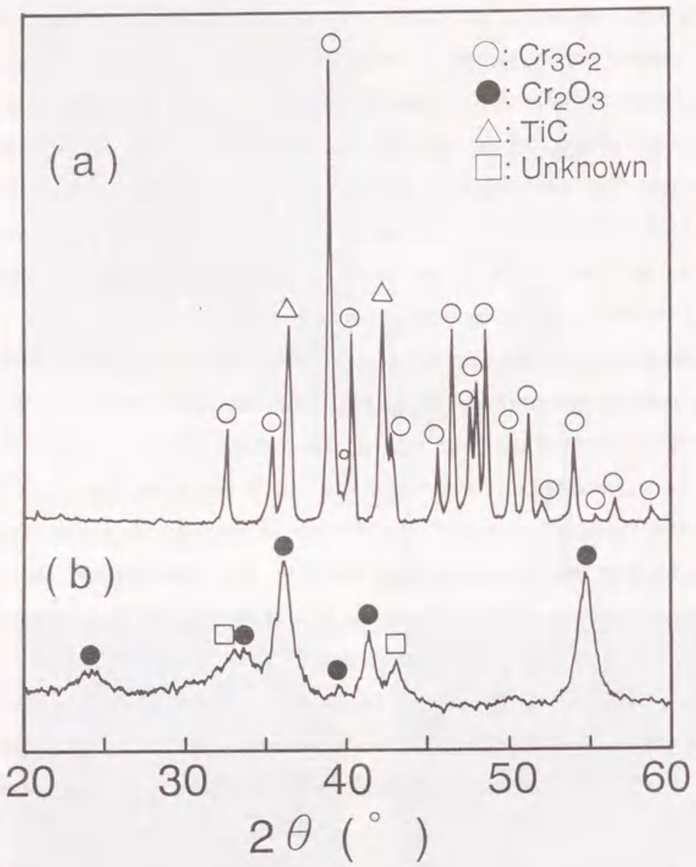

Fig.5-4 X-ray diffraction patterns of (a) CRT surface of the plate before the test and (b) wear debris produced at the sliding speed of 0.84m/s in water at 300℃.

Cr_2O_3 with low crystallinity, and both Cr_3C_2 and TiC phases are not detected. Therefore, the titanium oxide in the particulates accumulated on the worn surface at 300℃ as seen in figure 5-3(c) is considered to be amorphous TiO_2. The XRD pattern of the wear debris at 120℃ was the same as that at 300℃.

The production mechanism of the wear debris seems to be explained by the fact that the oxide layer, which is produced by the hydrothermal oxidation on the worn surface of CRT specimens due to the frictional heat, is removed at the sliding interface and/or that the particulates removed from the bulk are oxidized. At room temperature, the particulates could not be characterized because of its small amount. However, the same oxidation as that at 120 and 300℃ may be occurred at room temperature, since the color of the wear debris was similar at all sliding conditions.

It was found from the TG · DTA analysis of the wear debris produced at 0.84m/s in water at 300℃ that the exothermic peak with the decrease of its mass (about 8.8wt%) was observed at the temperature of 180～650℃, where the CO_2 production was also confirmed by gas chromatography. Therefore, this exothermic reaction is considered to be caused by combustion of the carbon in the wear debris.

5.3.4 Analysis of the gaseous products after the wear tests

Figure 5-5 shows the relationship between the sliding speed and each amount of the reaction products (H_2, CH_4, C_2H_6 and CO_2) existing in both gas- and liquid-phases, where the gases dissolved in water are calculated by applying Henrry's law. This figure also includes the corrosion data measured after immersing the CRT specimens statically in the same hydrothermal conditions as the wear tests at 300℃. In the static corrosion tests, H_2 and CH_4 gases are detected only after testing at 300℃, but in the wear tests these gases are produced at all sliding conditions. The amounts of H_2 and CH_4 produced during the wear tests are larger than those at the immersion tests. C_2H_6 could not be detected in the wear tests at the sliding speed above 0.4m/s in water at room temperature. The evolution of CO_2 is slightly confirmed only during the wear at 300℃. Thus the formation of H_2, CH_4, C_2H_6 and CO_2 gases may be expressed by the following tribochemical reactions:

$$2/9\ Cr_3C_2 + H_2O \rightarrow 1/3\ Cr_2O_3 + 4/9\ CH_4 + 1/9\ H_2 \qquad (5\text{-}1)$$

$$2/9\ Cr_3C_2 + H_2O \rightarrow 1/3\ Cr_2O_3 + 4/9\ C + H_2 \qquad (5\text{-}2)$$

$$2/9\ Cr_3C_2 + H_2O \rightarrow 1/3\ Cr_2O_3 + 2/9\ C_2H_6 + 1/3\ H_2 \quad (5\text{-}3)$$

$$2/17\ Cr_3C_2 + H_2O \rightarrow 3/17\ Cr_2O_3 + 4/17\ CO_2 + H_2 \quad (5\text{-}4)$$

$$1/2\ TiC + H_2O \rightarrow 1/2\ TiO_2 + 1/2\ CH_4 \quad (5\text{-}5)$$

$$1/2\ TiC + H_2O \rightarrow 1/2\ TiO_2 + 1/2\ C + H_2 \quad (5\text{-}6)$$

$$1/2\ TiC + H_2O \rightarrow 1/2\ TiO_2 + 1/4\ C_2H_6 + 1/4\ H_2 \quad (5\text{-}7)$$

$$1/4\ TiC + H_2O \rightarrow 1/4\ TiO_2 + 1/4\ CO_2 + H_2 \quad (5\text{-}8)$$

If activities of all substances are unity and the reaction products such as H_2, CH_4, C_2H_6 and CO_2 are ideal gases and the partial pressure of each gas is 0.1 MPa, the reactions (5-1) ~ (5-8) can thermodynamically proceed in water from room temperature to 300℃. (calculated from refs.9 and 10)

Although large amount of H_2 was produced during the static corrosion tests in water at 300℃, the weight of the specimens slightly increased with increasing the immersion time. This suggests that the oxidation rate of the CRT specimens is slightly larger than the dissolution rate of the reaction products of Cr_2O_3 and TiC. Therefore, it is expected that the thickness of the oxide layer increased with increasing the exposure time in spite of the dissolution of the oxide. However, because Cr and Ti in water after the corrosion tests were little detected by ICP, these constituent may be adsorbed on the wall of the pressure vessel (SUS316).

Figure 5-6 shows the relative molar ratio of H_2/CH_4 which is calculated by subtracting amount of each product such as H_2 and CH_4 obtained during static corrosion from that during the wear test, indicating the relative molar ratio of the gases produced at the sliding interface by the friction. This figure also involves the static corrosion data of the CRT specimens in water at 300℃. In the statical immersion at 300℃, the H_2/CH_4 ratio is above 30 and increases with increasing the immersion time as seen in fig.5-6 in similar to that of SiC in fig.4-8. The CO_2 production was not detected in the immersion at 300℃, in spite of the large amount of H_2. Moreover, the amount of the total carbonic acids of H_2CO_3, HCO_3^- and CO_3^{2-} in water was below the detection limit (0.5mg/l) of the strontium chloride-hydrochloric acid titration method, which was described in JIS K 0101.[11] Therefore, reactions (5-4) and (5-8) is considered hardly to progress, but reactions (5-2) and (5-6) to produce free-carbon and H_2 may occur. Yoshimura et al.[4] suggest that

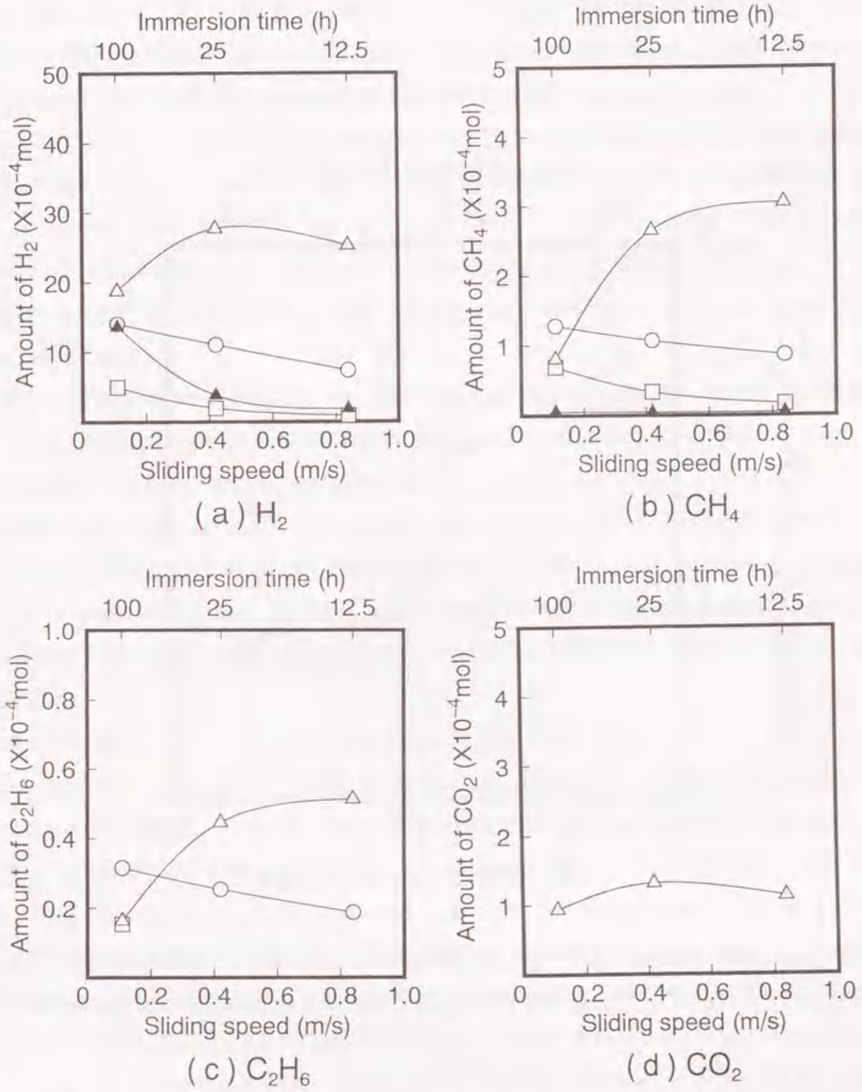

Fig.5-5 The each amount of H_2, CH_4, C_2H_6 and CO_2, gases existed in the gas- and liquid-phases as a function of sliding speed at room temperature (□), 120℃ (○) and 300℃ (△). In the figure, static corrosion data of CRT specimen at 300℃(▲) under the same hydrothermal conditions as the wear tests are also shown as a function of immersion time. The gases dissolved in water are calculated by applying the Henry's law: (a) H_2, (b) CH_4, (c) C_2H_6 and (d) CO_2.

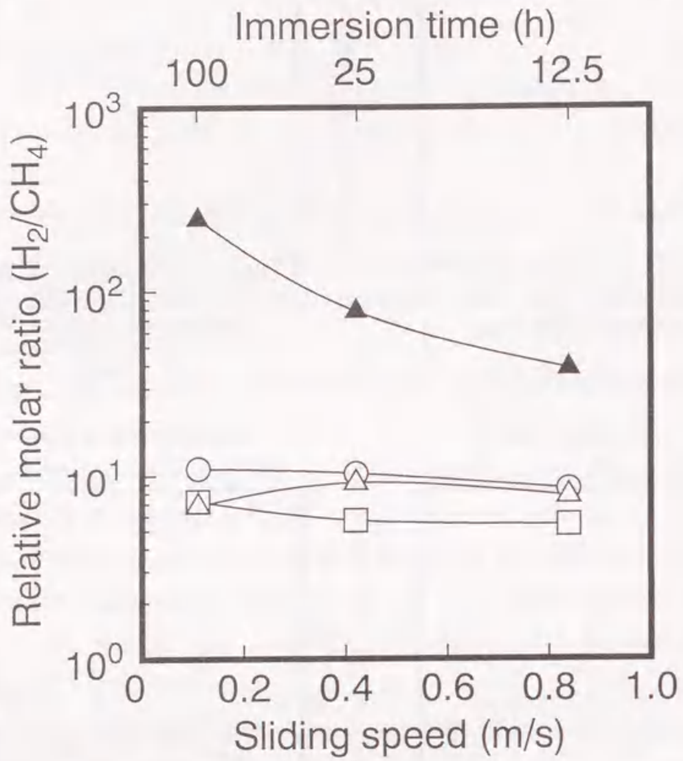

Fig.5-6 The relative molar ratio (H_2/CH_4) of CRT as functions of sliding speed at room temperature (□), 120℃(○) and 300℃(△), and that of static immersion time at 300℃ (▲).

the oxidation of TiC in water at 400～500℃ is controlled by the diffusion of CH_4 and CO_2 in the protective layer existed as the amorphous TiO_2 in the induction period, and after a certain period, this reaction changes to be reaction-controlled mechanism which was caused by losing the protective layer effect after the crystallization of the amorphous TiO_2. Since any cracks were not observed on the attacked surface of the CRT specimen after the immersion in water at 300℃ for 100h by SEM, the oxidation at the TiC region in CRT seems to be controlled by the diffusion of gaseous species. The reaction between the Cr_3C_2 region in CRT and H_2O may be also controlled by the diffusion of the gaseous products in the oxide layer.

If the carbon produced during the static immersion tests does not inhibit the diffusion of H_2 in the oxide layer, the preferential progress of the reactions (5-2) and (5-6) may be caused by the largest diffusivity of H_2 because the Van der Waals' radius of H_2 (0.353) is smaller than those of CH_4 (0.414nm) and C_2H_6 (0.473nm).[12] During the static corrosion of the specimens at 300℃, the increase of H_2/CH_4 ratio with increasing the immersion time as seen in fig.5-6 probably contributes to an enlargement of the difference of diffusivity of H_2 and CH_4 due to the development of the oxide layer formed on the CRT substrate.

As seen in fig.5-6, the relative molar ratio of H_2/CH_4 at the wear tests in water at 300 ℃ is lower than that at the static corrosion test, similarly to that of SiC in fig.4-8. This behavior may be attributed to the favorable progress for reactions (5-1) and (5-5) because of the decrease of the oxide diffusion layer thickness by friction and wear. The values of H_2/CH_4 ratio at the wear tests scarcely depend on the temperature and sliding speed, and are in the rage from 6 to 10. The values of C_2H_6/CH_4 ratio were also about 0.2, independent of sliding speed. Therefore, the tribochemical reactions of the CRT specimens may not be affected by the sliding conditions. However, the values of H_2/CH_4 ratio for the SiC specimens increased with increasing the sliding speed as seen in fig.4-8. We have already described in the section 4.3.6 that this tendency for SiC seems to be caused by the contribution of the hydrodynamic lubrication of water. For the CRT specimens, it is probably explained by the fact that the hydrodynamic lubrication of water is not achieved because of the very rough worn surfaces of the CRT specimens at all wear tests. The other reactions to produce H_2, CH_4, C_2H_6 and CO_2 except reactions (5-1)～(5-8) may be also considered to proceed, since a fresh surface of solids is sometimes highly activated for

chemical reactions by giving the mechanical energy as a friction.[13] For example, the carbon, which is produced with the progress of reactions (5-2) and (5-6), may be hydrogenated by exoelectrons released during the fracture of the CRT specimens at the sliding interface and may transform to CH_4 or C_2H_6.[14] Other reactions to produce the low order oxides or oxycarbide may also proceed due to the friction.

5.3.5 Friction and wear mechanisms

The author now discusses the contribution of each tribochemical reaction to the total wear, which is determined from the total weight loss of both plates and disk. The amounts of CH_4, H_2, C_2H_6 and CO_2 formed at the sliding interface are defined as the values corrected by subtracting the quantity of gaseous products in both gas- and liquid-phases under the static corrosion of the specimens from those obtained in the wear tests. Each wear component is estimated from the corrected values of CH_4, H_2, C_2H_6 and CO_2 by assuming that the evolution of the gaseous products following the equations (5-1)~(5-8) is proportional to the concentration of Cr_3C_2 and TiC in the CRT specimens. As seen in figure 5-7, the explainable tribochemical wear by using the equations (5-1)~(5-8) occupies 30~70% of the total wear volume at all sliding conditions, where the wear due to the equations (5-2) and (5-6) are the main participants and those due to other reactions give only a small contribution. The residual wear component is presumed to be caused by the participation of the tribochemical reactions to produce the lower order oxides and/or oxycarbide, because Cr_3C_2 and TiC were not detected in the wear debris by XRD as seen in fig.5-4.

As seen in fig.5-2, the dependence of the specific wear rate of the plate on the sliding speed was significantly different from that of the disk. This point is discussed as follows. The chromium and titanium oxides surface layers produced from the CRT specimens during the wear tests are considered to be hydrated in water. Since aluminum and silicon hydroxides have suggested to act as a solid lubrication,[15,16] it is expected that the chromium and titanium hydroxides also have a lubrication effect. The low friction coefficient of CRT in water at room temperature may be caused by this hydroxide film on the worn surface. However, the dehydration of the film may easily occur at higher testing temperature, and simultaneously disappearance of the lubricating ability probably leads to the increase of the friction coefficient at higher temperature. The specific wear rates of the

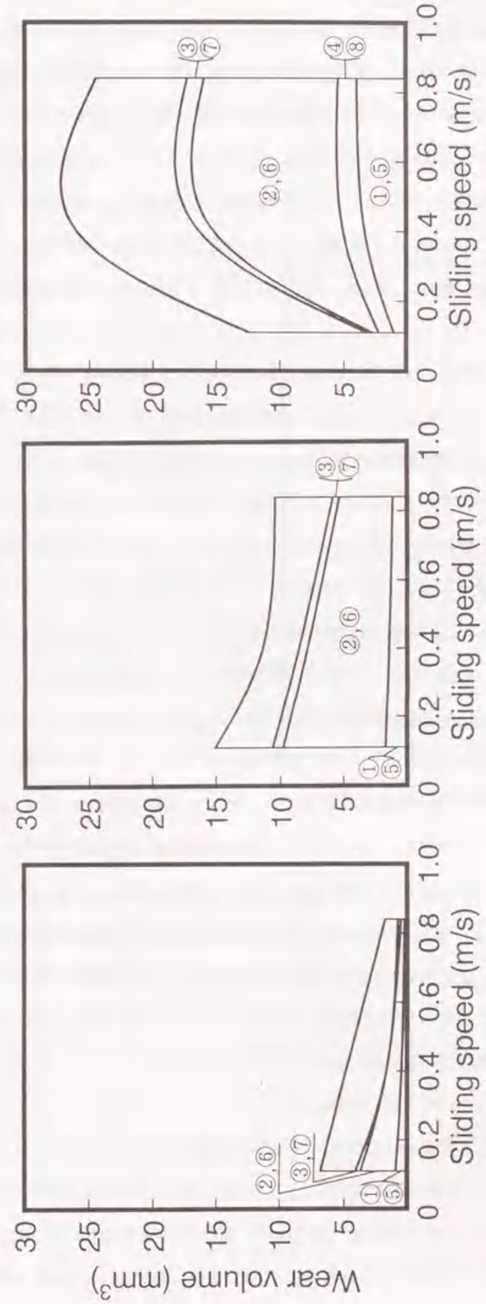

① $2/9\ Cr_3C_2 + H_2O \rightarrow 1/3\ Cr_2O_3 + 4/9\ CH_4 + 1/9\ H_2$
② $2/9\ Cr_3C_2 + H_2O \rightarrow 1/3\ Cr_2O_3 + 4/9\ C + H_2$
③ $2/9\ Cr_3C_2 + H_2O \rightarrow 1/3\ Cr_2O_3 + 2/9\ C_2H_6 + 1/3\ H_2$
④ $2/17\ Cr_3C_2 + H_2O \rightarrow 3/17\ Cr_2O_3 + 4/17\ CO_2 + H_2$
⑤ $1/2\ TiC + H_2O \rightarrow 1/2\ TiO_2 + 1/2\ CH_4$
⑥ $1/2\ TiC + H_2O \rightarrow 1/2\ TiO_2 + 1/2\ C + H_2$
⑦ $1/2\ TiC + H_2O \rightarrow 1/2\ TiO_2 + 1/4\ C_2H_6 + 1/4\ H_2$
⑧ $1/4\ TiC + H_2O \rightarrow 1/4\ TiO_2 + 1/4\ CO_2 + H_2$

Fig.5-7 The total wear volume and each wear component of CRT at (a) room temperature, (b) 120℃ and (c) 300℃ in water as a function of sliding speeds. In the figure, the total wear volume is determined from the weight loss of both the plates and disk, and each wear component is estimated from the reactions ①~⑧ to produce CH_4, H_2, C_2H_6 and CO_2 gases.

plate in water at 120 and 300℃ were larger than that at room temperature. This behavior may be responsible for the decrease of the lubricating ability of the film due to the dehydration and the acceleration of the hydrothermal oxidation of the substrate. The constant specific wear rates of the plate against the sliding speed at the temperature above 120℃ may be related to accumulation of the oxide particulates on the worn surface, where the local stress at the sliding interface decreases. That is to say, the depressing ability of the wear due to this inclusions seems to compensate for accelerating the wear due to the oxidation of the CRT specimens and the decrease of the hydroxides with increasing the testing temperature.

On the other hand, the worn surface of the disk is considered to be affected by the ambient water more than that of the plate, because the worn surface of the disk is periodical contact with the two plates. Since the hydroxide layer with lubricating ability may not be sufficiently formed in the early sliding stage in water at room temperature, higher frictional heat produced at the higher sliding speeds may accelerate of the oxidation reactions of the substrate. But, at higher sliding speeds, the hydroxide layer, which is able to protect the substrate, is formed in a shorter testing duration, resulting in the decrease of the specific wear rate of the disk at room temperature with increasing sliding speed. In water at 300℃, however, the specific wear rate of the disk oppositely increases with increasing the sliding speed. Because the dehydration of the lubricious film at the sliding interface in water at 300℃ due to the frictional heat may occur easily more than that at room temperature, it will be difficult to cool the worn surface of the disk at higher sliding speed. Thus, in water at 300℃ the dehydration of the film and oxidation of the CRT substrate seems to be still more accelerated with increasing the sliding speed. However, at the sliding speed of 0.84m/s at 300℃, a large amount of the particulates existing at the interface probably reduces the magnitude of the local stress due to contact between plate and disk. The specific wear rate of the disk in water at 120℃ did not depend on the sliding speed and was constant. It can be explained that the condition of the worn surface at 120℃ is an intermediate between those at room temperature and 300℃.

As seen in fig.5-2, the specific wear rates of the disk are larger than those of the plate at all sliding conditions, similarly to those for the Al_2O_3 ceramics (ALO-1 in fig.2-3 and ALO-2 in fig.2-9). On the contrary, the specific wear rates of both the plate and disk for the Si_3N_4 (SN-1, SN-2 and SN-3) and SiC ceramics are the same or those of the plate are

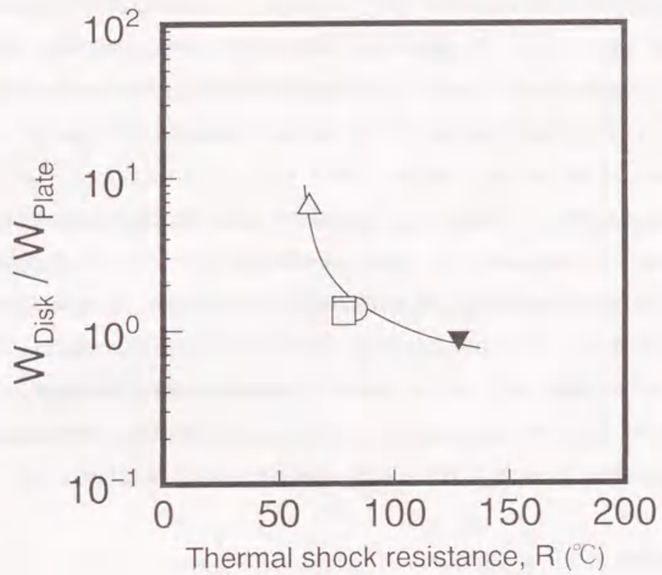

Fig.5-8 W_{disk}/W_{plate} ratios of CRT (△), ALO-1 (○), ALO-2 (□) and SiC (▼) as a function of the thermal shock resistance parameter *R*: W_{disk} and W_{plate} are the specific wear rates of the plate and disk at the sliding speed of 0.84 m/s in water at 300℃, respectively.

larger than those of the disk depending on the experimental conditions as seen in figs.3-2, 3-14, 3-18 and 4-2. These behavior seems to be related to an intrinsic property of the materials as will be discussed below. Figure 5-8 shows the W_{disk}/W_{plate} ratio as a function of the thermal shock resistance parameter, *R*, listed in table 1-2. In this figure, W_{disk} and W_{plate} are the specific wear rates of the disk and plate at the sliding speed of 0.84 m/s in water at 300℃, respectively. The W_{disk}/W_{plate} ratio above unity means that the wear of the disk is accelerated by the cyclic contact in addition to the shear stress at the interface. As seen in fig.5-8, the W_{disk}/W_{plate} ratio increases with decreasing the thermal shock resistance, and the ratio of CRT is significantly above unity. Thus, the wear of the disk for CRT is probably caused by the thermal shock fracture due to the frictional heat in addition to the oxidation of the substrate.

From these experiments, it is clear that the tribological characteristics of CRT in high temperature water are influenced by the hydrothermal oxidation and fracture of the substrate. The oxidation mechanism of CRT during the friction in water suggests to be different from that during the static corrosion, because the formation of CH_4 and C_2H_6 is easily occurred at the wear tests compared to the immersion tests. However, effects of the nonstoichiometry of TiC and the solubility of CRC to TiC on the tribology of CRT have not been unknown. Thus we will have to study about this point further.

5.4 Conclusions

(1) The friction coefficient increased at elevated temperatures at all sliding speeds, but decreased with increasing sliding speed. The specific wear rates of the plate at room temperature were in the order of $10^{-10}mm^2/N$, but those at 120 and 300℃ were about 10 times larger than that at room temperature. The specific wear rate of the plate slightly decreased with increasing the sliding speed at all temperatures. On the other hand, the specific wear rates of the disk were larger than those of the plate at all sliding conditions. At lower sliding speed, the specific wear rate of the disk did not depend on the testing temperature. However, those of the disk at room temperature decreased with increasing the sliding speed, those at 120℃ were constant and those at 300℃ oppositely increased.

(2) The tribochemical reactions to produce H_2, C, CH_4, C_2H_6 and CO_2 proceeded during the wear tests in water. The H_2/CH_4 and C_2H_6/CH_4 ratios due to the friction were constant at all sliding conditions. The H_2/CH_4 ratio at the wear tests in water at 300℃ was smaller than that at the immersion tests.

(3) The tribological characteristics of the CRT specimens seem to be controlled by the oxidation and microfracture of the specimens. Especially for the disk, the thermal shock fracture due to the frictional heat participates in the wear tests.

References

1 K.Tomita and Y.Terabayashi, *Genshiryoku kogyo*, 34,No.10,9(1988) (in Japanese).

2 K.Tada, *Tribologist*, 37,No.7,550(1992) (in Japanese).

3 T.Hachisuka, *Powder and Powder Metallrugy*, 38,4,516(1991) (in Japanese).

4 N.Saito, Y.Fuse, Y.Yasuda and M.Oishi, *Rroceedings of the Symposium on Boshoku Fushoku*, 355(1993) (in Japanese)

5 M.Yoshimura, M.Hayakawa and S.Somiya, *Yogyo Kyokai Shi*, 97,No.11,1139(1989) (in Japanese).

6 Y.Kanno, M.Yashima, M.Kakihana and M.Yoshimura, *J.Soc.Mat.Sci.,* 42,No.428,780 (1993) (in Japanese).

7 T.Hachisuka, *Powder and Powder Metallrugy*, 37,No.4,74(1990).

8 E.K.Storms, *The Refractory Carbides*, Chap. Ⅰ, Academic Press (1967) .

9 JANAF Thermochemical Tables Third Edition, *J.Phys.Chem.Ref.Data,* Vol.14, Suppl.1, (1985).

10 Ihsan Barin, Fried Sauert, Ernst Schultze-Rhonhof and Wang Shu Sheng, *VCH* (1989).

11 *Testing methods for industrial water, JIS K 0101*, Japanese Standards Association, 86(1991) (in Japanese).

12 A.R.Berens and H.B.Hopfenberg, *J.Menb.Sci.*, 10,283(1982).

13 S.Mori, *Bulletin of the Japan Institute of Metals*, 24,No.8,639(1985) (in Japanese).

14 T.Kubo, *Mechanochemistry Gairon*, Tokyo Kagaku Dojin, 227(1978) (in Japanese).

15 R.S.Gate, S.M.Hsu and E.E.Klaus, *Tribol.Trans.*, 32,No.3,357(1989).

16 T.E.Fischer and H.Tomizawa, *Wear*, 105,29(1985).

Chapter 6

Comparison of Tribological Behavior of the Ceramics

6 Comparison of Tribological Behavior of the Ceramics

6.1 Prediction of wear amount

It is clear from the previous chapters that the wear behavior of the various ceramics such as Al_2O_3 (ALO-1 and ALO-2), Si_3N_4 (SN-1, SN-2 and SN-3), SiC and CRT in high temperature water is strongly affected by the tribochemical reactions at the sliding interface. It has suggested that the wear of Al_2O_3 at room temperature and 120℃ was caused by the dissolution of this material through formation of hydrous alumina, but that at 300℃ was mainly contributed to stress corrosion cracking (SCC) and preferential dissolution of the grain boundary because of the disappearance of the hydrous alumina with lubricious ability due to frictional heat. For Si_3N_4 and SiC, we have found that the wear was mainly caused by the oxidation of these materials. The wear of CRT was related to the thermal shock fracture in addition to the oxidation of the specimens, especially for the disk specimen. Therefore, the tribochemical wear is discussed for the plate, because the wear of the disk is significantly affected by cooling the worn surface due to water during the periodical contact with the plates in addition of the tribochemical reactions at the interface.

The tribochemical wear models for the ceramics are proposed as shown in fig.6-1. As seen in fig.6-1, the wear of Al_2O_3 is assumed to be controlled by the dissolution of the material at the temperatures up to 120℃ (model Ⅰ), but only by the SCC at 300℃ (model Ⅲ) as seen in fig.6-1, although the contribution of the dissolution of the grain boundary layer to the wear amount of the material has not been apparent. The wear of the non-oxide ceramics is supposed to be caused only by the hydrothermal oxidation (model Ⅱ). The tribochemical reactions as the dissolution and oxidation are assumed to be caused by frictional heat transformed from frictional work at the real contact area, A_r, between plate and disk specimens, but the SCC is supposed to occur at the same contact area, where the subsurface layer is strained below the critical stress intensity (K_{IC}) for catastrophic failure by the friction as seen in fig.6-1. The contact area between plate and disk specimens with a diameter, $2a$, as seen in fig.6-1, is assumed to be given by

$$A_r = \frac{F_n}{p} = \pi a^2 \qquad (6-1)$$

where F_n is a contact load and p is the yield pressure of softer material (equal to hardness, H_v, of the ceramic in our experiments because of sliding the material on itself).[1] This

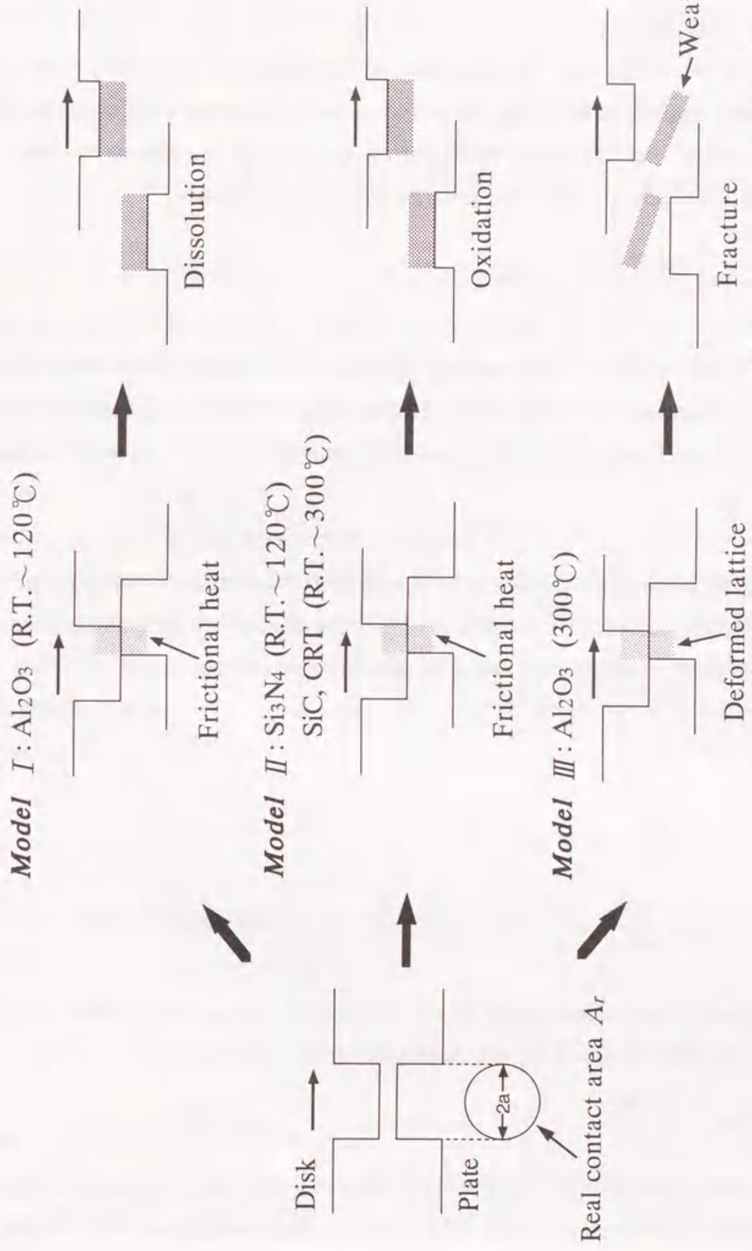

Fig. 6-1 Models of the tribochemical wear for the ceramics in water.

assumption makes the mathematics to be manageable, although the real contact area may not be truly circular. Suppose also that A_r is constant during the sliding.

6.1.1 Model I for Al_2O_3

At first, model I, where the wear is contributed to the dissolution of Al_2O_3 ceramic, is discussed. If these reactions proceed on the surface after an asperity contact at the flash temperature, T_c, where the frictional work during the contact transforms to only the frictional heat, this temperature T_c on the asperity can be described by[2]

$$T_c = \frac{\mu \cdot F_n \cdot v}{4 \cdot 2\kappa}\left(\frac{\pi \cdot H_v}{F_n}\right)^{1/2} + T_0 \qquad (6-2)$$

where μ is friction coefficient, v is sliding speed, κ is thermal conductivity of the material, and T_0 is ambient temperature. It is supposed that the reaction temperature T_c is maintained for the time t_1, which is equal to the lifetime of the asperity contact as follows:

$$t_1 = \frac{2a}{v}. \qquad (6-3)$$

In model I, the tribochemical dissolution of Al_2O_3 is also assumed to follow a linear rate law (reaction controll), because this reaction may proceed directly on the surface. Thus, the weight loss of the plate, ΔW_1, per A_r due to an asperity contact is given by

$$\left(\frac{\Delta W_1}{A_r}\right) = k \cdot t_1. \qquad (6-4)$$

where k is linear rate corrosion constant as

$$k = A_c \exp\left(-\frac{\Delta E}{RT_c}\right), \qquad (6-5)$$

where ΔE is apparent activation energy of the reaction, A_c is frequency factor and R is gas constant. On the other hand, ΔW_1 can be experimentally obtained by

$$\Delta W_1 = \frac{\rho \cdot \Delta V \cdot 2a}{L} \qquad (6-6)$$

where ΔV is volume of the plate, ρ is density of the material and L is sliding distance. If the hardness H_v of the material is independent of the surface temperature and constant at

all sliding conditions, the combination of equation (6-4) with (6-1), (6-3), (6-5) and (6-6) yields

$$\Delta V = \frac{L \cdot F_n}{\rho \cdot v \cdot H_v} \cdot A_c \exp\left(-\frac{\Delta E}{R \cdot T_c}\right). \qquad (6-7)$$

The equation (6-7) is rewritten as

$$U = Ln\left(\frac{v \cdot H_v \cdot \rho \cdot \Delta V}{F_n \cdot L}\right) = \mathrm{Ln}A_c - \frac{\Delta E}{R} \cdot \frac{1}{T_c}. \qquad (6-8)$$

In a plot of U vs. $1/T_c$ as shown in fig.6-2(a), ΔE and ln A_c are obtained from a slope and intercept on the U-axis, respectively, by fitting the data of ALO-1 at the testing temperature below 120℃ to equation (6-8). The figure shows a straight line with some scatter (correlation coefficient of r=0.80). ΔE and A_c for the dissolution of ALO-1 obtained from fig.6-2(a) are 20 kJ/mol and 84g/(m^2s), respectively, and listed in table 6-1.

6.1.2 Model Ⅱ for non-oxide ceramics

The tribochemical oxidation of Si_3N_4, SiC and CRT in water has been suggested to show diffusion-controlled reaction as described in Chapters 3, 4 and 5. Therefore, it is supposed for model Ⅱ that the oxidation of Si_3N_4, SiC and CRT shows a parabolic rate law. Thus the weight loss per unit contact area ($\Delta W_1 / A_r$) of the plate due to the asperity contact is given by

$$\left(\frac{\Delta W_1}{A_r}\right)^2 = k \cdot t_1. \qquad (6-9)$$

By substituting $\Delta V'$ for ΔV in equation (6-6), the combination of equation (6-9) with (6-1), (6-3), (6-5) and (6-6) becomes

$$\Delta V' = \frac{L}{\rho}\left\{\frac{\pi^{1/2} \cdot F_n^{3/2}}{2v \cdot H_v^{3/2}} \cdot A_c \exp\left(-\frac{\Delta E}{R \cdot T_c}\right)\right\}^{1/2}. \qquad (6-10)$$

Equation (6-10) is rewritten as

$$U' = Ln\left\{\frac{2v \cdot H_v^{3/2} \cdot \rho^2 \cdot \Delta V'^2}{\pi^{1/2} \cdot F_n^{3/2} \cdot L^2}\right\}^{1/2} = \mathrm{Ln}A_c - \frac{\Delta E}{R} \cdot \frac{1}{T_c}. \qquad (6-11)$$

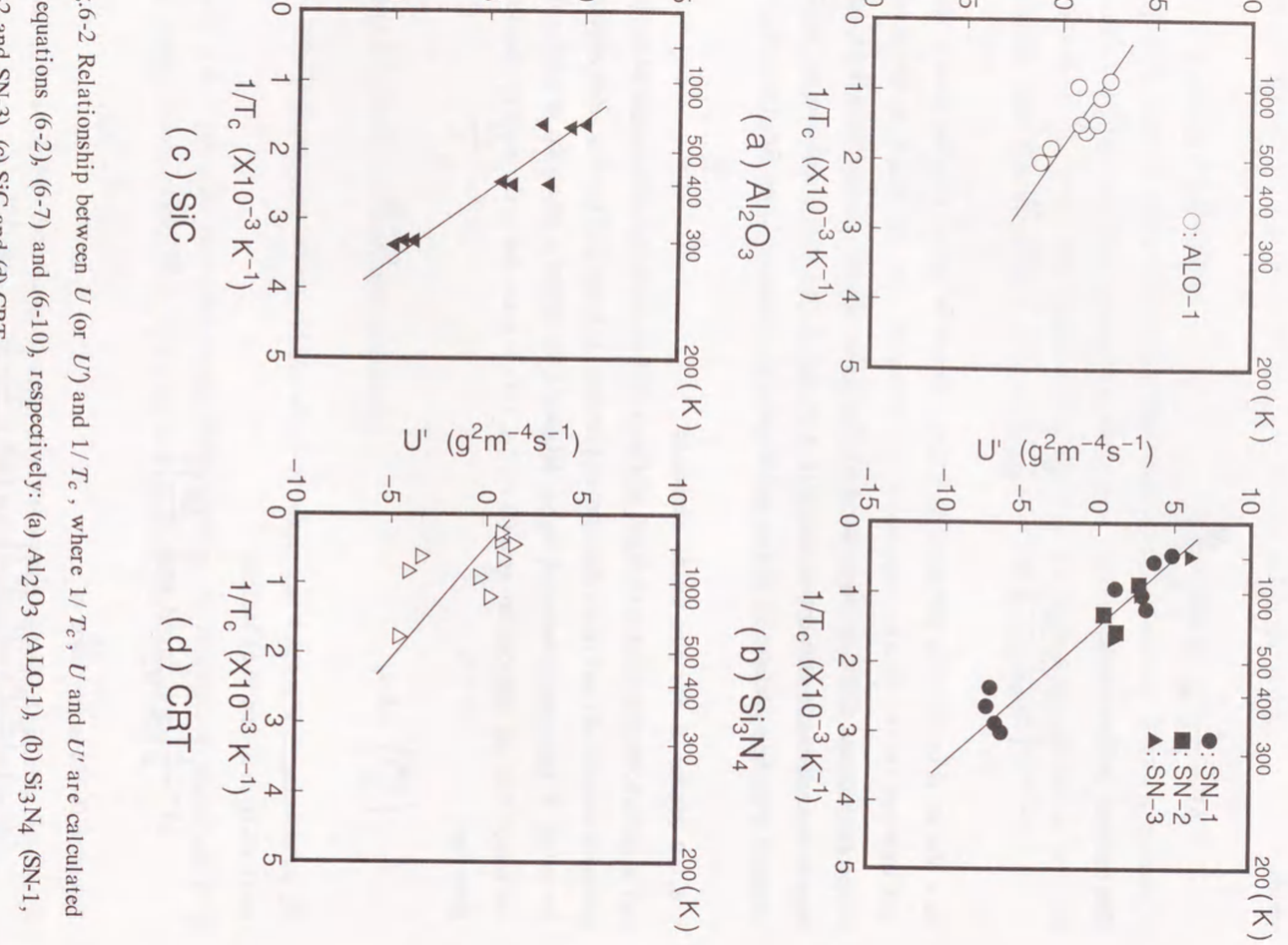

Fig.6-2 Relationship between U (or U') and $1/T_c$, where $1/T_c$, U and U' are calculated by equations (6-2), (6-7) and (6-10), respectively: (a) Al_2O_3 (ALO-1), (b) Si_3N_4 (SN-1, SN-2 and SN-3), (c) SiC and (d) CRT.

Table 6-1 The tribochemical reaction parameters of ceramics.

Materials	Temperature	Reactions	Kinetics	Activation energy	Frequency factor
ALO-1	R.T.～120℃	dissolution	linear	20 kJ/mol	84 (g/(m^2.s))
SN-1,2,3	R.T.～120℃	oxidation	parabolic	42 kJ/mol	2038 (g^2/(m^4.s))
SC	R.T.～300℃	oxidation	parabolic	41 kJ/mol	2614 (g^2/(m^4.s))
CRT	R.T.～300℃	oxidation	parabolic	25 kJ/mol	4 (g^2/(m^4.s))

Figure 6-2(b) shows that in a plot of U' vs. $1/T_c$, the U' values of the Si_3N_4 ceramics (SN-1, SN-2 and SN-3) give a straight line with r=0.95, although the friction and wear behavior of these materials in water at 120℃ is strongly affected by the composition and crystallinity of the grain boundaries as mentioned in section 3.3. This linear relationship may be correlated to the results that any wear of Si_3N_4 ceramics is mainly controlled by the oxidation to produce NH_3. The wear of SiC has suggested to be caused by the oxidation to produce H_2, C and CH_4 at the temperature below 120℃, but to produce H_2, CO_2, CH_4 and C_2H_6 at 300℃ as described in Chapter 4. Therefore, since the tribochemical mechanism of SiC at lower temperature is considered to be different from that at higher temperature, it is imagined that the plot of U' vs. $1/T_c$ shows a refraction of the line in the temperature range from 120 to 300℃. However, the U' values of the SiC ceramic may be expressed by a straight line with r=0.94 as seen in fig.6-2(c), because the presence of the refraction point is not clear due to some scatter values at higher T_c. As seen in fig.6-2(d), the U' values of the CRT ceramic deviate largely from the linear relationship and its correlation coefficient (r=0.60) is lower than those of other ceramics. Although this large deviation suggests the participation of other factors in addition to the oxidation, the wear amount is predicted approximately by using the experimental constants (ΔE and A_c) determined due to the linear approximation as will be discussed later.

The activation energies of the tribochemical reactions of all the ceramics are listed in table 6-1 and are in the range from 20 to 45kJ/mol, relatively independent of the materials. The activation energies of the tribochemical oxidation of the Si_3N_4 (42kJ/mol) and SiC (41kJ/mol) are much smaller than those values determined by the static immersion of the materials (73～108kJ/mol in water and 134kJ/mol in water vapor for Si_3N_4,[4,5] 167kJ/mol in water and 194kJ/mol in water vapor for SiC[3]). These are probably related to the difference of the diffusion coefficient of the gaseous products in different morphology of a silica, namely a silica sol ($Si(OH)_4$) for the tribochemical oxidation as described in Chapter 4 and an amorphous silica for the static oxidation. The diffusion of the gaseous products seems to occur through the $Si(OH)_4$ more easily than through the amorphous silica.

6.1.3 Model Ⅲ for Al_2O_3

In model Ⅲ, the frictional work carried out during the asperity contact is presumed to

transform to only the distortion of the α -alumina lattice, which induces SCC in the asperity, without frictional heat. It is so assumed to make the mathematics simple, although the frictional heat as much as dehydration of boehmite, which is thermodynamically stable in water at 300℃, is actually produced at the sliding interface as described in Chapter 2. Figure 6-3 shows representation of reaction coordinate for bond rupture in alumina. The main interesting point on the reaction coordinate is the energy levels of the activated complexe which exists at the time of bond rapture. For static immersion in water (solid line), the activation energy is the entire energy of the bridging bond which must be overcomed before bond rupture can occur. This energy barrier is stress free apparent activation energy ΔE_0 corresponding to the same condition as *step 2* for silica in fig.1-2. On the other hand, under the wear condition, when the alumina lattice is deformed by the change of the Al-O-Al or O-Al-O angle in the subsurface layer due to the shear stress during the asperity contact, this change may enhance the acid/base properties of alumina in the subsurface layer thereby making the chemical attack mechanism described in fig.1-2 in similar to the SCC mechanism proposed for silica.[6] The energy to make the SCC is assumed to be equal to the energy ΔW_f seen in fig.6-3, which is the frictional work per molar number of the discrete alumina at one asperity contact. Thus effect of the reduced energy barrier to the reaction can be modified as

$$k = A_c \exp\left(-\frac{\Delta E_0 - \Delta W_f}{RT_0}\right), \qquad (6-12)$$

The SCC of alumina may follow a linear rate law, because the reaction directly progress on the surface of the material. If the reaction time is also supposed to be equal to the lifetime of the asperity contact, by substituting $\Delta V''$ for ΔV in equation (6-6), the combination of equation (6-4) with (6-1), (6-3), (6-6) and (6-12) gives

$$\Delta V'' = \frac{L \cdot F_n}{\rho \cdot \nu \cdot H_v} \cdot A_c \exp\left(-\frac{\Delta E_0 - \Delta W_f}{RT_0}\right). \qquad (6-13)$$

The experimental constants of ΔE_0 and A_c can not be determined here, because the wear due to the participation of the SCC occurred only at 300℃. However, if the frictional work at one asperity contact transforms to the energy required to distort the alumina lattice in the surface layer, which is equal to 2 times of the wear amount of the plate during the

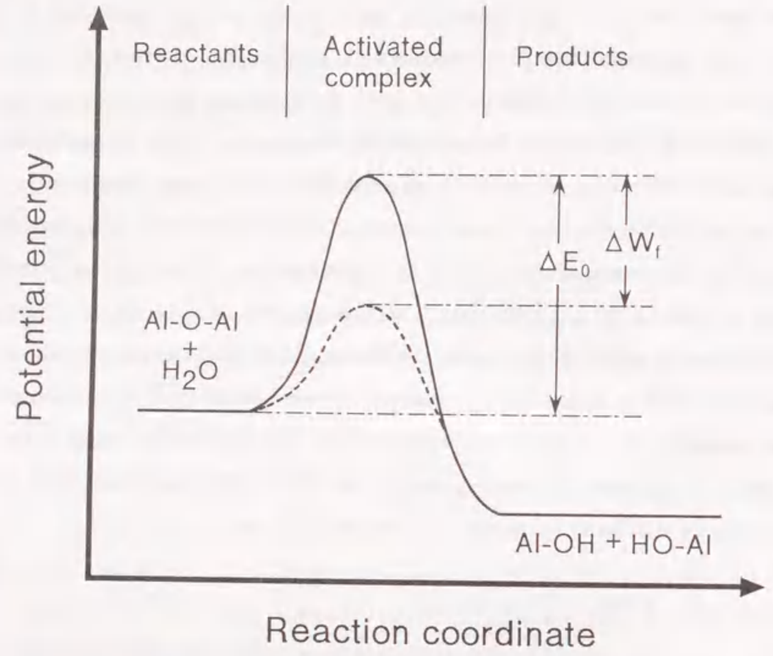

Fig. 6-3 Representation of reaction coordinate for bond rupture in alumina, where solid line and dashed line indicate rupture in water during static immersion and friction, respectively. ΔE_0 is stress free apparent activation energy and ΔW_f is energy required to distort alumina lattice at a contact asperity corresponding to frictional work at the asperity.

asperity contact (the wear amount of the disk is equal to that of the plate), ΔW_f can be written as

$$\Delta W_f = \frac{Frictional\ work\ at\ the\ asperity\ contact}{Molar\ number\ of\ the\ discrete\ alumina} = \frac{\mu \cdot F_n \cdot L \cdot M}{2\Delta V'' \cdot \rho} \qquad (6-14)$$

where M is molecular weight of alumina. The ΔW_f values of both ALO-1 and ALO-2 in this experiment are in the order of $10^4 \sim 10^6$kJ/mol and unbelievably large. This is probably related to the unsuitable assumption, where the frictional work transforms only to the deformation of the alumina lattice due to changing the Al-O-Al or O-Al-O angle. It can not be negligible that the frictional work transformed to the frictional heat and plastic deformation due to initiation and development of the dislocation in the subsurface layer etc. Unfortunately, the author has not been able to estimate the energy dissipation due to these factors.

6.1.4 Applicability of equations derived for models I and II

The author now discusses the general applicability of equations (6-7) and (6-10) for models I and II, respectively. Figure 6-4 shows the relationship between calculated wear volume of the plate (ΔV_{cal}) and the experimental one (ΔV_{exp}). In this figure, ΔV_{cal} is calculated from equations (6-7) and (6-10), where the experimental constants presented in table 6-1 and the friction coefficient in the steady state are used, and ΔV_{exp} is determined from the weight loss of the plate. The ΔV_{exp} values of ALO-1 and ALO-2 at 300℃ are not included in this figure, because equations (6-7) and (6-10) can not be applied to ALO-1 and ALO-2 at 300℃. As seen in fig.6-4, the ΔV_{exp} values are in relatively agreement with the ΔV_{cal} values for all the materials.

The wear amounts of other ceramics predicted by using equations (6-7) and (6-10) are compared with the experimental data reported by other investigators. Figure 6-5 shows relationship between ΔV_{exp} and ΔV_{cal}, where ΔV_{exp} is the wear volume of the pin specimens obtained at the total sliding distance (the symbols except ■, ▲ and ▼) for the ceramics (Al_2O_3, Si_3N_4 and SiC)[7,8,9], and ΔV_{cal} is determined from equation (6-7) for Al_2O_3 and equation (6-10) for Si_3N_4 and SiC by using the average friction coefficient in the steady state and our experimental constants listed in table 6-1. This figure also includes the V_{exp} values (■, ▲ and ▼) determined at the steady state by Loffelbein et al.,[9]

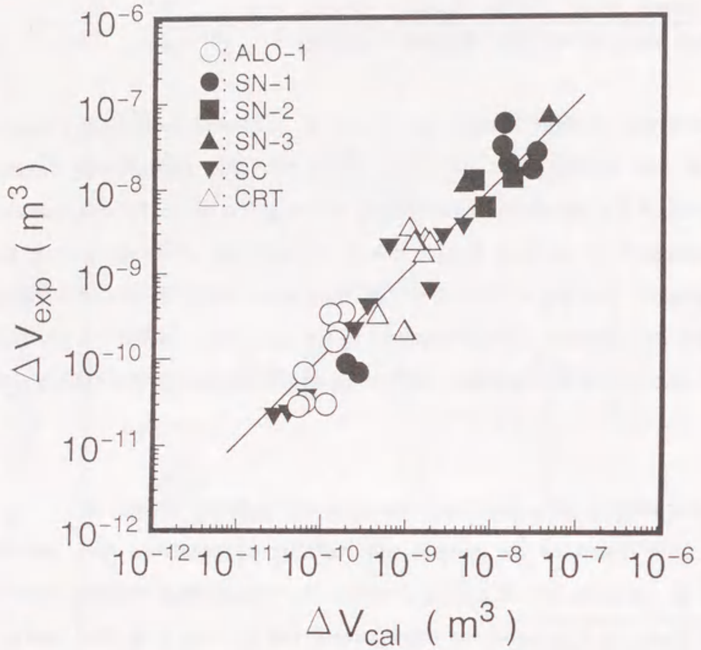

Fig.6-4 Calculated wear volume of the plate specimen (ΔV_{cal}) versus experimental one (ΔV_{exp}) obtained at the sliding speed of 0.11～0.84m/s, contact load of 19.6N and sliding distance of 38,000m in water at room temperature, 120 and 300℃ where is determined from equation (6-7) for ALO-1 and equation (6-10) for non-oxide ceramics (SN-1, SN-2, SN-3, SiC and CRT).

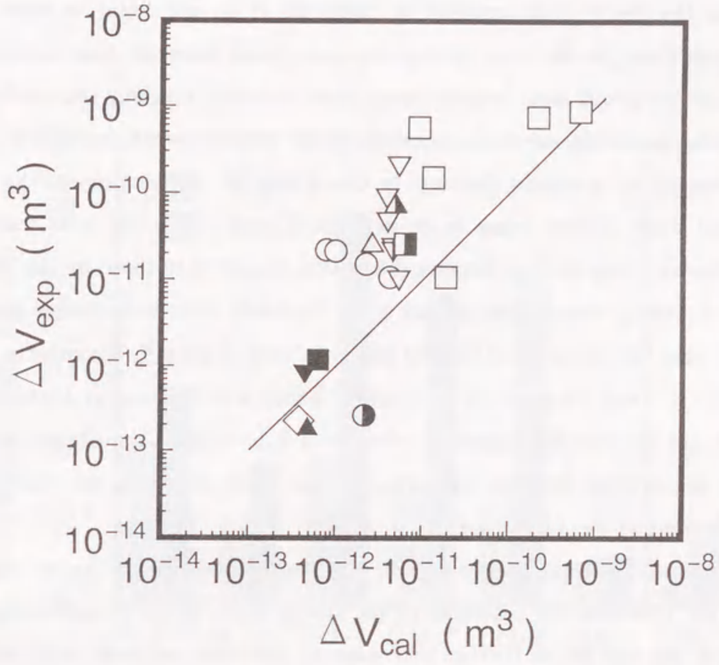

Fig.6-5 Calculated wear volume of the pin specimen (ΔV_{cal}) versus experimental one (ΔV_{exp}), where ΔV_{cal} is determined from equation (6-7) for Al_2O_3 and equation (6-10) for non-oxide ceramics (Si_3N_4 and SiC).

Pin-on-disk type tribometer, T_0=20℃, F_n=50N, v=0.1～0.8m/s, L=1,256m, ΔV_{exp} = Total wear volume and μ = Friction coefficient in the steady state by Sasaki.[7] (○: Al_2O_3, □: Si_3N_4 and ▽: SiC)

Pin-on-disk type tribometer, T_0=22℃, F_n=10N, v=0.1m/s, L=2,500m, ΔV_{exp} = Total wear volume and μ = Friction coefficient in the steady state by Andersson.[8] (◇: Al_2O_3 and △: SiC)

Pin-on-disk type tribometer, T_0=23℃, F_n=22N, v=0.1m/s, L=2,000m, ΔV_{exp} = Total wear volume and μ = Friction coefficient in the steady state by Löffelbein et al.[9]
(◑: Al_2O_3, ◨: Sintered Si_3N_4, ◭: HIP-reaction bonded Si_3N_4 and ▼: SiC).

Pin-on-disk type tribometer, T_0=23℃, F_n=22N, v=0.1m/s, L=2,000m, ΔV_{exp} = The wear volume in the steady state and μ = Friction coefficient in the steady state by Löffelbein et al.[9]
(■: Sintered Si_3N_4, ▲: HIP-reaction bonded Si_3N_4 and ▼: SiC).

where the frictional constant is constant. As seen in fig.6-5, the almost all values of ΔV_{exp} obtained at the total sliding distance are larger than the ΔV_{cal} values. However, the ΔV_{exp} values at the steady state reported by Loffelbein et al. are closer to their ΔV_{cal} values rather than those at the total sliding distance. These behavior may suggest that initial wear before the steady state is much larger than that after reaching the steady state, because the friction coefficient of the ceramics in water decreases with increasing sliding distance and saturates at a certain distance. In this study, the contribution of the initial wear to the total wear amount seems to be negligibly small, since the wear tests were carried out at the very long sliding distance (38,000m) compared to those by the previous studies (1,250～2,500m), where wear amount after the steady state was smaller than that of total amount from the initial state to final state. As seen in fig.6-5, the minima of the ΔV_{exp} values (○, □ and ▽) reported by Sasaki[7], which was obtained at higher sliding speed of 0.8m/s, are also in good agreement with the ΔV_{cal} values. This may be related to the result that the sliding distance for tribochemical wear to reach the steady state decreased with increasing the sliding speed.[7]

Therefore, equations (6-7) and (6-10) may be applicable to the prediction of the wear amount due to the tribochemical reactions in the steady state. If the tribochemical wear models in fig.6-1 are applied to friction and wear of advanced ceramics in water, it is expected from these equations that the ceramics with high hardness and high thermal conductivity have an excellent wear resistance in water. Therefore, the wear amount of the SiC ceramic may be the smallest of all the ceramics in this experiment. In order to estimate the wear amount of the disk specimen during the cyclic contacts, The participation of the thermal shock fracture or oppositely the depression of the tribochemical wear due to the cooled worn surface should be considered in addition to those models.

6.2 Applicability of ceramics to nuclear power plants

6.2.1 Comparison of static corrosion resistance of ceramics

The corrosion resistance of the ceramics in water is one of the important indications to evaluate the applicability of the materials to nuclear power plants. Figure 6-6 shows weight change of the ceramics (ALO-1, ALO-2, SN-1, SN-2, SN-3, SiC and CRT) at 120 and 300℃ for 100h in water with dissolved oxygen concentration of 8.5mg/l for both ALO-1 and ALO-2 and below 0.02mg/l for other ceramics. As seen in fig.6-6, the weight

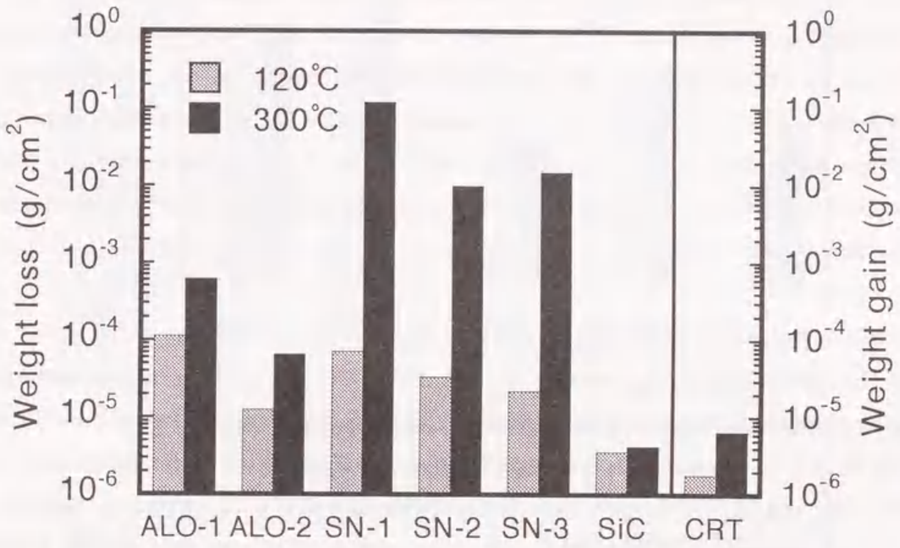

Fig.6-6 Weight change of the ceramics in distilled water at 120 and 300℃ for 100h. The concentration of dissolved oxygen in water is 8.5mg/l for the Al_2O_3 ceramics (ALO-1 and ALO-2) and below 0.02mg/l for other ceramics (SN-1, SN-2, SN-3, SiC and CRT). The V/A value is 2.6m, where V (m^3) is the amount of water and A (m^2) is the sum of the initial surface areas of the specimens.

loss is observed for all ceramics except CRT, but the weight gain for CRT. The weight changes of SiC and CRT at the both temperatures were in the order of 10^{-6}g/cm^2, which is close to the identification limit (1.7×10^{-6}g/cm^2) of the gravimeter used in this experiment, and those were too lower than other ceramics. The weight changes of SiC and CRT slightly increased with increasing the immersion temperature compared to other ceramics, but those of the Si_3N_4 ceramics (SN-1, SN-2 and SN-3) significantly increased. These results suggest that SiC and CRT may be hopeful to the application to the triboelements in water even though the temperature on the worn surface locally rises due to frictional heat. On the contrary, the application of the Si_3N_4 ceramics should be avoided, especially to the parts used under the severe sliding conditions, where a large amount of frictional heat is produced.

6.2.2 Selection of tribomaterials in nuclear power plants

The applicability of the ceramics (ALO-1, SN-1, SiC and CRT) to the tribomaterials is also discussed by comparing with the tribological characteristics of the stellite (ST), which has been widely used for the present LWR. Figure 6-7 shows the friction coefficients of the ceramics and ST in the steady state at the sliding speeds of 0.11 and 0.84m/s in water at room temperature, 120 and 300℃. The wear tests at 300℃ for SN-1 are not conducted, because Si_3N_4 ceramics are too corroded in water at 300℃ as seen in fig.6-6. As seen in fig.6-7, the friction coefficients of SiC at the sliding speeds of both 0.11 and 0.84m/s are lower than those of other materials at all testing temperatures. The friction coefficients of SN-1 at room temperature are lower than those of other materials except SiC, but those at 120℃ are the largest of all materials.

If the triboelements consist of a combination of the same materials such as mechanical seals of a primary coolant pump in PWR, the wear resistance of the materials should be evaluated by the total wear amount of both the two plates and disk. Figure 6-8 shows the total wear volume of the materials at the sliding conditions corresponding to those in fig.6-7. Under the sliding conditions except the sliding speed of 0.11m/s in water at 120 ℃, the total wear volume of SiC is smaller than those of other materials as seen in fig.6-8, similarly to that for the static corrosion behavior in fig.6-6. The wear volume of SN-1 at 120℃ in fig.6-8 is very large compared to that at room temperature in similar to the

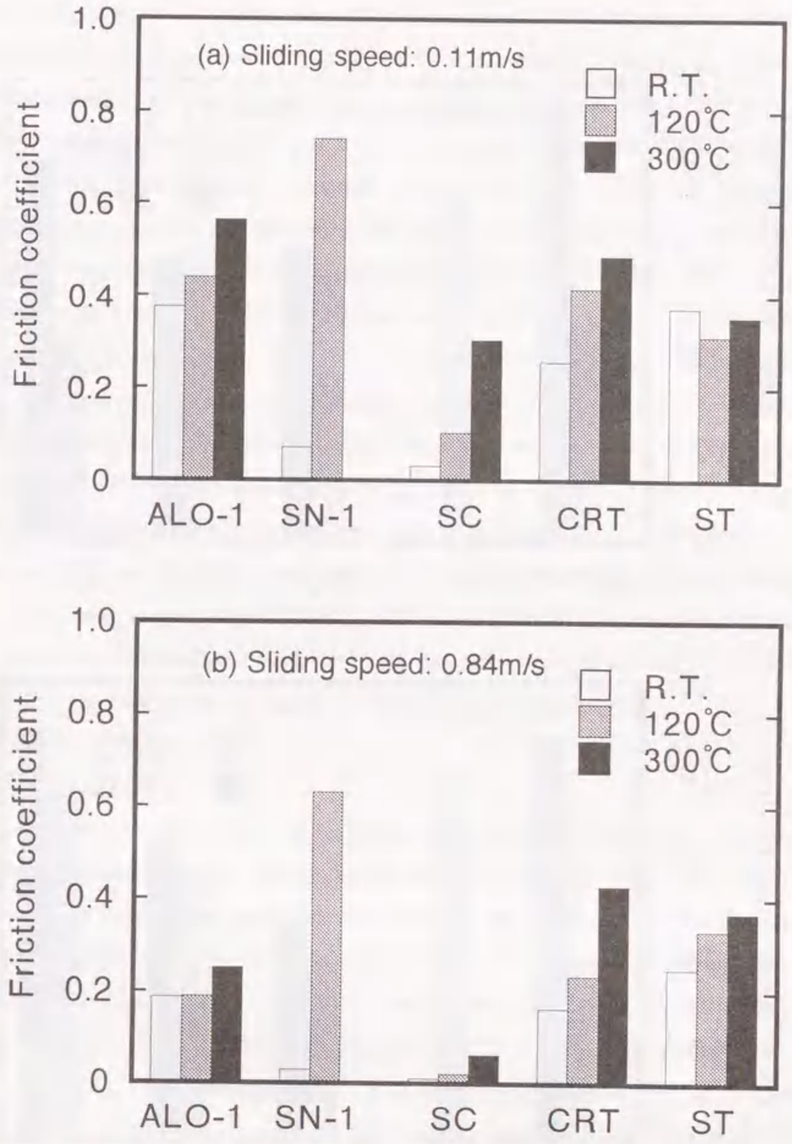

Fig.6-7 Friction coefficients of the materials at the sliding speeds of 0.11 and 0.84m/s in water at room temperature, 120 and 300℃.

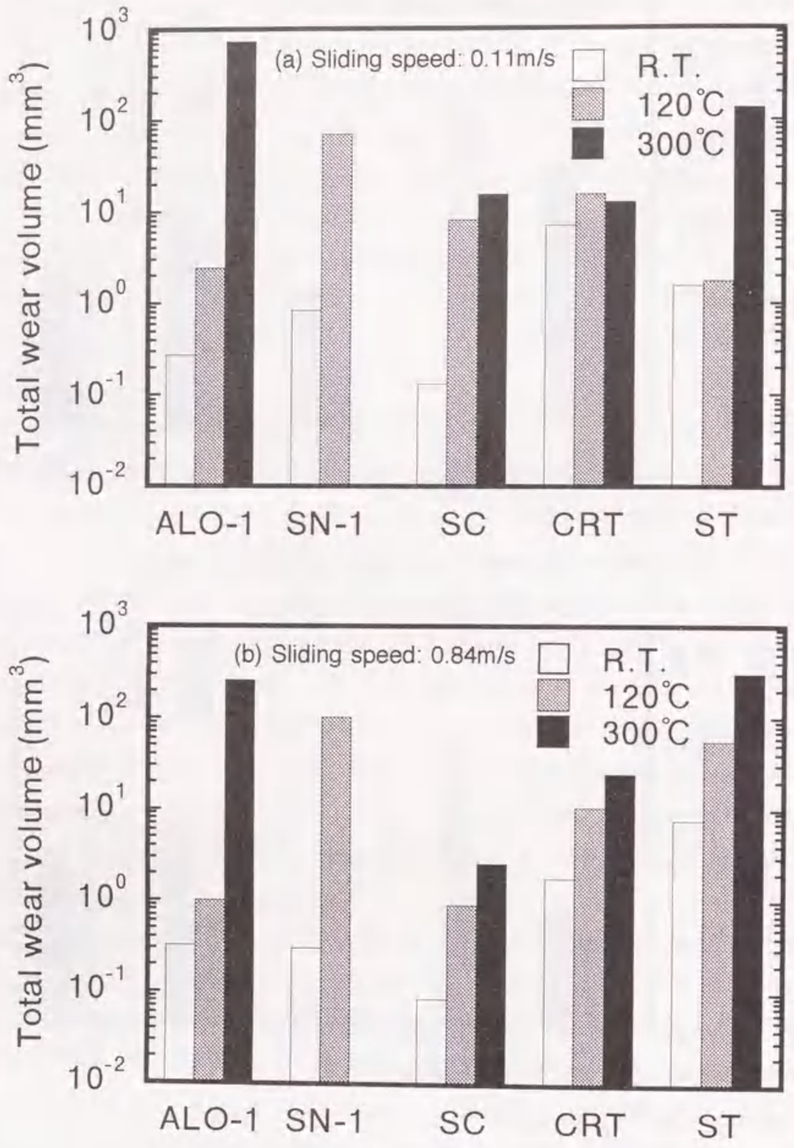

Fig.6-8 Total wear volume of both the two plates and disk at the sliding speeds of 0.11 and 0.84m/s in water at room temperature, 120 and 300℃.

temperature dependence of the friction coefficient in fig 6-7. This is probably related to the rapid acceleration of the corrosion rate of the SN-1 in spite of a slight rise in temperature on the worn surface as seen in fig.6-6. On the other hand, the wear volume of ALO-1, especially at higher sliding speed of 0.84m/s, significantly increases with increasing the temperature in spite of the small increment of the friction coefficient. This suggests to be caused by the fact that the Al_2O_3 grains fall off due to the preferential dissolution of the intergranular layers of ALO-1 as mentioned in Chapter 2.

It is now clear that the SiC ceramic tends to have the low friction and excellent wear resistance in high temperature water compared to other materials in addition to the excellent static corrosion resistance, especially at higher sliding speed in water at 300℃. This is also consistent with the prediction from equations (6-7) and (6-10) as mentioned above. Thus, the SiC ceramic may have a bright prospect of application as a substitute for the stellite. However, the big problem for this application is that the SiC ceramic is fractured easily by an impact stress because of its low fracture toughness (K_{IC}) as shown in table 1-1, resulting in the low reliability of the tribomaterial. If a composite with the SiC matrix, which has higher K_{IC} in addition to the excellent wear resistance, is developed, one can apply this material to nuclear power plants with confidence.

6.3 Conclusions

(1) The equations to predict the wear amount of the plate specimen were proposed on the base of the tribochemical wear models of the ceramics (Al_2O_3, Si_3N_4, SiC and CRT) in high temperature water. The equations proposed by the wear due to the dissolution of Al_2O_3 or oxidation of Si_3N_4 and SiC may be effective for the prediction of the wear amount under the steady state condition. The wear behavior of CRT suggests to be caused by the participation of other factors in addition to the oxidation. In the tribology of Al_2O_3 in water at 300℃, the frictional work may be transformed not only to the energy to change the Al-O-Al or O-Al-O angle at the asperity contact, where the stress corrosion cracking occurs, but to the frictional heat and plastic deformation due to initiation and development of the dislocation in the subsurface layer etc.

(2) If these models can be applied for the dissolution or oxidation to the tribological behavior of the ceramics, it is expected that new materials with high hardness and high thermal conductivity have an excellent wear resistance in water.

(3) The corrosion resistance of SiC and CRT at 120 and 300℃ was more excellent than other ceramics.

(4) The friction coefficient and total wear amount of the SiC specimens tended to be lower than those of other materials (ALO-1, SN-1, CRT and ST), especially at higher sliding speed in water at 300℃. This result was in good agreement with the prediction from the wear models. Thus, this ceramic may be applicable to mechanical parts in nuclear water plants as the tribomaterial instead of ST. However, advanced materials such as composites of the SiC-matrix will have to be futher developed to increase the reliability of the triboelements because the SiC itself has a low K_{IC}.

References

1 See for instance: H.Czichos, *Tribology*, Elsevier, Amsterdam, (1978); D.A.Rigney, Ed. *Fundamentals of Friction and Wear Materials*, American Society for Metals, Metals Park, OH(1981); F. P. Bowden and D. Tabor, *The Friction and Lubrication of Solid*, Clarendon Press, Oxford(1986).

2 E. Rabinowic, *Friction and Wear of Materials*, Wiley, New York, 88(1965).

3 M.Yoshimura, J.Kase and S.Somiya, *J.Mater.Res.*, 1,No.1,100(1986).

4 M.Yoshimura, J.Kase and S.Somiya, *Yogyo Kyokai Shi*, 94,No.1,129(1986) (in Japanese).

5 T.Sato, T.Murakami, T.Endo, M.Shimada, K.Komeya, T.Kameda and M.Komatsu, *J.Mater.Sci*., 26,1749(1991).

6 B.C.Bunker and T.A.Michalske, *Fract.Mech.Ceram.* Vol.8, 391(1986).

7 S.Sasaki, *J.Soc.Lubrication Eng.*, 33,No.8,620(1988) (in Japanese).

8 P.Andersson, *Wear*, 154,37(1992).

9 B.Loffelbein, M.Woydt and K.-H.Habig, *Wear*, 162-164,220(1993).

Chapter 7

Conclusions

7 Conclusions

The applications of advance ceramics to triboelements in nuclear power plants have been desired from the viewpoints of increasing the reliability and lifetime of the mechanical parts and decreasing the radiation exposure. Tribological characteristics of the ceramics sliding on themselves in water were investigated under the various sliding conditions to evaluate the applicability of ceramics materials as the mechanical parts comparing with those of stellite (ST) used for the present LWR and to make clear the wear mechanisms and further to obtain the information on developing materials with the more excellent wear resistance in water. The results of this study are summarized as follows.

In Chapter 1, significance of development of the ceramics as tribomaterials in nuclear power plants were reported, and the principles and chemical aspects of the tribology of the ceramics were also presented. The previous studies on the static corrosion behavior of the ceramics in high temperature and high pressure water, which may strongly affect the friction and wear of these materials, were also described. It was pointed out that the tribology of the ceramics in higher temperature water was scarcely investigated and the friction and wear mechanisms were not clear. After that, aim and summary of this work were mentioned.

In Chapter 2, the effects of temperature, sliding speed, contact load and impurities on the tribological characteristics of 99.3wt% α -Al_2O_3 (ALO-1) and 99.9wt% α -Al_2O_3 (ALO-2) in water were investigated at the temperatures up to 300℃ and the tribochemical mechanisms between the alumina and water at 300℃ were discussed. The specific wear rate of ALO-1 at all sliding speeds significantly increased with increasing the testing temperature, but the friction coefficient slightly increased at lower sliding speeds and was weakly dependent on the temperature at higher sliding speeds. The specific wear rates of ALO-1 at 300℃ were larger than those of ALO-2 at lower loads, whereas those of both ALO-1 and ALO-2 were similar values at higher loads. These behavior may be mainly caused by the dissolution of intergranular impurities and stress corrosion cracking which may be affected by the crack tip blunting due to the dissolution. The streaked film containing γ -alumina particulates appeared on the worn surface at increasing sliding speeds and contact loads in water at 300℃. The γ -alumina particulates may be formed by

the stress induced phase transformation and/or decomposition of boehmite produced on the worn surface due to frictional heat.

In Chapter 3, the effects of temperature, sliding speed, contact load, hydrostatic pressure, dissolved oxygen concentration and sintering aids on tribology of three kinds of Si_3N_4 ceramics (SN-1, SN-2 and SN-3) in water were investigated at room temperature and 120℃. The friction coefficients and specific wear rates of disk and plates of SN-1 at 120℃ were much larger than those at room temperature. This is probably related to decrease of the hydrated silica layer, which possessed a lubrication ability, due to dissolution in water. The friction coefficient and specific wear rate of SN-1 increased with increasing the load and saturated at about 60N under 0.2 and 10MPa in water at 120℃. Those values of SN-1 at 0.2MPa were large compared to those at 10MPa. This seems to be caused by the direct contact between disk and plates and cavitation erosion due to vaporization of water. In water at 120℃, the friction coefficients and specific wear rates of plate for SN-1 were larger than those of SN-2 and SN-3 at lower sliding speeds, but decreased in order of SN-3, SN-1 and SN-2 at higher sliding speeds above 0.4m/s.

The wear of the Si_3N_4 materials at lower sliding speeds and lower loads in water at 120℃ was caused mainly by the hydrothermal oxidation of Si_3N_4 to produce NH_3. This phenomenon seems to be responsible for the contact stress on the asperities formed by the dissolution of the grain boundaries. On the other hand, the wear at higher sliding speeds and higher loads occurred by the microfracture and the hydrothermal oxidation to produce H_2 in addition to NH_3. Especially, the wear of SN-1 at higher sliding speeds may be affected by the oxide film formed on the worn surface and that of SN-3 is probably caused by the preferential oxidation of $Y_{10}(SiO_4)_6N_2$. These tribochemical oxidation of Si_3N_4 also suggests little participation of the dissolved oxygen in water, because the tribochemical properties of SN-1 were independent of dissolved oxygen concentrations for all sliding conditions in water at room temperature and 120℃.

In Chapter 4, the effects of the temperature and sliding speed on the tribological characteristics of a SiC ceramic in deoxygenated water were investigated in the temperatures up to 300℃. The friction coefficient and specific wear rates of disk and plate increased with a rise of the temperature at all sliding speeds and decreased with increasing

the sliding speed at 120 and 300℃. The wear amounts estimated from the evolution of the gaseous products such as H_2, CH_4 and C_2H_6 were similar values to that determined from the total weight loss of two plates and disk at 120 and 300℃. The worn surface morphology at room temperature was very smooth and resembled very closely that at 300 ℃. The wear mechanisms of the SiC ceramic in the range from room temperature to 300℃ were probably governed by the tribochemical oxidation to produce H_2, C, CO_2, CH_4 and C_2H_6. The increases of the friction and wear with increasing the temperature were considered to be contributed to the acceleration of the hydrothermal oxidation of SiC, simultaneously with dissolution of silica. The decreases of the friction and wear with increasing the sliding speed were probably caused by the hydrodynamic lubrication and by depressing the hydrothermal oxidation due to a decrease of the testing duration with increase of the sliding speed under the constant sliding distance.

In Chapter 5, the effects of temperature and sliding speed on the tribological behavior of CRT in deoxygenated water were evaluated in the range from room temperature to 300℃. The friction coefficient increased at elevated temperatures at all sliding speeds, but decreased with increasing sliding speed. The specific wear rates of the plate at room temperature were in the order of $10^{-10}mm^2/N$, but those at 120 and 300℃ were about 10 times larger than that at room temperature. The specific wear rate of the plate slightly decreased with increasing the sliding speed. On the other hand, the specific wear rates of the disk were larger than those of the plate at all sliding conditions. At lower sliding speed, the specific wear rate of the disk did not depend on the testing temperature. However, those of the disk at room temperature decreased with increasing the sliding speed, those at 120℃ were constant, and those at 300℃ increased oppositely. The friction and wear properties of the material are considered to be controlled by the tribochemical oxidations to form the same gaseous products as those for SiC and by the microfracture, especially for the disk by the participation of the thermal shock fracture due to the frictional heat.

In Chapter 6, equations were proposed to predict the wear amount of the plate specimen of the ceramics (Al_2O_3, Si_3N_4, SiC and CRT) and the applicability of the ceramics to the triboelements in nuclear power plants was discussed by comparing with friction and wear

of stellite (ST) used for the present LWR. The equations, which were based on the assumptions of the wear proceeded only due to the tribochemical reactions such as dissolution of Al_2O_3 or oxidation of Si_3N_4 and SiC, may be effective for the prediction of the wear amount under the steady state condition. According to these equations, ceramics materials with high hardness and high thermal conductivity will be expected to have an excellent wear resistance in water. The wear behavior of CRT suggests to be controlled by the participation of other factors in addition to the oxidation. In order to predict the wear amount of Al_2O_3 in water at 300℃, it is necessary to take into account not only on the transformation of the frictional work to the energy to change the Al-O-Al or O-Al-O angle at the asperity contact, but on that to the frictional heat and the plastic deformation due to initiation and development of the dislocation etc.

The SiC ceramic has the most excellent static corrosion resistance of all the ceramics. Moreover, the friction coefficient and total wear amount of the SiC specimens were tend to be lower than those of other materials, especially at higher sliding speed in water at 300 ℃. This result probably reflects that prediction for the wear due to the dissolution or oxidation. Thus, the SiC ceramic may be most applicable to the mechanical parts as the tribomaterial instead of ST. If only the mechanical fracture resistance of the SiC ceramic is improved by composite of the SiC-matrix, the reliability of this material will be further increased in addition to its excellent tribochemical wear resistance in water.

Acknowledgements

The present thesis is the collection of studies which have been carried out under the direction of Prof. Dr. Toshio KATOH and Prof. Dr. Toshihide TSUJI of Department of Nuclear Engineering, Faculty of Engineering, Nagoya University, and Mr. Yoshimi YAMAGUCHI who is the chief management researcher, Japan Fine Ceramics Center (JFCC), during 1991～1994. The author expresses grateful acknowledgement to Prof. Dr. Toshio KATOH, Prof. Dr. Toshihide TSUJI and Mr. Yoshimi YAMAGUCHI for their valuable suggestion, discussion and continuous encouragement throughout his work.

The thesis was completed through the discussions and suggestions by Prof. Dr. Toshio KATOH, Prof. Dr. Toshihide TSUJI, Prof. Dr. Kenji MORITA, Prof. Dr. Kunihito KOUMOTO, Prof. Dr. Kanji TASAKA and Assoc. Prof. Dr. Tsuneo MATSUI. I would like to express my thanks to them.

The author is deeply indebted to Dr. Mitsuo ISOTANI who was the former Laboratory Director of JFCC and Dr. Yasushi IKEDA who is the chief researcher of JFCC for providing the chance to carry out his work.

Grateful acknowledgement is made to Dr. Hiroshi OKUDA who was the onetime Laboratory Director of JFCC, Mr. Kōji SATO and Mr. Kazumi KASHIWAGI of JFCC and Yoshihide TAKAHASHI of Shikoku Electric Power Corporation for their continuous assistance in various stages of his work.

Finally the author expresses his gratitude heartily to his wife, Michie KITAOKA and to his parents, Mr. Kazuo KITAOKA, Mrs. Kazuko KITAOKA, and also to his parents by marriage, Mr. Toshiharu HATTORI, Mrs. Sachiko HATTORI.

July, 1994

Satoshi KITAOKA

List of published papers

(1) Tribological Characteristics of α-Alumina in High-Temperature Water
S.Kitaoka, Y.Yamaguchi and Y.Yoshihide
J.Am.Ceram.Soc.,75,No.11,3075(1992)

(2) Tribological Characteristics of Si_3N_4 Ceramic in High-Temperature and High-Pressure Water
S.Kitaoka, T.Tsuji, T.Katoh, Y.Yamaguchi and K.Sato
J.Am.Ceram.Soc.,77,No.2,580(1994)

(3) Effects of Load and Hydrostatic Pressure on Tribological Characteristics of Si_3N_4 Ceramic at 120℃ in Water
S.Kitaoka, T.Tsuji, T.Katoh, Y.Yamaguchi and K.Sato
in Proceedings of IUMRS-ICAM-93, Elsevier, London, U.K., (1994) (in press)

(4) Effects of Sintering Aids on Tribological Characteristics of Si_3N_4 Ceramics at 120℃ in Water
S.Kitaoka, T.Tsuji, T.Katoh, Y.Yamaguchi and K.Sato
in Proceedings of the 6th Nordic Symposium on Tribology NORDTRIB'94, (1994) (in press)

(5) Tribological Characteristics of SiC Ceramic in High-Temperature and High-Pressure Water
S.Kitaoka, T.Tsuji, T.Katoh, Y.Yamaguchi and K.Sato
J.Am.Ceram.Soc., (1994) (in press)

(6) Tribological Characteristics of Cr_3C_2 Ceramic with Addition of TiC in High-Temperature and High-Pressure Water
S.Kitaoka, T.Tsuji, T.Katoh, Y.Yamaguchi and K.Kashiwagi
J.Soc.Mater.Sci., 43,No.489,646(1994) (in Japanese)